

SHAPING ANTENNA PHASE AND AMPLITUDE DISTRIBUTIONS FOR LOW SIDELOBES

BY

Charles P. Burns, H. Allen Ecker and Edward B. Joy

GEORGIA TECH RESEARCH INSTITUTE
Atlanta, Georgia 30332

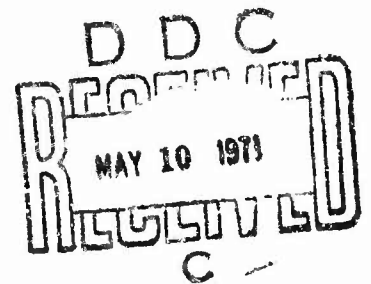
Contract No. F19628-70-C-0169

Project No. 4609

Task No. 460010

Work Unit No. 46001001

FINAL REPORT



Period Covered: 1 February 1970 through 31 January 1971

28 February 1971

This research was performed at the Electronics Division
of Georgia Institute of Technology

Contract Monitor: Allan C. Schell
Microwave Physics Laboratory

This document has been approved for public
release and sale; its distribution is unlimited.



Prepared for

AIR FORCE CAMBRIDGE RESEARCH LABORATORIES
AIR FORCE SYSTEMS COMMAND
UNITED STATES AIR FORCE
BEDFORD, MASSACHUSETTS 01730

AD 722718

Unclassified

Security Classification

DOCUMENT CONTROL DATA - R & D

Security classification of title, body of abstract and indexing annotation must be entered when the overall report is classified)

1. ORIGINATING ACTIVITY (Corporate author) Georgia Tech Research Institute Atlanta, Georgia 30332		2a. REPORT SECURITY CLASSIFICATION Unclassified	
		2b. GROUP	
3. REPORT TITLE SHAPING ANTENNA PHASE AND AMPLITUDE DISTRIBUTIONS FOR LOW SIDELOBES			
4. DESCRIPTIVE NOTES (Type of report and inclusive dates) Scientific. Final 1 February 1970 to 31 January 1971			Approved: 30 March 1971
5. AUTHOR(S) (First name, middle initial, last name) Charles P. Burns Harry A. Ecker Edward B. Joy			
6. REPORT DATE 28 February 1971	7a. TOTAL NO. OF PAGES 98	7f. NO. OF REFS 17	
8a. CONTRACT OR GRANT NO. F19628-70-C-0169 Project, Task, Work Unit Nos. 4600-10-01 DoD Element 62702F DoD Subelement 674600		9a. ORIGINATOR'S REPORT NUMBER(S) 9b. OTHER REPORT NO(S) (Any other numbers that may be assigned this report) AFCL-71-0180	
10. DISTRIBUTION STATEMENT This document has been approved for public release and sale; its distribution is unlimited.			
11. SUPPLEMENTARY NOTES This research was performed at the Electronics Division of Georgia Institute of Technology		12. SPONSORING MILITARY ACTIVITY Air Force Cambridge Research Laboratories L. G. Hanscom Field (LZ) Bedford, Massachusetts 01730	
13. ABSTRACT For many radar applications, extremely low antenna sidelobes can improve system performance. Current techniques utilize only the antenna amplitude distribution to produce lower sidelobes. This report presents results of an investigation of combined amplitude and phase tapering to produce lower sidelobes. Combinations of phase and amplitude distributions and the resulting far-field patterns were studied theoretically through computer analysis. Gaussian phase tapers with cosine and modified Taylor amplitude distributions were studied in detail. Experimental work included the construction of a dielectric lens for a horn antenna that significantly lowered the sidelobe level. Design information was compiled to demonstrate tradeoffs between amplitude tapering alone and combined phase and amplitude tapering.			

KEY WORDS	LINK A		LINK B		LINK C	
	ROLE	WT	ROLE	WT	ROLE	WT
Aperture Distribution Antenna Sidelobes Phase Taper Near-Field Far-Field						

SHAPING ANTENNA PHASE AND AMPLITUDE
DISTRIBUTIONS FOR LOW SIDELOBES

BY

Charles P. Burns, H. Allen Ecker and Edward B. Joy

Georgia Tech Research Institute
Atlanta, Georgia 30332

Contract No. F19628-70-C-0169

Project No. 4600

Task No. 460010

Work Unit No. 46001001

FINAL REPORT

Period Covered: 1 February 1970 through 31 January 1971

28 February 1971

This research was performed at the Electronics Division
of Georgia Institute of Technology

Contract Monitor: Allan C. Schell
Microwave Physics Laboratory

This document has been approved for public
release and sale; its distribution is unlimited.

Prepared for

AIR FORCE CAMBRIDGE RESEARCH LABORATORIES
AIR FORCE SYSTEMS COMMAND
UNITED STATES AIR FORCE
BEDFORD, MASSACHUSETTS 01730

FOREWORD

This work was performed by the Electronics Division of the Georgia Institute of Technology under United States Air Force Contract No. F19628-70-C-0169 during the period February 1970 to January 1971.

This report is the result of efforts by a large number of individuals. Contributors in addition to the authors include D. G. Bodnar, K. B. Barfield, T. M. Hedges, and E. C. Burdette. Special acknowledgement is made of the contributions of Dr. Allan Schell of the Air Force Cambridge Research Laboratories.

ABSTRACT

For many radar applications, extremely low antenna sidelobes can improve system performance. Current techniques utilize only the antenna amplitude distribution to produce lower sidelobes. This report presents results of an investigation of combined amplitude and phase tapering to produce lower sidelobes. Combinations of phase and amplitude distributions and the resulting far-field patterns were studied theoretically through computer analysis. Gaussian phase tapers with cosine and modified Taylor amplitude distributions were studied in detail. Experimental work included the construction of a dielectric lens for a horn antenna that significantly lowered the sidelobe level. Design information was compiled to demonstrate tradeoffs between amplitude tapering alone and combined phase and amplitude tapering.

TABLE OF CONTENTS

<u>Section</u>	<u>Page</u>
I. INTRODUCTION	1
II. BACKGROUND	3
III. THEORETICAL INVESTIGATIONS	11
1. CURVE FITTING	14
2. COSINE PHASE DISTRIBUTION	14
3. GAUSSIAN PHASE DISTRIBUTION.	17
4. PHASE TAPERING APPLIED TO TAYLOR AMPLITUDE DISTRIBUTIONS . .	19
(a) Modified Taylor Distribution	21
(b) End Point Phase Requirements	26
5. THE OPTIMUM LINE SOURCE DISTRIBUTION	26
(a) General Line Source Optimization	26
(b) Optimization of a Monopulse Line Source Distribution . .	36
IV. EXPERIMENTAL WORK	39
1. NEAR-FIELD PROBE	39
2. SQUARE HORN	43
(a) Near-Field Measurements	49
(b) Far-Field Measurements	49
3. STANDARD GAIN HORN	53
4. LINE SOURCE	58
V. DESIGN INFORMATION	63
1. OPTIMUM PHASE AND AMPLITUDE TAPERS	63
2. GAIN FACTOR CURVES	68

LIST OF FIGURES

<u>Number</u>		<u>Page</u>
2-1.	The far-field radiation patterns of (a) a 23.0-inch aperture employing an unfolded geodesic Luneberg lens, and (b) a 23.6-inch aperture employing a folded geodesic Luneberg lens	4
2-2.	The amplitude and phase distributions for (a) a 23.0-inch aperture employing an unfolded geodesic Luneberg lens, and (b) a 23.6-inch aperture employing a folded geodesic Luneberg lens	6
2-3.	The far-field radiation patterns of an X-band lens-horn feed at (a) 9.95 GHz and (b) 10.00 GHz.. . . .	8
3-1.	Aperture distribution and computed far-field pattern for a uniform illumination	13
3-2.	Folded geodesic Luneberg lens aperture distribution, and computed far-field pattern	15
3-3.	Folded geodesic Luneberg lens aperture distribution with no phase variation, and computed far-field pattern	15
3-4.	Folded lens aperture distribution fitted to a fourth-order polynomial, and computed far-field pattern	16
3-5.	Folded lens aperture distribution fitted to a sixth-order polynomial, and computed far-field pattern	16
3-6.	Folded lens aperture distribution with a phase distribution of the form $A(1 + \cos \pi X)$, and computed far-field pattern	18
3-7.	Folded lens aperture distribution with a Gaussian phase distribution, and computed far-field antenna pattern	18
3-8.	Modified Taylor amplitude distribution and computed far-field pattern, with a sidelobe level of -30 dB	23
3-9.	Aperture distribution and computed far-field pattern for the amplitude distribution of Figure 3-8, but with a Gaussian phase distribution	23
3-10.	Modified Taylor amplitude distribution and computed far-field pattern, with a sidelobe level of -35 dB	24

TABLE OF CONTENTS (Continued)

<u>Section</u>	<u>Page</u>
VI. CONCLUSIONS AND RECOMMENDATIONS	81
APPENDIX	83
REFERENCES	87

LIST OF FIGURES (Continued)

<u>Number</u>		<u>Page</u>
3-11.	Aperture distribution and computed far-field pattern for the amplitude distribution of Figure 3-10, but with a Gaussian phase distribution	24
3-12.	Modified Taylor amplitude distribution with a nominal side-lobe level of -25 dB with a twenty degree end point Gaussian phase distribution, and computed far-field pattern	27
3-13.	Modified Taylor amplitude distribution with a nominal side-lobe level of -25 dB with a forty degree end point Gaussian phase distribution, and computed far-field pattern	27
3-14.	Modified Taylor amplitude distribution with a nominal side-lobe level of -20 dB with a forty degree end point Gaussian phase distribution, and computed far-field pattern	28
3-15.	Modified Taylor amplitude distribution with a nominal side-lobe level of -20 dB with a sixty degree end point Gaussian phase distribution, and computed far-field pattern	28
3-16.	Line source coordinate system	31
4-1.	Front view of near-field probe and X-Y-Z positioner	40
4-2.	Side view of near-field probe and X-Y-Z positioner	41
4-3.	Measured near-field pattern of an X-band horn antenna, E-plane cut	42
4-4.	Normalized aperture distribution and computed far-field pattern using the near-field pattern shown in Figure 4-3	44
4-5.	Measured far-field pattern of the antenna shown in Figure 4-4	45
4-6.	Measured aperture distribution and computed far-field pattern of the test horn	46
4-7.	Test horn aperture distribution with a Gaussian phase distribution, and computed far-field pattern	47
4-8.	Measured aperture distribution and computed far-field pattern of the test horn with lens at 9375 MHz	50

LIST OF FIGURES (Continued)

<u>Number</u>		<u>Page</u>
4-9.	Measured aperture distribution and computed far-field pattern of the test horn with lens at 9385 MHz	51
4-10.	Measured aperture distribution and computed far-field pattern of the test horn with lens at 9405 MHz	52
4-11.	Measured far-field pattern of the test horn with lens at 9385 MHz	54
4-12.	Measured far-field pattern of the test horn at 9385 MHz	55
4-13.	Measured far-field pattern of the test horn with lens at 9405 MHz	56
4-14.	Measured far-field pattern of the test horn at 9405 MHz	57
4-15.	Measured aperture distribution and computed far-field pattern of the X-band standard gain horn	59
4-16.	Standard gain horn aperture distribution with a Gaussian phase distribution, and computed far-field pattern	59
4-17.	Measured aperture distribution and computed far-field antenna pattern of the line source antenna	60
4-18.	Line source aperture distribution with a Gaussian phase distribution and computed far-field pattern	60
4-19.	Measured line source distribution and computed far-field pattern, showing the effect of mutual coupling on the aperture distribution	62
4-20.	Measured line source distribution and computed far-field pattern, showing the effect of an abrupt change in the phase distribution	62
5-1.	Optimized modified Taylor amplitude and Gaussian phase aperture distribution for a sidelobe level of -15 dB	64
5-2.	Optimized modified Taylor amplitude and Gaussian phase aperture distribution for a sidelobe level of -20 dB	64
5-3.	Optimized modified Taylor amplitude and Gaussian phase aperture distribution for a sidelobe level of -25 dB	65

LIST OF FIGURES (Continued)

<u>Number</u>		<u>Page</u>
5-4.	Optimized modified Taylor amplitude and Gaussian phase aperture distribution for a sidelobe level of -30 dB	65
5-5.	Optimized modified Taylor amplitude and Gaussian phase aperture distribution for a sidelobe level of -35 dB	66
5-6.	Optimized modified Taylor amplitude and Gaussian phase aperture distribution for a sidelobe level of -40 dB	66
5-7.	Optimized modified Taylor amplitude and Gaussian phase aperture distribution for a sidelobe level of -45 dB	67
5-8.	Optimized modified Taylor amplitude and Gaussian phase aperture distribution for a sidelobe level of -50 dB	67
5-9.	Gain Factor and sidelobe level as a function of amplitude taper, with no phase variation	70
5-10.	Gain Factor and sidelobe level as a function of amplitude taper, with a maximum phase variation of twenty degrees . .	71
5-11.	Gain Factor and sidelobe level as a function of amplitude taper, with a maximum phase variation of thirty degrees	72
5-12.	Gain Factor and sidelobe level as a function of amplitude taper, with a maximum phase variation of forty degrees	73
5-13.	Gain Factor and sidelobe level as a function of amplitude taper, with a maximum phase variation of fifty degrees	74
5-14.	Gain Factor and sidelobe level as a function of amplitude taper, with a maximum phase variation of sixty degrees	75
5-15.	Gain Factor and sidelobe level as a function of amplitude taper, with a maximum phase variation of seventy degrees	76
5-16.	Gain Factor and sidelobe level as a function of amplitude taper, with a maximum phase variation of eighty degrees	77
5-17.	Gain Factor and sidelobe level as a function of amplitude taper, with a maximum phase variation of ninety degrees	78
5-18.	Gain Factor and sidelobe level as a function of amplitude taper, with a maximum phase variation of one hundred degrees . .	79

LIST OF FIGURES (Continued)

<u>Number</u>		<u>Page</u>
5-19.	Use of the design curves to determine if phase tapering will result in a higher gain factor at sidelobe levels of -20 dB and -35 dB	80
A-1.	Three-dimensional error map of deviation in probe position from a true X-Y plane	86

LIST OF TABLES

<u>Table</u>		<u>Page</u>
3-1.	Theoretical Performance of Several Phase Tapers for the Folded Lens Amplitude Distribution	20
3-2.	Theoretical Performance of Modified Taylor Amplitude Tapering and Gaussian Phase Tapering	25
4-1.	Performance Comparison of Test Horn and Test Horn with Lens at Several Frequencies	48
4-2.	Theoretical Performance of Standard Gain Horn with Quadratic and Gaussian Phase Distributions	58
5-1.	Optimized Modified Taylor Amplitude and Gaussian Phase Distributions	69

SECTION I

INTRODUCTION

For many radar and communication applications, extremely low antenna sidelobes can improve the overall system performance. It is common practice to taper the antenna amplitude distribution to produce lower sidelobes at the expense of lower gain factor and larger beamwidth. However, current sidelobe reduction techniques do not employ a modification to the phase distribution in addition to the tapered amplitude distribution. It is the purpose of this report to present results of an investigation of combined amplitude and phase tapering to produce low sidelobe levels.

Specific instances of low sidelobe antennas have been observed at Georgia Tech when non-uniform phase distributions were produced in folded geodesic lens antennas and horn antennas with dielectric lenses. As described in Section II, phase tapering combined with amplitude tapering produced antennas with unusually low sidelobes. The approach in this investigation was to start with phase and amplitude distributions known to produce low sidelobes and to examine the far-field pattern as the parameters controlling the phase distribution were varied. Rapid phase variations were avoided so that realizable distributions and reasonable gain factors would result.

Initially, combinations of phase and amplitude distributions and the resulting far-field patterns were investigated theoretically through computer analysis. Gaussian phase tapers with cosine and modified Taylor amplitude distributions were considered in detail. Horn-lens combinations and line source arrays were fabricated to confirm the theoretical results. From the results of the theoretical and experimental work, design information was compiled to show

tradeoffs between amplitude tapering and combined phase and amplitude tapering. Potential practical applications of phase tapering were examined with particular emphasis on their use in monopulse systems and phased arrays.

SECTION II

BACKGROUND

The increasing need for better target discrimination and improved detection capabilities in radar applications has resulted in more stringent requirements being placed on radar antenna systems. In particular, these requirements have resulted in the demand for antennas having lower sidelobes than are usually achieved in practical radar antennas. Although a great deal of theoretical work has been devoted to the optimization of antenna directivity for specified sidelobe levels^{1,2,3} and to the synthesis of arbitrary patterns,⁴ there remains a definite need for information concerning the design and construction of efficient, practical antennas which can meet the existing directivity and low sidelobe requirements.

Two notable observations of significant sidelobe reduction with either minor or immeasurable changes in the far-field gains and 3-dB beamwidth have been made on antennas designed, constructed, and tested at Georgia Tech. The results obtained from these observations indicate that phase shaping can be combined with the amplitude shaping of antenna apertures to yield efficient antennas which have very low sidelobes in their far-field radiation patterns.

1. GEODESIC LENS OBSERVATIONS

The first observation of significant sidelobe reduction was made in comparing the radiation pattern of a 23.0-inch line source aperture employing a folded geodesic Luneberg lens⁵ to that of a similar 23.6-inch line source aperture which employed an unfolded geodesic Luneberg lens.^{6,7} The radiation patterns of both antennas at 70 GHz are shown in Figure 2-1. At this frequency

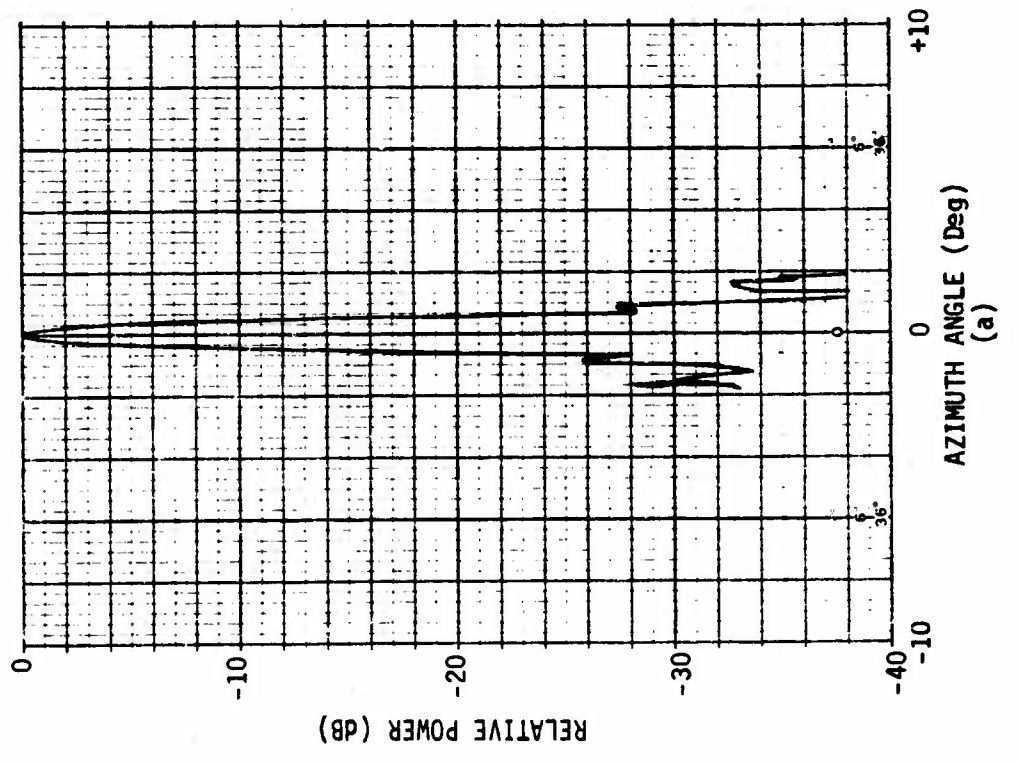
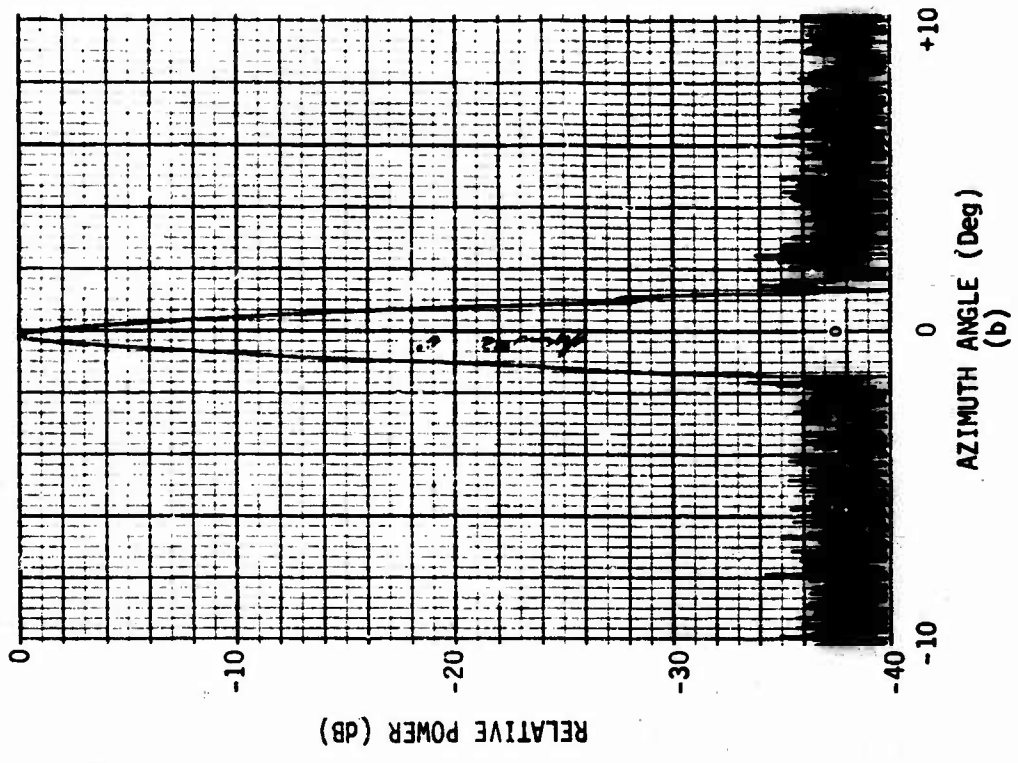


Figure 2-1. The far-field radiation patterns of (a) a 23.0-inch aperture employing an unfolded geodesic Luneberg lens, and (b) a 23.6-inch aperture employing a folded geodesic Luneberg lens.

both antennas exhibited a 3-dB beamwidth of about 0.5 degrees. The major difference between the radiation patterns of the two antennas was the difference in sidelobe levels. The sidelobes of the antenna employing the unfolded lens were 26 dB or more down from the peak of the main lobe, whereas the sidelobes of the antenna employing the folded lens were more than 36 dB down from the peak of the main lobe. The measured sidelobe levels in the radiation pattern of the antenna employing the unfolded lens agreed with those predicted by transforming the primary feed horn pattern through the lens. However, the sidelobe levels achieved in the radiation pattern of the antenna employing the folded lens were much lower than the predicted levels. It was surmised that the very low sidelobes resulted from a modification of the amplitude and phase distributions of the folded lens aperture due to the presence of higher order modes in the lens folds. A far-field pattern calculation using measured amplitude and phase distributions verified that the sidelobe level improvement was due to the changes in the amplitude and phase distribution caused by the effects of folding the lens.

The amplitude and phase distributions which produced the observed far-field patterns of the antennas employing the unfolded and folded geodesic lenses are shown in Figures 2-2a and 2-2b, respectively. Note, in Figure 2-2b, that the effect of the lens folds was to concentrate more energy toward the center of the aperture and to introduce a symmetrical phase taper (with a phase lag of about 90 degrees at the edges of the aperture) having two minor peaks located ± 9 inches from the center of the aperture. The increase of energy near the center of the folded lens aperture tended to compensate for the loss in aperture efficiency caused by the presence of the phase taper.

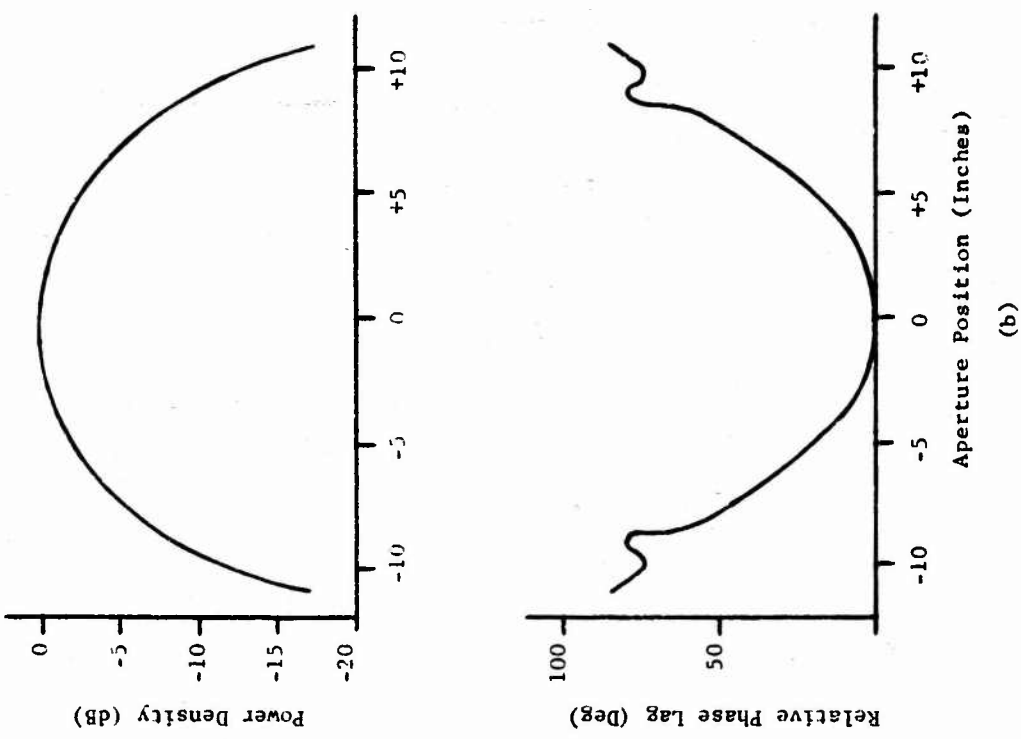


Figure 2-2. The amplitude and phase distributions for (a) a 23.0-inch aperture employing an unfolded geodesic Luneberg lens, and (b) a 23.6-inch aperture employing a folded geodesic Luneberg lens.

A careful comparison of the two patterns illustrated in Figure 2-1 shows that the first pair of sidelobes present in Figure 2-1a has merged with the main lobe of the pattern in Figure 2-1b. Note, however, that the second pair of sidelobes present in Figure 2-1a has been suppressed in the pattern of Figure 2-1b. The merging of the first sidelobes with the main beam and the suppression of the outlying sidelobes was accompanied by some broadening of the main beam below the -10 dB level. However, the main lobe pattern achieved is more desirable than the very broad pattern which is usually obtained when a quadratic phase taper is added to a constant phase aperture distribution^{8,9}.

2. LENS-HORN FEED OBSERVATIONS

The second observation of significant sidelobe reduction was made in the testing of an X-band feed which consisted of a quarter-wave step-matched dielectric lens mounted in the throat of a horn. The establishment of higher order modes in the throat of the horn made the lens-horn feed combination frequency sensitive. The patterns of the lens-horn feed at 9.95 GHz and 10.00 GHz are shown in Figures 2-3a and 2-3b, respectively. The feed exhibited the same gain and a 3-dB beamwidth of 27 degrees at both frequencies. However, the sidelobes present at 10.00 GHz were more than 36 dB below the peak of the main lobe. The 12-dB sidelobe suppression observed in the lens-horn feed tests is particularly interesting since the sidelobe suppression did not significantly broaden the base of the main lobe. Preliminary measurements of the amplitude and phase distributions of the feed aperture at 9.95 GHz and 10.00 GHz have indicated that the amplitude distribution is essentially the same at both frequencies. However, the phase distribution changes noticeably

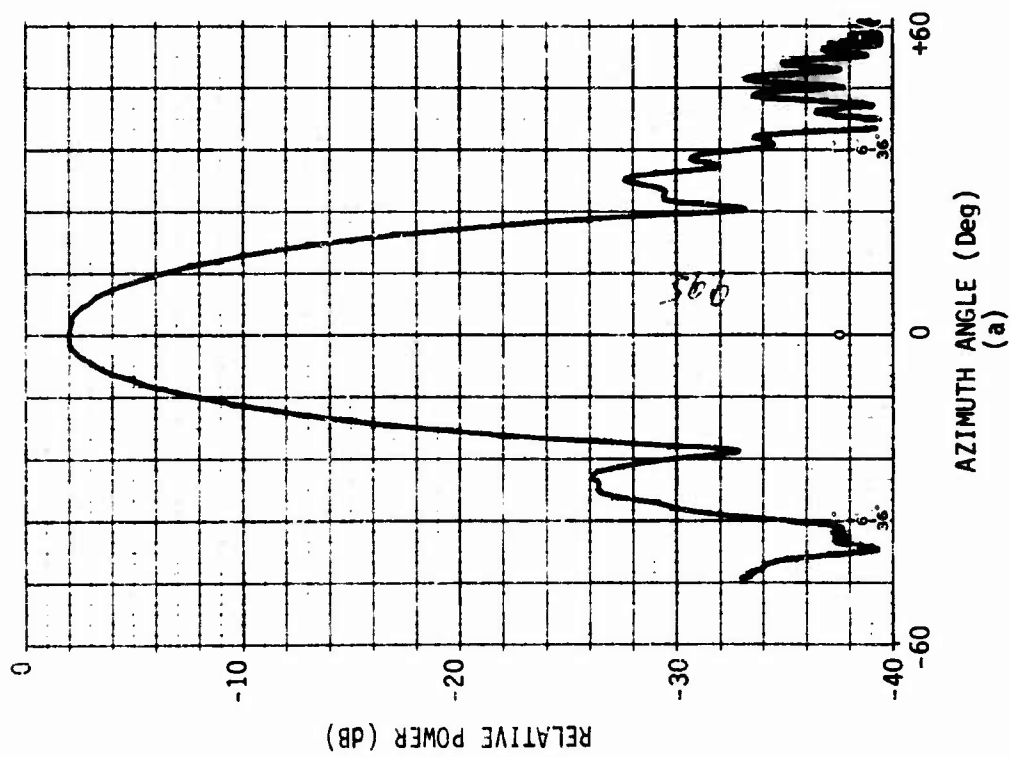
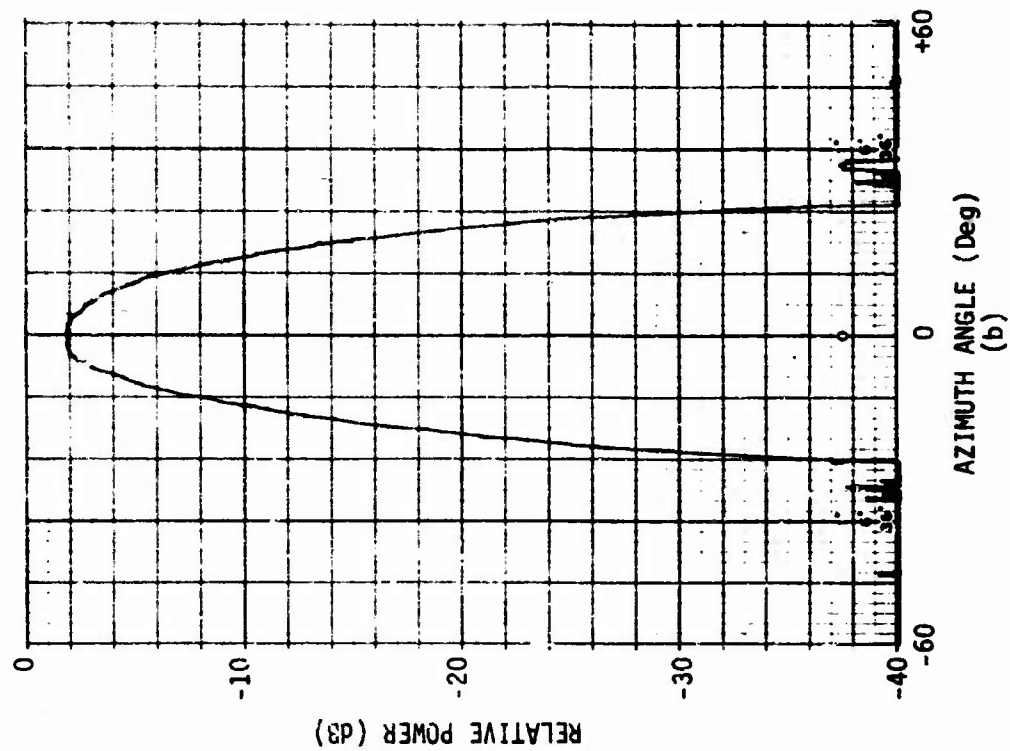


Figure 2-3. The far-field radiation patterns of an X-band lens-horn feed at (a) 9.95 GHz and (b) 10.00 GHz.

between 9.95 GHz and 10.00 GHz. Thus, the improved performance at 10.00 GHz is due largely to the changed phase distribution.

3. DESIGN APPROACH

The two observations discussed above suggest that the sidelobe levels in the far-field radiation patterns of highly directive, efficient antennas can be reduced with no significant changes in the directivity or efficiency if 1) the usual constant-phase aperture distribution is replaced by a properly shaped, non-uniform phase distribution, and 2) the existing amplitude distribution is slightly modified to overcome the loss in aperture efficiency which results from the replacement of the constant-phase aperture distribution by the shaped non-uniform phase distribution. This approach to sidelobe level reduction contrasts with the more familiar approaches to sidelobe reduction in that no attempt is made to achieve the maximum directivity for a given sidelobe level. The required directivities and sidelobe levels are obtained by combining a practical amplitude distribution with realizable shaping of the aperture phase distribution. This approach is highly practical and avoids the class of inefficient, supergain antennas.

SECTION III

THEORETICAL INVESTIGATIONS

As described in Section II, phase tapering combined with amplitude tapering produced antennas with unusually low sidelobes in research at Georgia Tech. The approach in the theoretical portion of the contract was to start with phase and amplitude distributions known to produce low sidelobes and to examine the far-field pattern as the parameters controlling the phase distribution were varied.

Fourier integral techniques were utilized to analyze the effects of changes in the aperture amplitude and phase distributions on far-field patterns. The far-field pattern of a line source aperture is given by¹⁰

$$g(\theta) = \int_{-a/2}^{a/2} F(z) e^{jkz \sin \theta} dz \quad (3-1)$$

where

a is the length of the aperture

z is the distance along the line source

$k = 2\pi/\lambda$ where λ is the wavelength

θ is the angular coordinate

$F(z)$ is the complex current distribution

This can be written in normalized form as

$$g(\mu) = \frac{a}{2} \int_{-1}^1 f(x) e^{j\mu x} dx \quad (3-2)$$

where

$$\mu = \frac{\pi a}{\lambda} \sin \theta, \quad x = \frac{2z}{a}$$

The normalized notation has the advantage that the far-field pattern of the antenna does not have to be recalculated if the aperture size or frequency is changed, as long as the aperture distribution is unchanged.

A computer program using the Fast Fourier Transform to calculate far-field patterns from aperture distributions was developed that included subroutines for plotting the input phase and amplitude aperture distributions and normalized far-field pattern. The normalized 3-dB beamwidth, aperture gain factor, and first sidelobe level are recorded on each plot of an antenna pattern. The normalized beamwidth is related to the true beamwidth by

$$\overline{BW}_{\text{normalized}} = \frac{a}{\lambda} \overline{BW} \quad (3-3)$$

and the gain factor is defined as¹¹

$$G = \frac{G_M}{G_O} \quad (3-4)$$

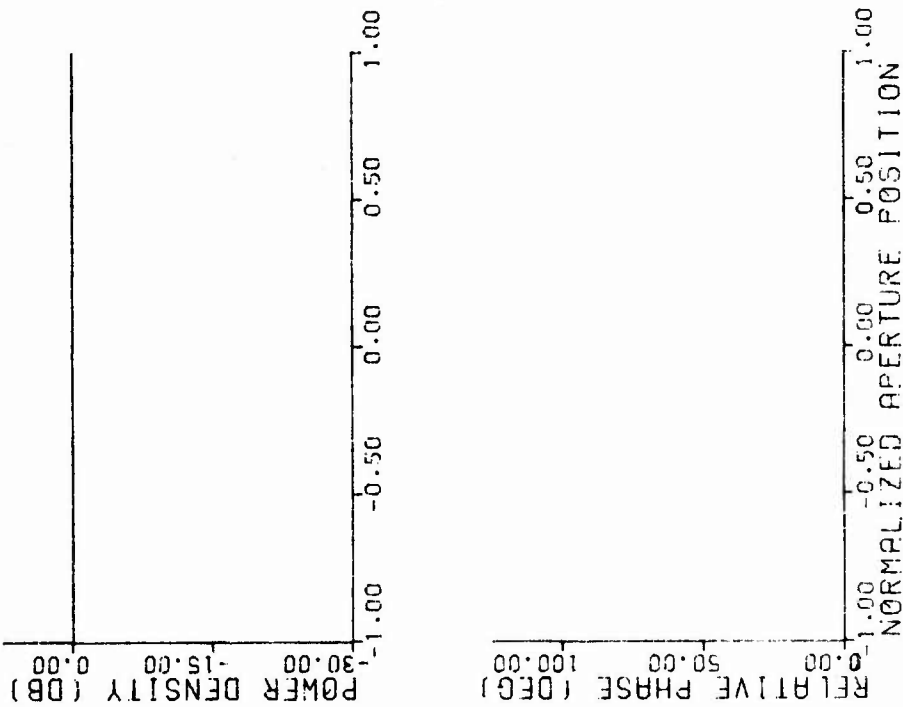
where

G_M is the gain of the aperture, and

G_O is the gain of a uniformly illuminated aperture.

Figure 3-1 shows a typical computer-plotted input aperture distribution and far-field pattern.

Test distributions for which the exact radiation patterns are known were used to determine the accuracy of the Fast Fourier Transform solution. Among those tested were the uniform illumination of Figure 3-1, and the cosine-squared distribution; gain factor errors were less than one percent, and first sidelobe level errors were on the order of 0.1 dB.



FIRST SIDELOBE - -13.26 DB
 GAIN FACTOR - 1.0000
 BEAMWIDTH - 50.63 DEGREES

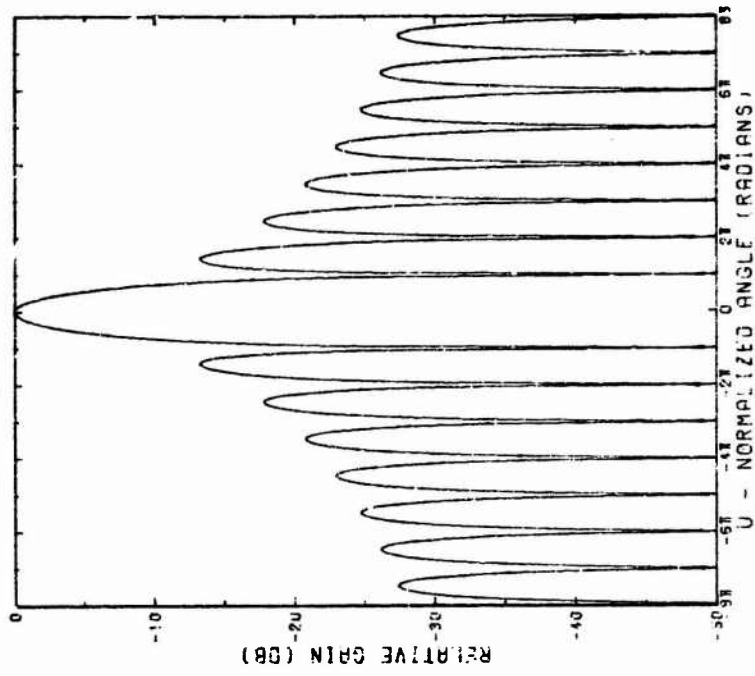


Figure 3-1. Aperture distribution and computed far-field pattern for a uniform illumination.

1. CURVE FITTING

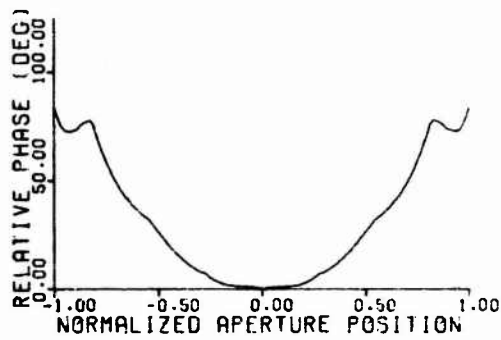
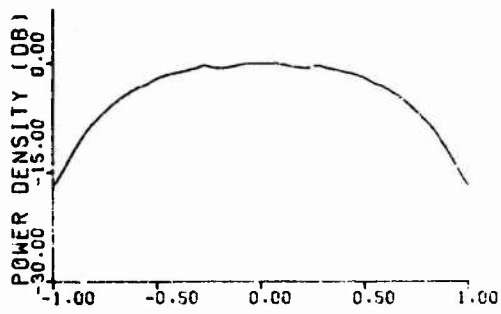
Polynomial curve fitting techniques were applied to the aperture distribution of the folded geodesic lens described in Section II. Figure 3-2 shows the amplitude and phase distribution of this antenna and the computed far-field pattern; the first sidelobe level is -32 dB. The shape of the phase distribution of this antenna is irregular; by successively approximating the shape of this curve with higher-order polynomials, the effect of small changes in the phase distribution on the sidelobe level can be determined.

Figure 3-3 shows the amplitude and phase distribution and computed far-field pattern for the folded lens with no phase variation (zero order polynomial); the first sidelobe level is -21 dB. Figures 3-4 and 3-5 show the effect on the far-field pattern when the aperture distribution is approximated by fourth and sixth order polynomials, respectively. The sixth order polynomial approximation produced the best combination of sidelobe level, gain factor, and beamwidth. However, no substantial improvement over the performance of the measured phase distribution resulted from this approach.

The curve fitting experiments did reveal that the sidelobe level is extremely sensitive to small changes in the phase distribution, but that the rapid phase change at the ends of the measured phase distribution (the "curls" in Figure 3-2) were not necessary to achieve the measured sidelobe level.

2. COSINE PHASE DISTRIBUTION

The phase distribution of Figure 3-5 is a well-behaved function, but would be difficult to express analytically. However, the general shape suggested a sinusoidal variation. A phase distribution of the form



FIRST SIDELOBE - -31.74 DB
 GAIN FACTOR - 0.7429
 BEAMWIDTH - 68.19 DEGREES

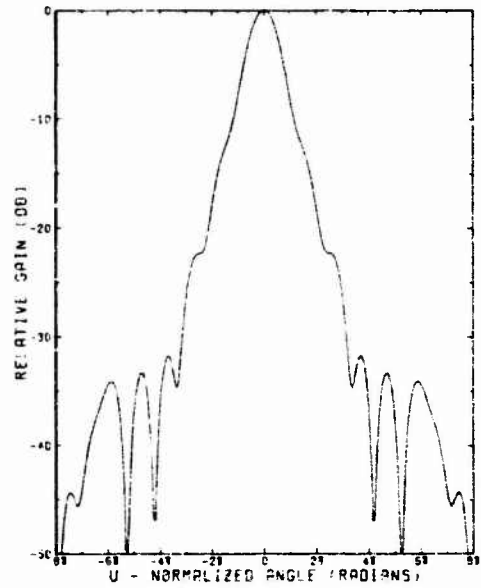
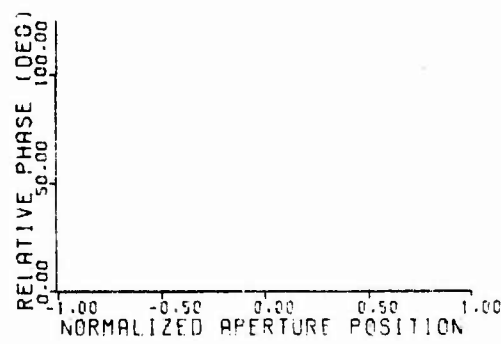
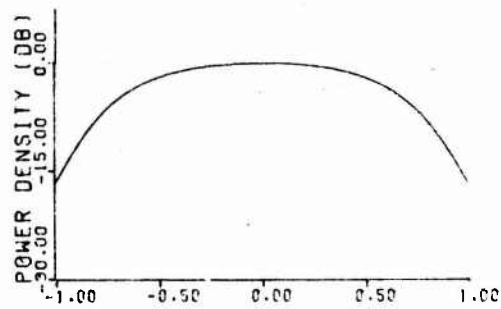


Figure 3-2. Folded geodesic Luneberg lens aperture distribution, and computed far-field pattern.



FIRST SIDELOBE - -20.93 DB
 GAIN FACTOR - 0.9730
 BEAMWIDTH - 63.46 DEGREES

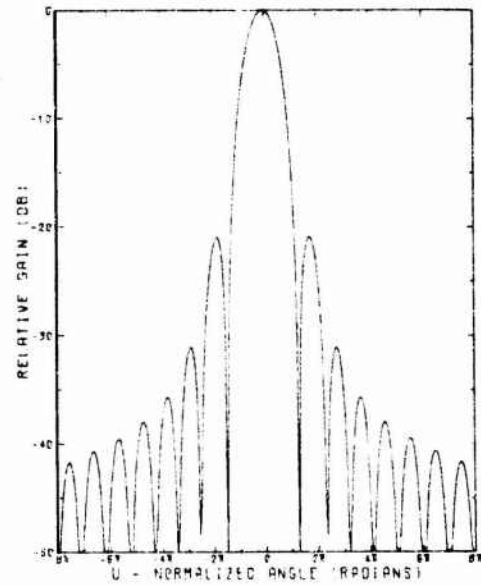
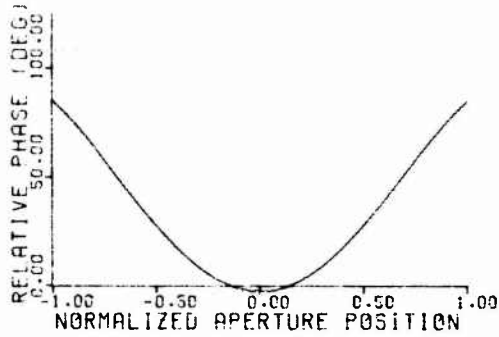
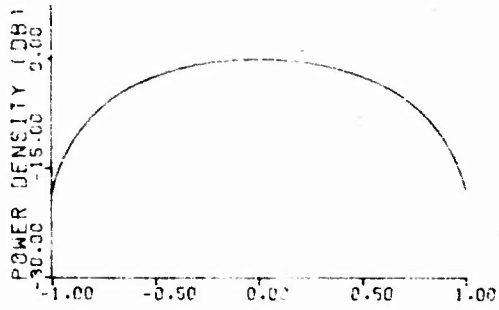


Figure 3-3. Folded geodesic Luneberg lens aperture distribution with no phase variation, and computed far-field pattern.



FIRST SIDELobe - -25.13 DB
 GAIN FACTOR - 0.7375
 BEAMWIDTH - 67.66 DEGREES

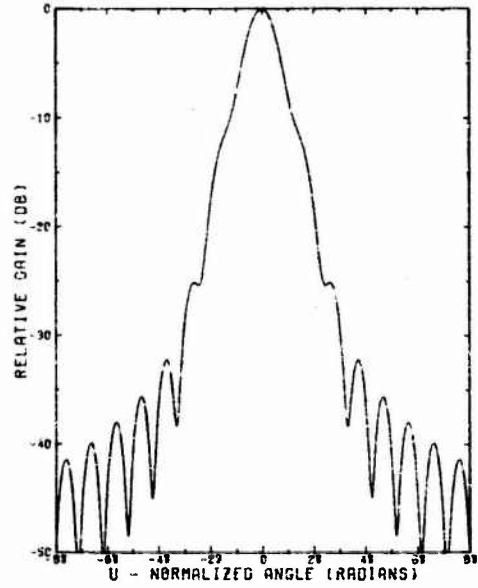
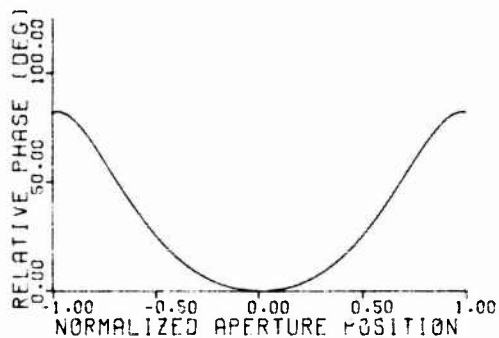
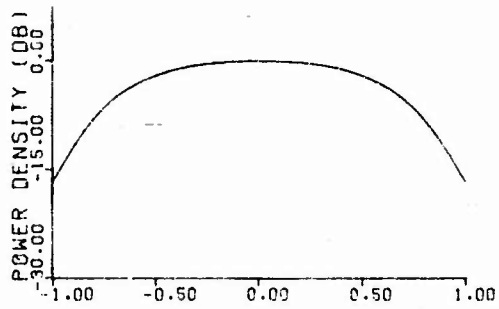


Figure 3-4. Folded lens aperture distribution fitted to a fourth-order polynomial, and computed far-field pattern.



FIRST SIDELobe - -32.32 DB
 GAIN FACTOR - 0.7383
 BEAMWIDTH - 68.20 DEGREES

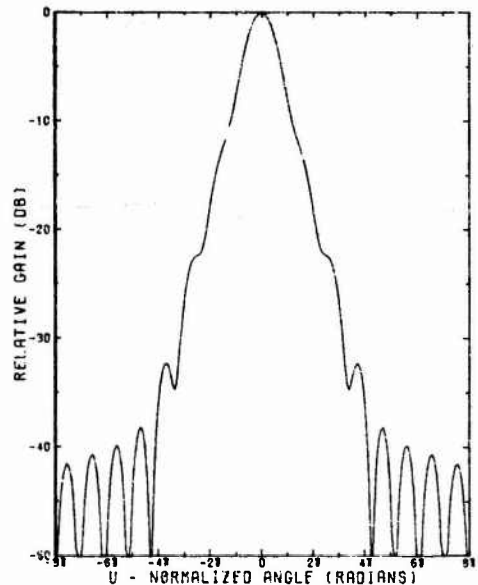


Figure 3-5. Folded lens aperture distribution fitted to a sixth-order polynomial, and computed far-field pattern.

$$\begin{aligned} \phi(X) &= A(1 + \cos \pi X) & (3-5) \\ -1 &\leq X \leq 1 \\ 5^\circ &\leq A \leq 50^\circ \end{aligned}$$

was investigated to determine the effect on the sidelobe level of this type of distribution. A phase distribution with a maximum variation of eighty degrees resulted in the computed antenna pattern and distributions shown in Figure 3-6. The first sidelobe level has been lowered to -38 dB, although the gain factor and beamwidth are less desirable than those produced by the phase distributions shown in Figures 3-2 and 3-5. However, it was encouraging to find that the same amplitude distribution could be used to achieve a reduction in sidelobe level of almost 100 percent by changing the phase distribution alone.

3. GAUSSIAN PHASE DISTRIBUTION

The shape of the cosine phase distribution suggested the possibility of using a Gaussian phase distribution to achieve similar results. Since a Gaussian distribution is a function of two variables, the effective width of the phase distribution could be varied along with the height. A phase distribution of the form

$$\begin{aligned} \phi(X) &= A\left(1 - e^{-\frac{(CX)^2}{2}}\right) & (3-6) \\ -1 &\leq X \leq 1 \\ 10^\circ &\leq A \leq 100^\circ \\ 1.75 &\leq C \leq 2.5 \end{aligned}$$

was investigated; a phase distribution with a maximum variation of approximately fifty degrees and standard deviation of 0.4 resulted in the computed antenna pattern shown in Figure 3-7. The first sidelobe level is -34 dB, and the gain factor is 0.82. This inverted Gaussian phase distribution resulted in the best combination of sidelobe level, gain factor, and beamwidth for the folded lens

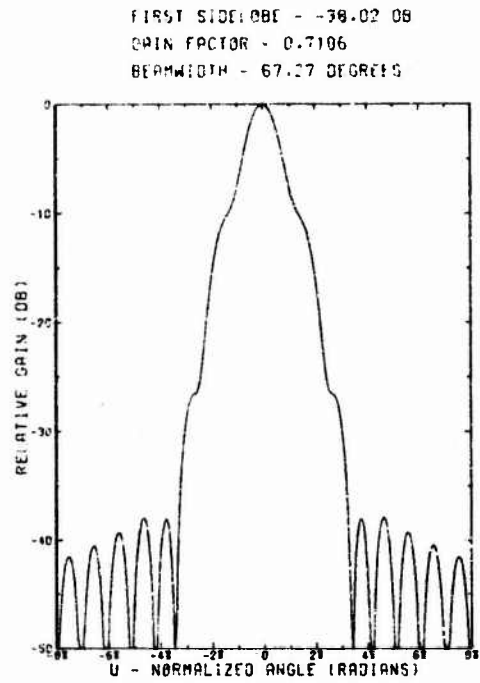
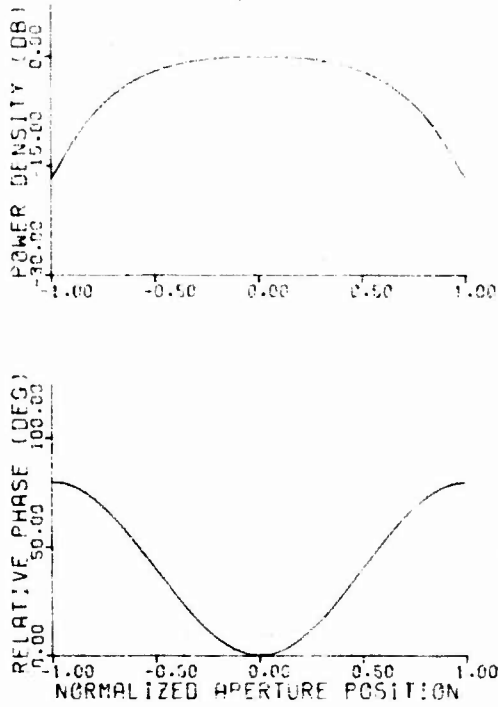


Figure 3-6. Folded lens aperture distribution with a phase distribution of the form $A(1 + \cos \pi X)$, and computed far-field pattern.

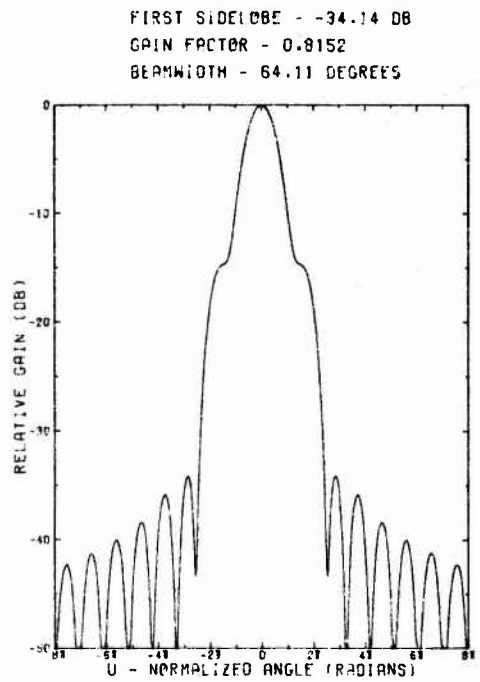
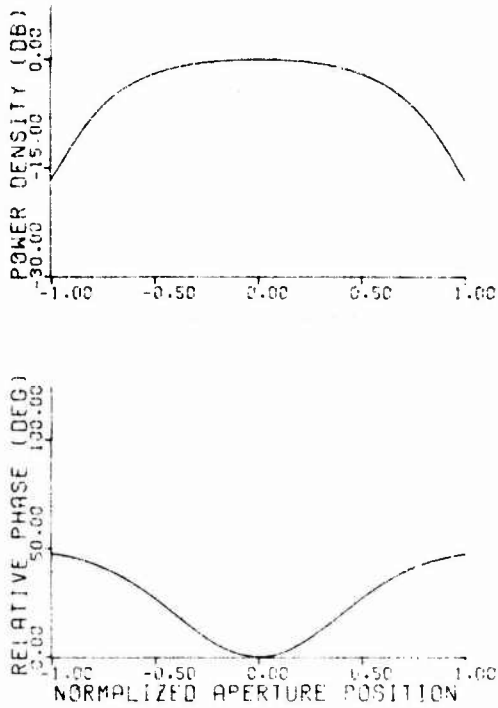


Figure 3-7. Folded lens aperture distribution with a Gaussian phase distribution, and computed far-field antenna pattern.

amplitude distribution. The results of the theoretical investigation of phase distributions for the folded lens amplitude distribution are summarized in Table 3-1.

As shown in the table, this Gaussian phase distribution results in a 13 dB improvement in first sidelobe level over that obtained with no phase variation, with a reduction in gain factor of less than six percent. The 3 dB beamwidth increases by less than one percent; the first significant beam broadening occurs at a level of approximately -14 dB.

Of course, it is possible to achieve a theoretical first sidelobe level of -34 dB using amplitude tapering only. However, using a cosine-squared amplitude taper and no phase taper results in a first sidelobe level of -32 dB and a gain factor of only 0.67, or 18 percent less gain than is possible using the folded lens amplitude taper and a Gaussian phase taper.

4. PHASE TAPERING APPLIED TO MODIFIED TAYLOR AMPLITUDE DISTRIBUTIONS

The improvement in sidelobe level possible with phase tapering described in the previous section was for only one amplitude distribution, the measured folded geodesic lens distribution. To be useful, phase tapering has to work for many different amplitude tapers (and therefore different sidelobe levels). The modified Taylor distribution was chosen as the amplitude distribution to be used in subsequent tests of phase tapering techniques. The modified Taylor distribution is an ideal choice for testing because it is considered a practical approximation to the "optimum" aperture distribution for continuous sources, and can generate a wide range of sidelobe levels.^{12,13}

TABLE 3-1

THEORETICAL PERFORMANCE OF SEVERAL PHASE TAPERS
FOR THE FOLDED LENS AMPLITUDE DISTRIBUTION

Phase Distribution	First Sidelobe Level (dB)	Gain Factor	3-dB Beamwidth (degrees)	10-dB Beamwidth (degrees)
Constant	-21	0.87	63.5 λ/a	110 λ/a
Measured	-32	0.74	68.2 λ/a	135 λ/a
Curve Fitting	-32	0.74	68.2 λ/a	135 λ/a
Cosine	-38	0.72	67.3 λ/a	155 λ/a
Gaussian	-34	0.82	64.1 λ/a	115 λ/a
Cosine-squared amplitude distribution, Constant Phase	-32	0.67	83.2 λ/a	165 λ/a

(a) Modified Taylor Distribution

The modified Taylor amplitude distribution is given by

$$\phi(X) = I_0(\pi B \sqrt{1 - X^2}) \quad \begin{array}{l} |X| \leq 1 \\ |X| < 1 \end{array} \quad (3-7)$$

where

X is the normalized distance along the source,

I_0 is the modified Bessel function of the first kind of order one, and

B is a constant to be specified.

The far-field pattern and first sidelobe level can be determined exactly; the sidelobe level is

$$R = 4.603 \frac{\sinh(\pi B)}{\pi B} \quad (3-8)$$

where R is the voltage ratio of the main beam to the first sidelobe.

Equation 3-8 can be used to determine the constant B for any desired sidelobe level. Six different values of B were used to generate patterns with first sidelobe ratios of approximately 15, 20, 25, 30, 35, and 40 dB, with no phase variation. For each amplitude taper, phase distributions of the form

$$\phi(X) = A \left(1 - e^{-\frac{(CX)^2}{2}} \right) \quad \begin{array}{l} -1 \leq X \leq 1 \\ 20^\circ \leq A \leq 100^\circ \\ 1.75 \leq C \leq 2.5 \end{array} \quad (3-9)$$

were investigated to determine the effect on sidelobe level, gain factor, and beamwidth. Changes in A correspond to variations in end point phase, or height, while changes in C correspond to changes in the standard deviation, or width,

of the Gaussian phase distribution. The range of values for A and C given above are the ones that generated the most desirable far-field patterns although many others were tried.

Figure 3-8 shows the aperture distribution and computed far-field pattern for a modified Taylor distribution with a first sidelobe level of approximately -30 dB and gain factor of 0.81. Figure 3-9 shows the aperture distribution and far-field for the same amplitude taper but with a Gaussian phase distribution ($A = 30^\circ$, $C = 2$). The first sidelobe level is -36 dB, and the gain factor is 0.80. However, merely lowering the sidelobe level is not significant. Figure 3-10 shows the real justification for using phase tapering. This figure shows the aperture distribution and far-field pattern for a modified Taylor amplitude distribution with a first sidelobe level of -35 dB and gain factor of 0.75. Thus, by using both amplitude and phase tapering, it is possible to achieve a higher gain factor for a given sidelobe level than is possible using the "optimum" amplitude taper alone. Note also that the 3-dB beamwidth is smaller for the phase tapering case, at a given sidelobe level, than for amplitude tapering alone. The first significant broadening of the beam, using phase tapering, occurs at a level of -20 dB.

Figure 3-11 shows the aperture distribution and far-field pattern for the case where the amplitude taper of Figure 3-10 is combined with a Gaussian phase distribution ($A = 20^\circ$, $C = 2$) to produce a pattern with a sidelobe level of -41.3 dB and a gain factor of 0.75. Table 3-2 summarizes the results achieved with phase and amplitude tapering and compares them to the results possible using amplitude tapering alone. In each case, using phase tapering results in a higher gain factor and smaller 3-dB beamwidth for the same sidelobe level.

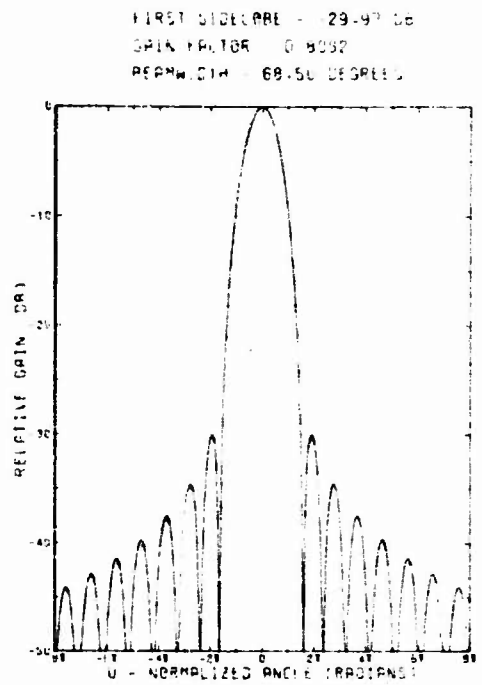
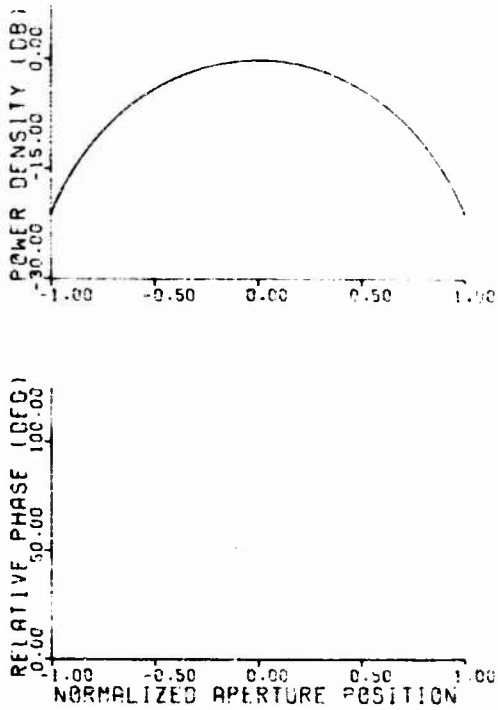


Figure 3-8. Modified Taylor amplitude distribution and computed far-field pattern, with a sidelobe level of -30 dB.

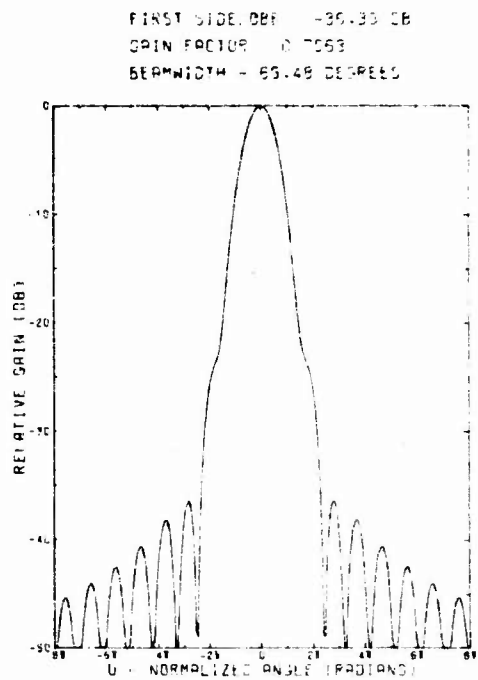
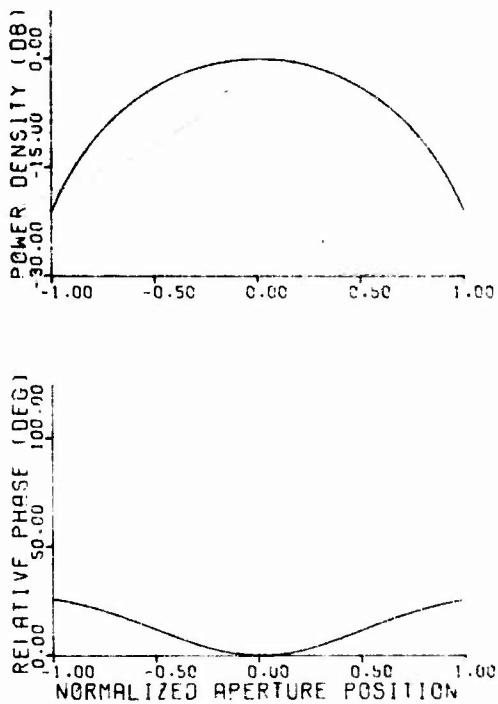


Figure 3-9. Aperture distribution and computed far-field pattern for the amplitude distribution of Figure 3-8, but with a Gaussian phase distribution.

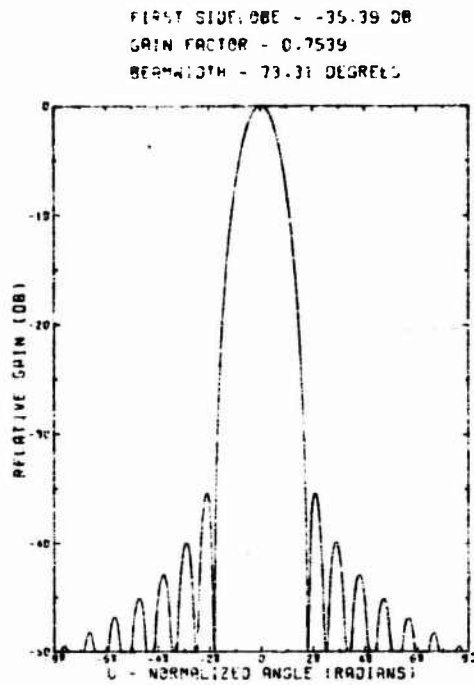
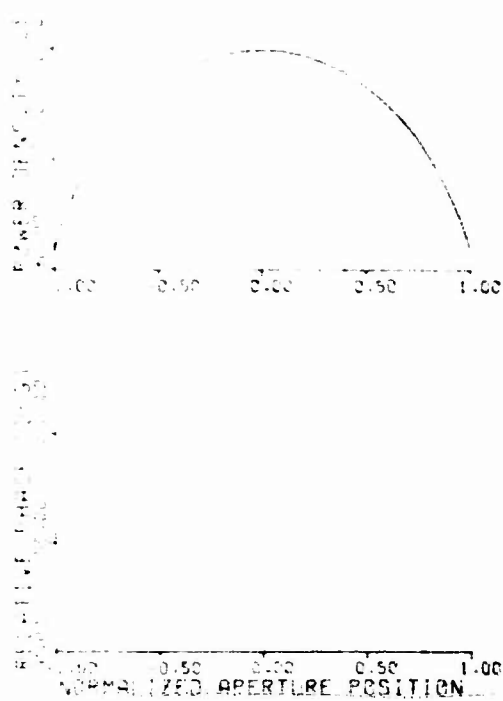


Figure 3-10. Modified Taylor amplitude distribution and computed far-field pattern, with a sidelobe level of -35 dB.

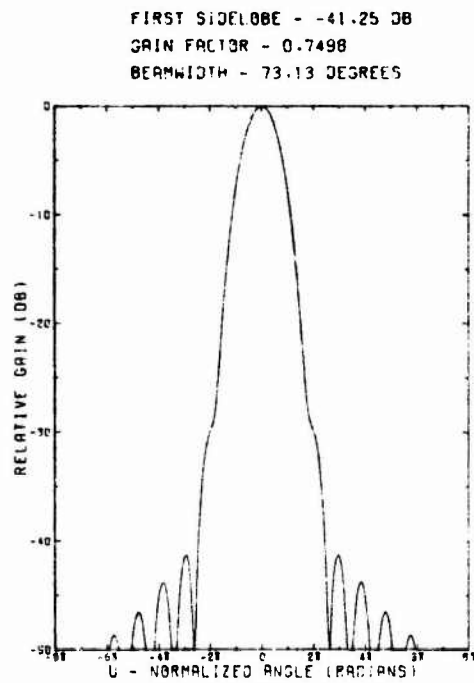
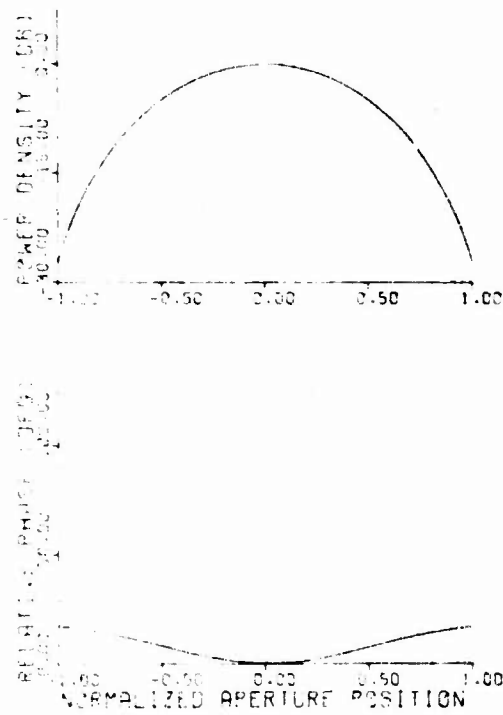


Figure 3-11. Aperture distribution and computed far-field pattern for the amplitude distribution of Figure 3-10, but with a Gaussian phase distribution.

TABLE 3-2

**THEORETICAL PERFORMANCE OF MODIFIED TAYLOR AMPLITUDE
TAPERING AND GAUSSIAN PHASE TAPERING**

Amplitude Taper (dB)	Phase Distribution	First Sidelobe Level (dB)	Gain Factor	3-dB Beamwidth (degrees)
9.0	Constant	-19.9	.940	58.4
9.0	Gaussian Taper	-25.4	.870	58.9
15.2	Constant	-24.9	.870	63.7
15.2	Gaussian Taper	-30.6	.857	63.5
21.1	Constant	-30.0	.808	68.5
21.1	Gaussian Taper	-36.4	.796	68.5
27.2	Constant	-35.4	.754	73.3
27.2	Gaussian Taper	-41.3	.750	73.1
32.6	Constant	-40.2	.713	77.4
32.6	Gaussian Taper	-45.6	.709	77.2

(b) End Point Phase Requirements

The maximum phase variation required to achieve an improvement in sidelobe level depends on the amplitude taper. In general, as the amplitude taper increases, the end point phase required to merge the first sidelobe with the main beam decreases. As shown in Figure 3-11, an end point phase of approximately twenty degrees is sufficient to improve the sidelobe level of a modified Taylor amplitude distribution with a nominal sidelobe level of -35 dB. However, if the same phase variation is applied to a modified Taylor amplitude distribution with a nominal sidelobe level of -25 dB, the first sidelobe does not merge with the main beam (Figure 3-12). Increasing the end point phase to forty degrees (with the same amplitude distribution) does result in the improved sidelobe level shown in Figure 3-13. Similarly, a forty degree phase variation does not merge the first sidelobe with the main beam if the amplitude distribution has a nominal sidelobe level of -20 dB (Figure 3-14), but a sixty degree phase variation does achieve the improved pattern shown in Figure 3-15.

5. THE OPTIMUM LINE SOURCE DISTRIBUTION

(a) General Line Source Optimization

The preceding demonstration of sidelobe reduction by phase tapering suggests an optimum distribution may be found in which both the amplitude and phase are system variables. Work is now underway to apply non-linear optimization theory to the problem of line source synthesis. Optimization theory has long been used in control and communication system synthesis and recently Sandrin and Glatt¹⁴ have applied it to the synthesis of phased arrays.

Basically, the optimization process locates the maximum or minimum of a real function of the system variables by the method of steepest descent. Let

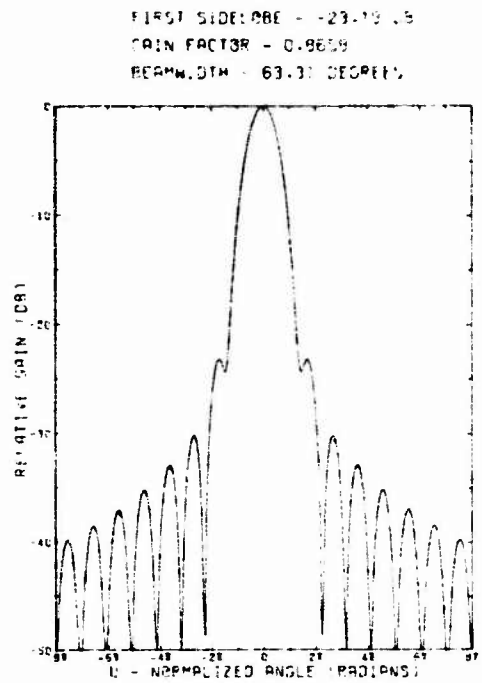
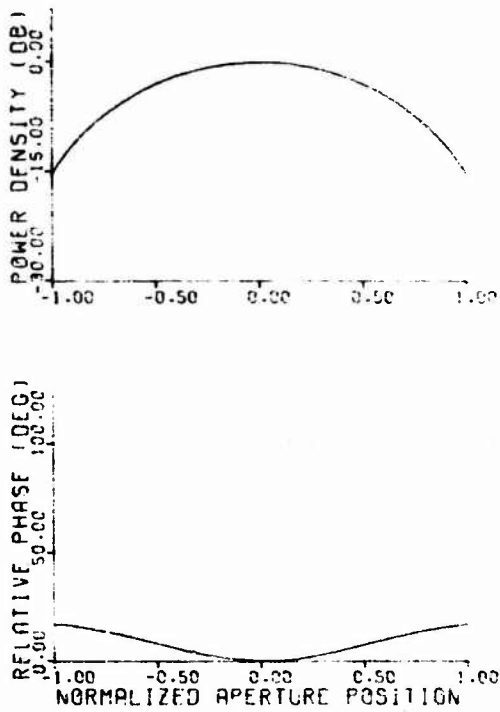


Figure 3-12. Modified Taylor amplitude distribution with a nominal sidelobe level of -25 dB with a twenty degree end point Gaussian phase distribution, and computed far-field pattern.

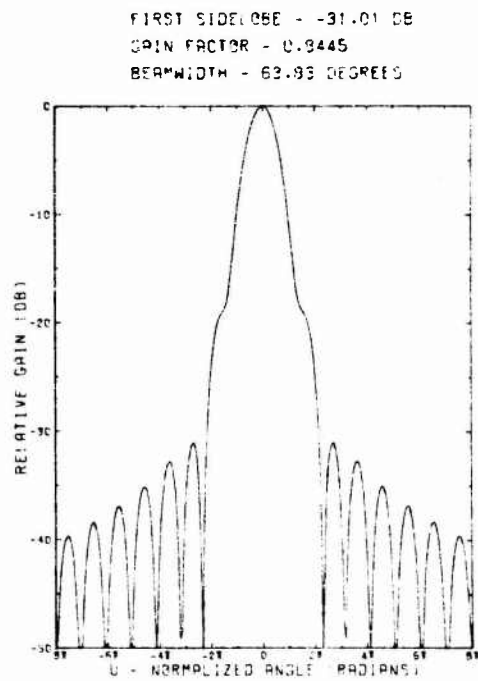
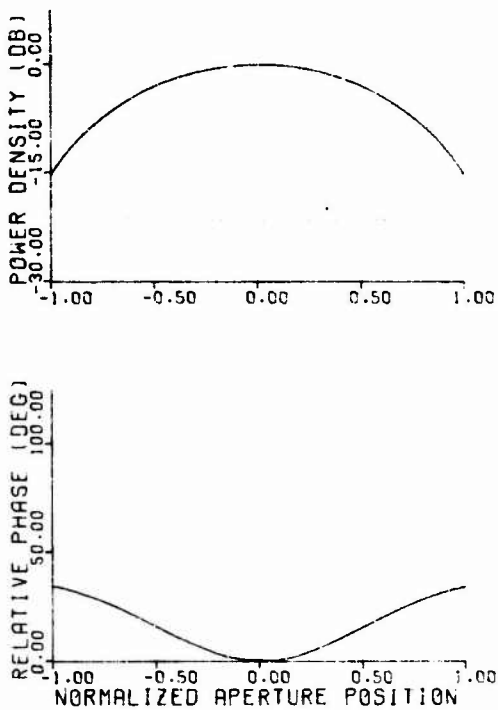


Figure 3-13. Modified Taylor amplitude distribution with a nominal sidelobe level of -25 dB with a forty degree end point Gaussian phase distribution, and computed far-field pattern.

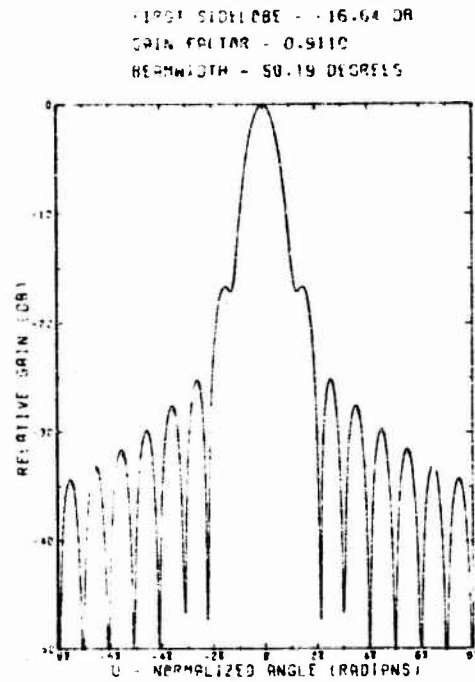
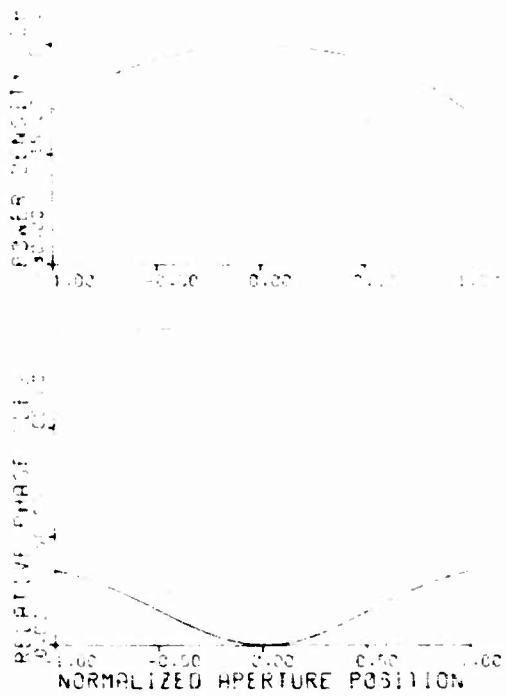


Figure 3-14. Modified Taylor amplitude distribution with a nominal side-lobe level of -20 dB with a forty degree end point Gaussian phase distribution, and computed far-field pattern.

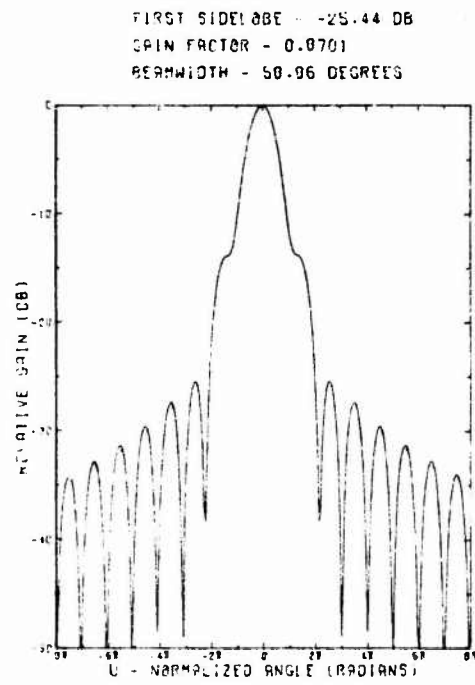
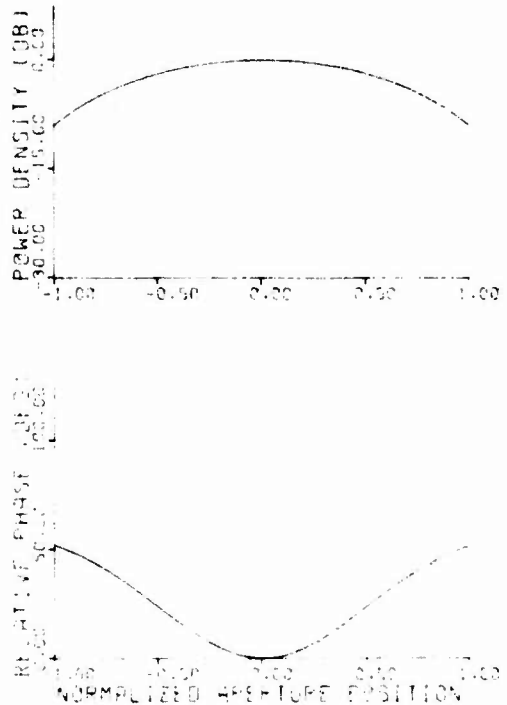


Figure 3-15. Modified Taylor amplitude distribution with a nominal side-lobe level of -20 dB with a sixty degree end point Gaussian phase distribution, and computed far-field pattern.

$S(X)$ be a complex line source distribution. $S(X)$ may be represented by complex samples equally spaced at intervals less than $\lambda/2$. In this work $S(X)$ is represented by $N + 1$ samples spaced at $\lambda/4$ intervals as

$$S(X) = \sum_{i=-\frac{N}{2}}^{\frac{N}{2}} S(\lambda/4 i) \quad (3-10)$$

$S(X)$ may also be written in terms of its amplitude and phase distributions as

$$S(X) = A(X)e^{jP(X)} \quad (3-11)$$

In line source synthesis the system variables are the amplitude and phase of the line source at each of the $N + 1$ sample points. As pointed out later the variables are not independent and constraints must be placed on their values.

Let f_j be a function of the system variables. The sequential process for finding the minimum of f_j may be written as

$$f_j(S_{n+1}(X)) = f_j(S_n(X)) + d \nabla f_j(S_n(X)) \quad (3-12)$$

where

$S_n(X)$ is the n^{th} state of the source distribution,

$\nabla f_j(S_n(X))$ is the gradient of f_j with respect to the system variables, $S(X)$, evaluated at the n^{th} state,

d is the step size between the $n + 1^{\text{th}}$ and the n^{th} value of f_j , and

$$S_{n+1}(X) = S_n(X) + \nabla f_j(S_n(X))$$

The iterative procedure is repeated until the gradient becomes zero indicating a local minimum has been reached. Several tests are available to determine

if the local minimum is the global minimum. One such test is to repeat the minimization procedure several times starting from random initial source distribution states.

Constraints may be added to the optimization procedure by forming a new system function $g_j(S(X))$ as follows

$$\begin{aligned}
 g_j(S_n(X)) = & f_j(S_n(X)) + \sum_{m=1}^{M_1} \frac{r_m}{C_m - f_m(S_n(X))} \\
 & + \sum_{m=M_1+1}^{M_2} \frac{r_m}{f_m(S_n(X)) - C_m} \\
 & + \sum_{m=M_2+1}^{M_3} r_m (C_m - f_m(S_n(X)))^2
 \end{aligned} \tag{3-13}$$

where

$f_j(S_n(X))$ is the system function to be minimized evaluated at the n^{th} state of the source variables,

$f_m(S_n(X))$ for $1 \leq m \leq M_1$ is a real system function to be constrained less than the constant C_m ,

$f_m(S_n(X))$ for $M_1 + 1 \leq m \leq M_2$ is a real system function to be constrained greater than the constant C_m ,

$f_m(S_n(X))$ for $M_2 + 1 \leq m \leq M_3$ is a real system function to be constrained to be equal to the constant C_m , and

r_m is a real parameter which is decreased in magnitude during the optimization process.

The minimization of g_j is carried out as described for f_j for fixed values of

the r_n 's. When a minimum is reached, the r_m 's are decreased and a new minimum is found. The process is repeated until the magnitude of all the r_m 's are vanishingly small. The reduction in the r_m values allows the constrained functions to approach their constraint C_m 's if necessary. Thus a system function can be optimized or constrained.

The definitions of several system functions which are important and useful in line source synthesis follow. The system functions are divided into two classes. The first class includes those system functions which are dependent on the far field pattern of the source distribution. The second class of system functions include those which are direct functions of the source distribution $S(X)$.

The far field is related to the system variables through a Fourier transform and can be expressed as¹⁵

$$F(S_n(X), \varphi) = \frac{j2\pi}{\lambda} e^{jk \cdot r} \sin \varphi \int_{-\infty}^{\infty} S_n(X) e^{j \frac{2\pi}{\lambda} X \cos \varphi} dX \quad (3-14)$$

where

$F(S_n(X), \varphi)$ is the far field of the n^{th} state of the source distribution,

k is the free space wavenumber, and

r and φ are as shown in Figure 3-16.

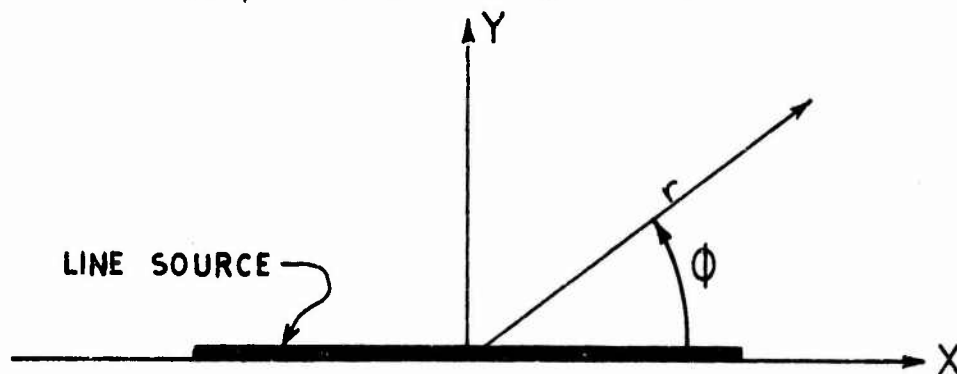


Figure 3-16. Line source coordinate system

The integral in the above equation is recognized as the Fourier transform integral. Computationally the Fast Fourier Transform algorithm is used to greatly increase the speed of computation.

The first class of system functions are as follows:

1. Directivity at an angle $\varphi = \varphi_c$.

$$f_1(S(X)) = \frac{F^2(S(X), \varphi_c)}{\int_0^\pi F^2(S(X), \varphi) d\varphi} \quad (3-15)$$

2. RMS sidelobe level.

$$f_2(S(X)) = \sqrt{\frac{1}{\pi - (\varphi_2 - \varphi_1)} \left[\int_0^{\varphi_1} F^2(S(X), \varphi) d\varphi + \int_{\varphi_2}^\pi F^2(S(X), \varphi) d\varphi \right]} \quad (3-16)$$

where φ_2 and φ_1 define the angular limits of the mainbeam.

3. Maximum sidelobe level.

$$f_3(S(X)) = \frac{\text{MSLL}}{\pi - (\varphi_2 - \varphi_1)} \left[\int_0^{\varphi_1} \frac{1}{\text{MSLL} - F^2(S(X), \varphi)} d\varphi \right. \\ \left. + \int_{\varphi_2}^\pi \frac{1}{\text{MSLL} - F^2(S(X), \varphi)} d\varphi \right] \quad (3-17)$$

where MSLL is the specified maximum sidelobe level,

φ_2 and φ_1 define the angular limits of the mainbeam, and The initial value of MSLL should be set greater than all sidelobes of $F^2(S(X), \varphi)$.

4. Beamwidth of mainbeam at a specified level below peak.

$$f_4 (S(X)) = \varphi_2 - \varphi_1 \quad (3-18)$$

To determine the beamwidth the angle of maximum radiation is first located as φ_c . φ is then increased until $F^2(S(X), \varphi)$ drops to the specified level at $\varphi = \varphi_2$. φ is returned to φ_c and then decreased to locate φ_1 .

5. Super gain ratio.

Let $k_x = (2\pi/\lambda) \cos \varphi$ in the Fourier transform integral of Equation (3-14). The integral then becomes

$$\int_{-\infty}^{\infty} S(X) e^{j \frac{2\pi}{\lambda} \cos \varphi X} dX = \int_{-\infty}^{\infty} S(X) e^{j k_x X} dX \quad (3-19)$$

$$-2\pi/\lambda \leq k_x \leq 2\pi/\lambda$$

which describes the spectrum of the radiation pattern. To obtain the spectrum of the evanescent waves the wavenumber limits must be extended to infinity. The supergain ratio may then be defined as

$$f_5 (S(X)) = \frac{\int_{-\infty}^{\infty} \int_{-\infty}^{\infty} S(X) e^{j k_x X} dX dk_x}{\int_{-2\pi/\lambda}^{2\pi/\lambda} \int_{-\infty}^{\infty} S(X) e^{j k_x X} dX dk_x} \quad (3-20)$$

6. Gain factor or efficiency.

$$f_6 (S(X)) = \frac{f_1 (S(X))}{f_1 (S'(X))} \quad (3-21)$$

where $S'(X)$ is the constant amplitude and phase distribution.

7. Mean square error between the calculated far field power pattern and a desired far-field power pattern.

$$f_7(S(X)) = \int_0^\pi [F_d^2(\varphi) - F^2(S(X), \varphi)]^2 d\varphi \quad (3-22)$$

where F_d^2 is the desired far-field power pattern.

8. Monopulse difference pattern sensitivity ratio.¹⁶

$$f_8(S''(X)) = \frac{\sqrt{3} \int_0^\pi \varphi F^2(S''(X), \varphi) d\varphi}{\left[\int_0^\pi F^2(S''(X), \varphi) d\varphi \right]^{1/2}} \quad (3-23)$$

where $S''(X)$ is the source distribution associated with the difference pattern of a monopulse antenna.

9. Signal-to-noise ratio.

$$f_9(S(X)) = \frac{V_{\varphi_s} F^2(S(X), \varphi_s)}{\int_0^\pi N^2(\varphi) F^2(S(X), \varphi) d\varphi} \quad (3-24)$$

where $N^2(\varphi)$ is the angular distribution of noise power and V_{φ_s} is the power of the plane wave signal at $\varphi = \varphi_s$.

The second class of system functions includes the following:

1. Size of the line source.

$$f_{10}(S(X)) = N \lambda / 4 \quad (3-25)$$

2. Phase variation limited to the interval $-P_{MAX} \leq P(X) \leq P_{MAX}$.

$$f_{11}(S(X)) = \frac{1}{(P_{MAX} - P(X)) (P_{MAX} + P(X))} \quad (3-26)$$

where the initial state of $P(X)$ must lie within the restricted region.

3. Amplitude taper of the source.

$$f_{12}(S(X)) = \frac{1}{\sum_{i=-N/2}^{N/2} A(\lambda/4 i)} \sum_{i=-N/2}^{N/2} \frac{A(\lambda/4 i)}{(N/2 + i)(N/2 - i) + L} \quad (3-27)$$

where L is a constant weighting factor.

4. Smoothness of the amplitude distribution.

$$f_{13}(S(X)) = \frac{1}{N+2} \sum_{i=-N/2}^{N/2+1} (A(\lambda/4(i-1)) - A(\lambda/4 i))^2 \quad (3-28)$$

where $A(\lambda/4(-N/2-1)) = A(\lambda/4(N/2+1)) = 0$.

5. Smoothness of the phase distribution.

$$f_{14}(S(X)) = \frac{1}{N} \sum_{i=-N/2+1}^{N/2} (P(\lambda/4(i-1)) - P(\lambda/4 i))^2 \quad (3-29)$$

6. Error between an amplitude distribution and a naturally occurring amplitude distribution.

$$f_{15}(S(X)) = \frac{1}{N} \sum_{i=-N/2}^{N/2} (A_n(\lambda/4 i) - A(\lambda/4 i))^2 \quad (3-30)$$

where $A_n(X)$ is the naturally occurring amplitude distribution.

7. Error between a phase distribution and a naturally occurring phase distribution.

$$f_{16}(S(X)) = \frac{1}{N} \sum_{i=-N/2}^{N/2} (P_n(\lambda/4 i) - P(\lambda/4 i))^2 \quad (3-31)$$

where $P_n(X)$ is the naturally occurring phase distribution.

(b) Optimization of a Monopulse Line Source Distribution

An approach to the synthesis of optimum monopulse line source distributions is outlined below. In conventional amplitude monopulse systems, two single beam patterns, one with maximum radiation at $\varphi = \pi/2 + \alpha/2$, the other with maximum radiation at $\varphi = \pi/2 - \alpha/2$, are added together to form a sum pattern with maximum at $\varphi = \pi/2$ and subtracted to form a difference pattern. Equivalently two source distributions with maximum radiation at $\varphi = \pi/2$ are phase shifted, one by $k x \cos(\pi/2 + \alpha/2)$ and the other by $k x \cos(\pi/2 - \alpha/2)$, and added together to form a sum distribution and subtracted to form a difference distribution. For ease of analysis it is assumed that the single beams have the same pattern shape, differing only by a constant angular shift α . This is indeed an approximation as the beam patterns are usually distorted in the shift process. However, much insight concerning monopulse source synthesis may be gained from the simpler analysis.

If $S(X)$ is the complex distribution associated with a single beam pattern with maximum radiation in the $\varphi = \pi/2$ direction, then the sum distribution is given by

$$\begin{aligned} S_s(X) &= S(X)e^{j k x \cos(\pi/2 - \alpha/2)} + S(X)e^{j k x \cos(\pi/2 + \alpha/2)} \quad (3-32) \\ &= S(X)e^{j k x \sin(\alpha/2)} + S(X)e^{-j k x \sin(\alpha/2)} \\ &= 2S(X) \cos(k x \sin \alpha/2) \end{aligned}$$

and the difference distribution is given by

$$\begin{aligned}
 S_d(X) &= S(X)e^{j k x \cos(\pi/2-\alpha/2)} - S(X)e^{j k x \cos(\pi/2+\alpha/2)} & (3-33) \\
 &= S(X)e^{j k x \sin(\alpha/2)} - S(X)e^{-j k x \sin(\alpha/2)} \\
 &= j 2 S(X) \sin(k x \sin \alpha/2)
 \end{aligned}$$

Thus, in synthesizing monopulse line source distributions, the complex line source distribution $S(X)$ is the significant system variable.

Two system functions compete for optimization. First, the gain factor of the sum pattern f_6 and second, the monopulse difference pattern sensitivity ratio f_8 . A possible first solution would maximize the monopulse difference pattern sensitivity ratio with the gain of the sum pattern constrained to be greater than some desirable level. A second solution would maximize a new system function formed as a combination of the difference pattern sensitivity ratio and sum pattern gain factor. A combination of these two functions was suggested by Kinsey¹⁶ and is given by

$$f_{17}(S(X)) = (f_6(S_s(X)))^{\frac{1}{2}} f_8(S_d(X)) \quad (3-34)$$

If unrealizable amplitude and phase distributions are synthesized using the optimization process, source constraints (system functions f_{10} through f_{16}) are added to the optimization process to smooth the synthesized solution. Constraining the super gain ratio to values near unity also helps in achieving realizable distributions.

SECTION IV

EXPERIMENTAL WORK

The previous section described theoretical sidelobe levels that are possible when both phase and amplitude shaping of the aperture distribution are used. The purpose of the experimental work was to determine if these results could be achieved with practical antennas. The major portion of the work concentrated on a precision X-band square horn with an eight-inch aperture, although several other antennas were studied in less detail. The experimental work would have been impossible without a convenient means of measuring the aperture amplitude and phase distributions; a brief description of the system used in this work is given below.

1. NEAR-FIELD PROBE

Measurement of the phase and amplitude aperture distributions of antennas can be accomplished at Georgia Tech with a large precision X-Y-Z positioner that is used with a phase and amplitude receiving system to probe the near-field of antennas directly. This unit is located in the basement of the Electronics Division building, and is securely mounted in concrete to minimize the effects of vibrations. The positioner is 14 feet square, but can be positioned to an accuracy of ± 0.025 inches. Over smaller segments of the probed area, accuracy is ± 0.005 inches; see the Appendix. All exposed metal parts and the area behind the probe are covered by panels of microwave absorbing material. The near-field probe and positioner are shown in Figures 4-1 and 4-2. A detailed description of the positioner is given in the Appendix.

Figure 4-3 illustrates a typical measured near-field pattern of a horn antenna. The E-plane normalized aperture distribution and computed far-field

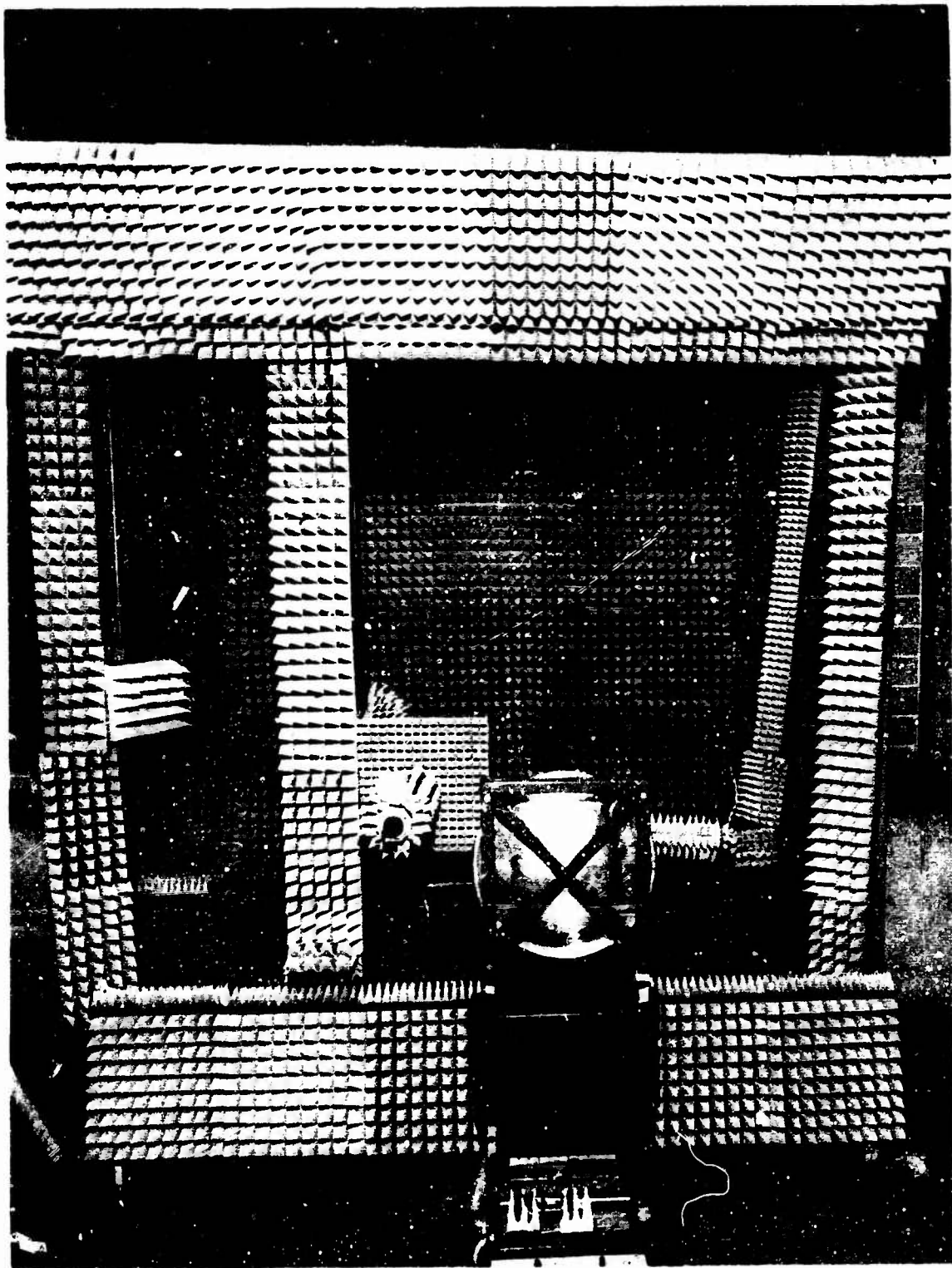


Figure 4-1. Front view of near-field probe and X-Y-Z positioner.

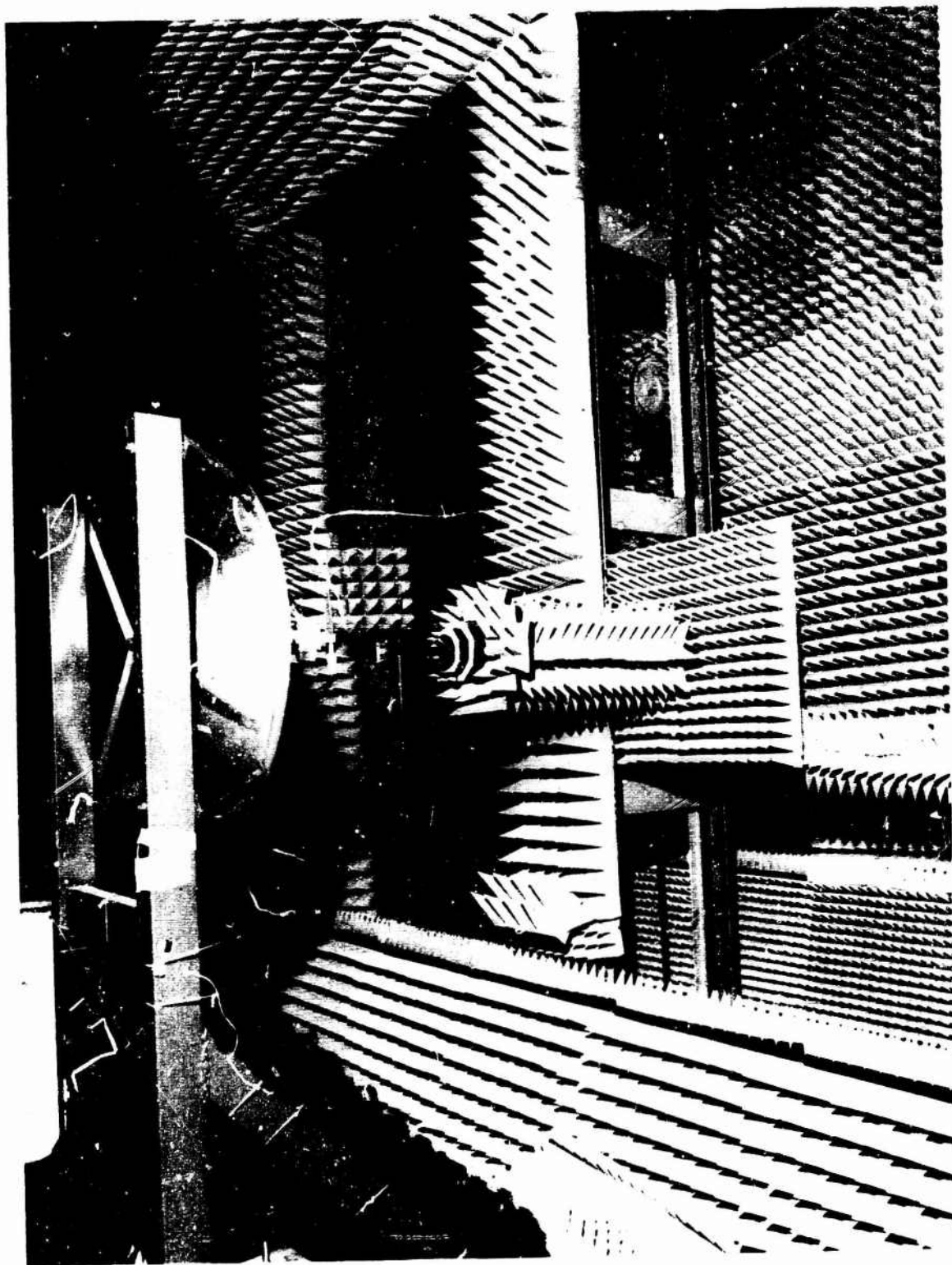


Figure 4-2. Side view of near-field probe and X-Y-Z positioner.

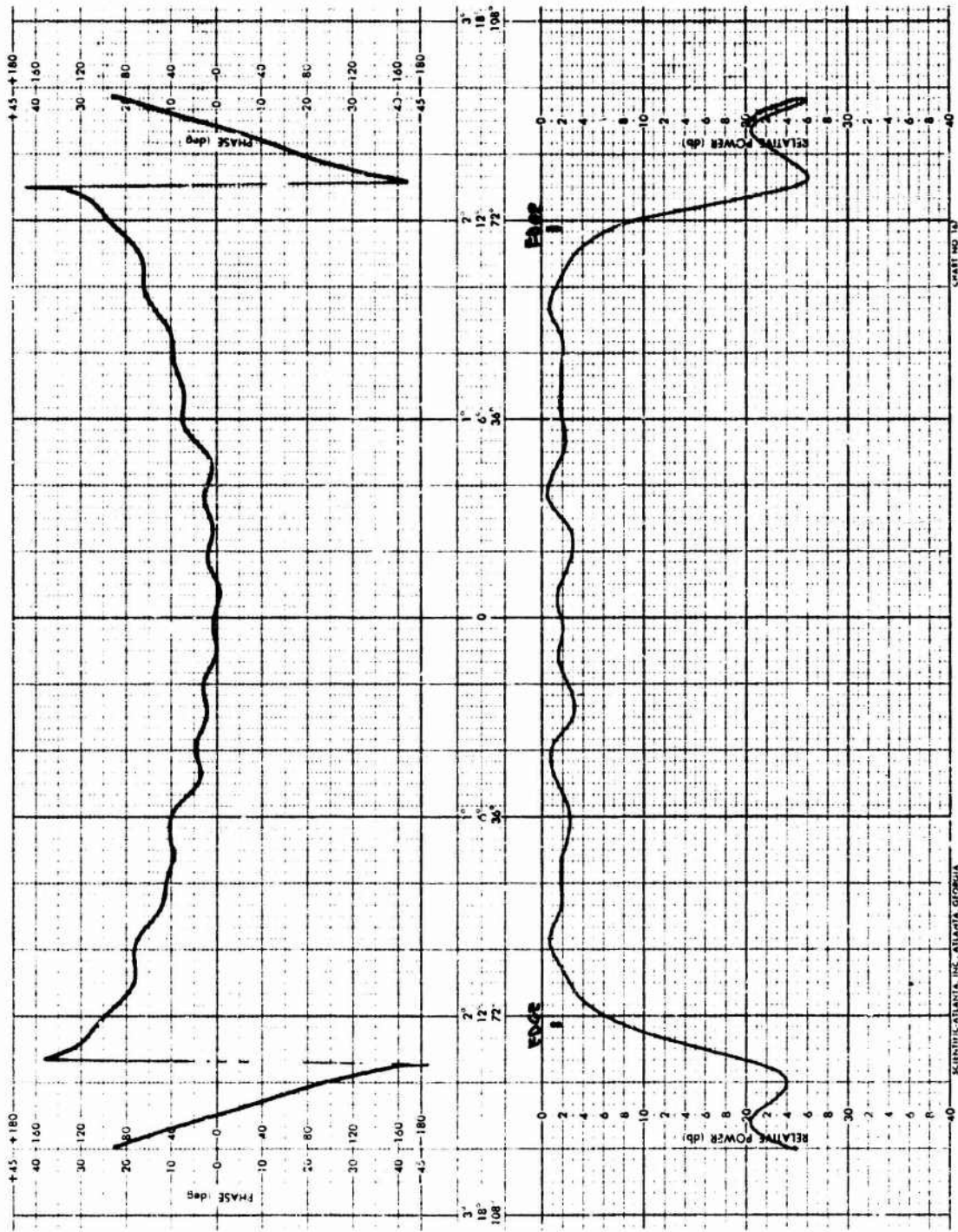


Figure 4-3. Measured near-field pattern of an X-band horn antenna, E-plane cut.

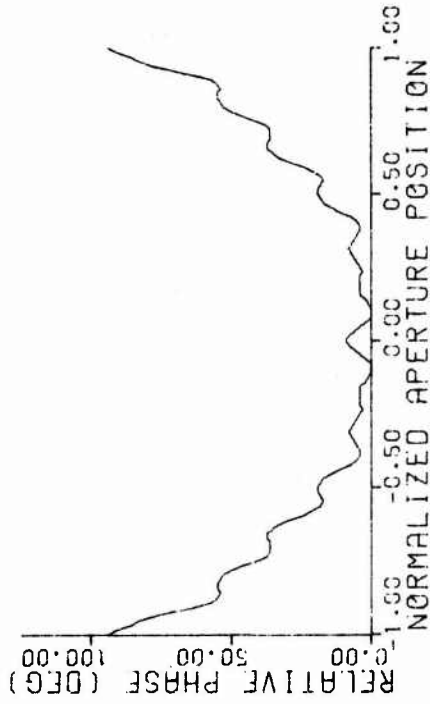
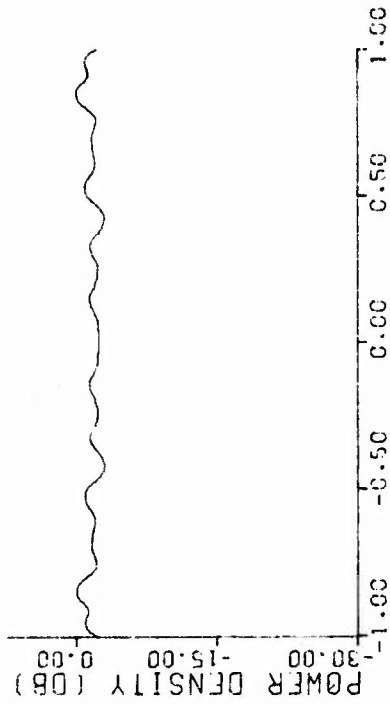
pattern are shown in Figure 4-4; the measured far-field pattern is reproduced in Figure 4-5. The agreement between the predicted and measured far-field patterns is very good, even for the higher-order sidelobes.

2. SQUARE HORN

An existing X-band horn antenna, with an amplitude aperture distribution similar to the distribution of the folded geodesic lens studied in the theoretical work, was chosen as a test horn for the experimental work. The H-plane amplitude and phase distributions were measured using the near-field probe; the aperture distribution and computed far-field pattern are shown in Figure 4-6. Note that the normal phase distribution for this antenna is quadratic, a result typical for conventional flared horns.

The Gaussian phase distributions discussed in Section III were substituted for the measured quadratic phase distribution of the test horn. The most improved far-field pattern was obtained with a Gaussian phase distribution with a standard deviation of 0.5 and an end point phase of approximately fifty degrees; the aperture distribution and computed far-field pattern are shown in Figure 4-7. The substitution of a Gaussian phase distribution for the measured phase distribution resulted in a theoretical improvement in sidelobe level, gain factor, and beamwidth. As shown in Table 4-1, modifying the phase distribution with a dielectric lens should result in an 11-dB reduction in sidelobe level, an improvement of more than eight percent in gain factor, and a six percent narrower 3-dB beamwidth.

A dielectric lens was designed for the test horn to modify the existing phase distribution to approximate the Gaussian phase distribution of Figure 4-7. Due to budget limitations, no attempt was made to match the lens using zoning techniques.



FIRST SIDELOBE - -9.62 DB
 GAIN FACTOR - 0.9137
 BEAMWIDTH - 51.01 DEGREE

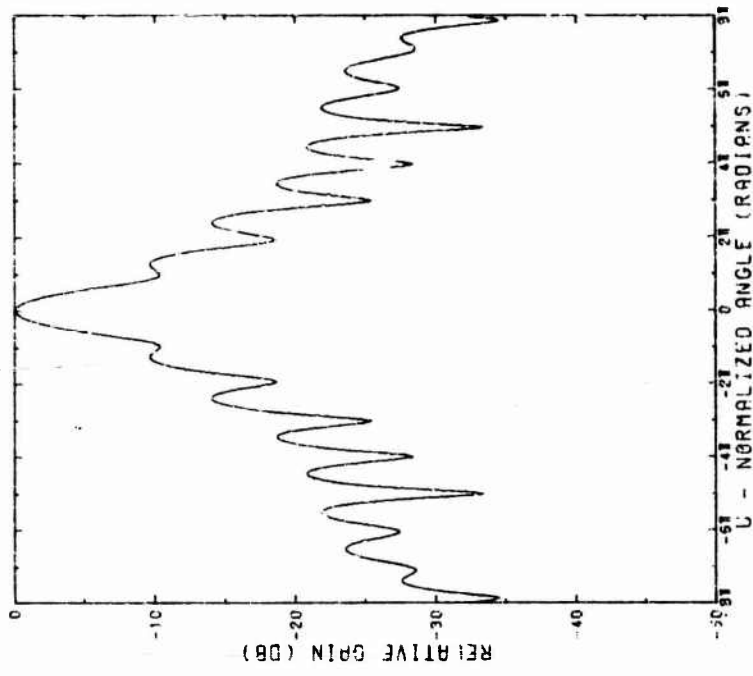


Figure 4-4. Normalized aperture distribution and computed far-field pattern using the near-field pattern shown in Figure 4-3.

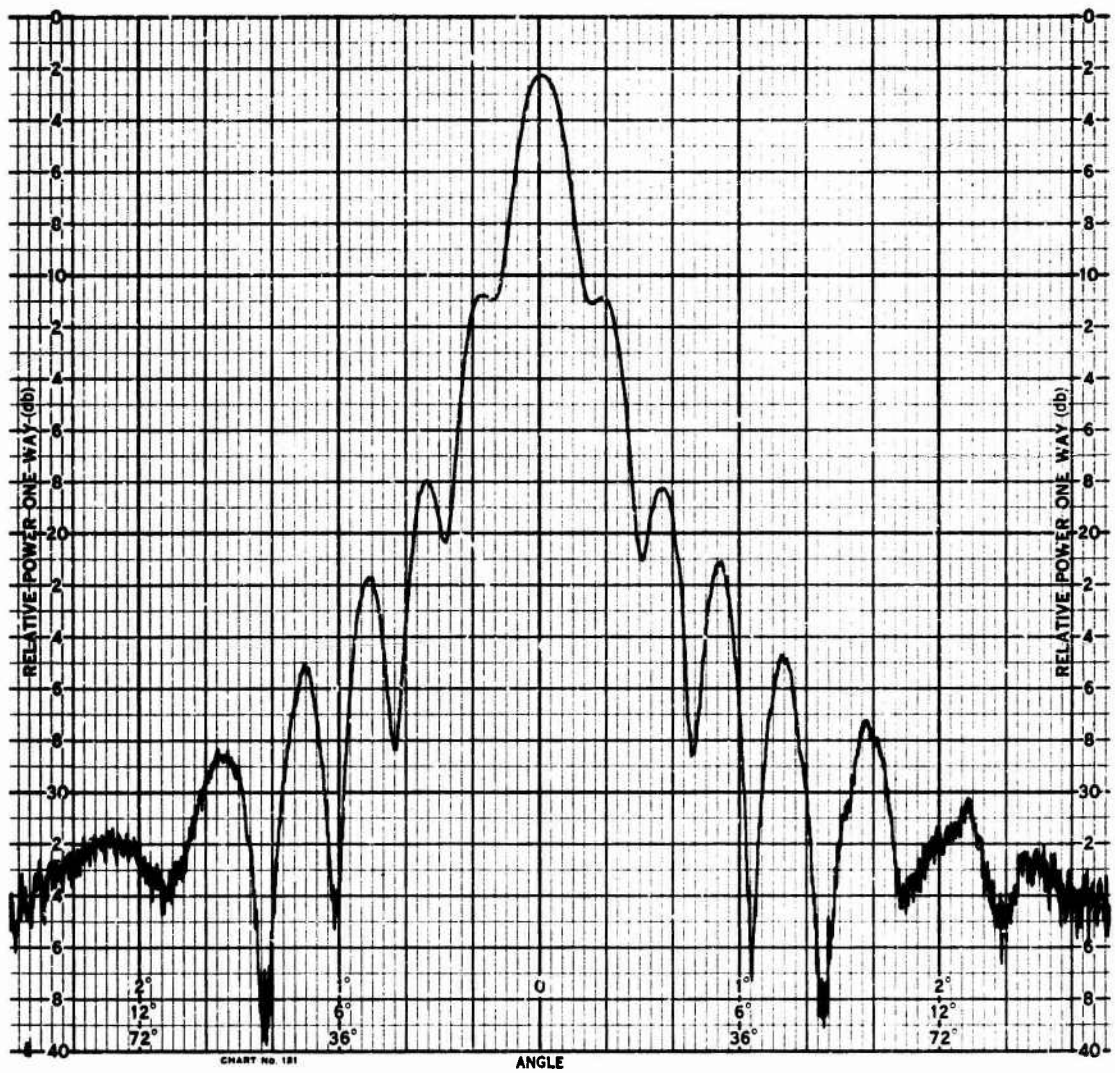
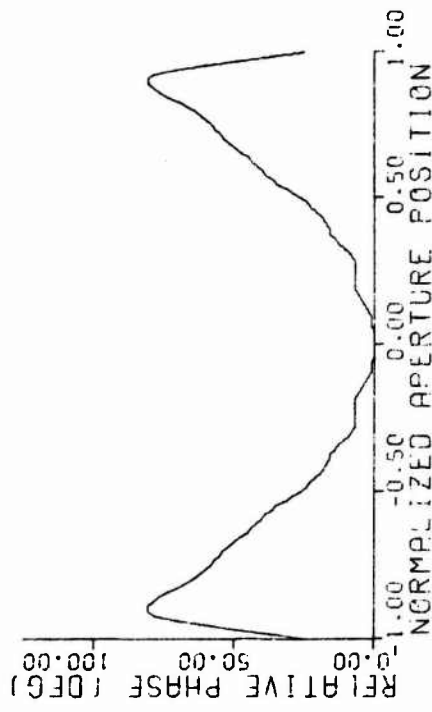
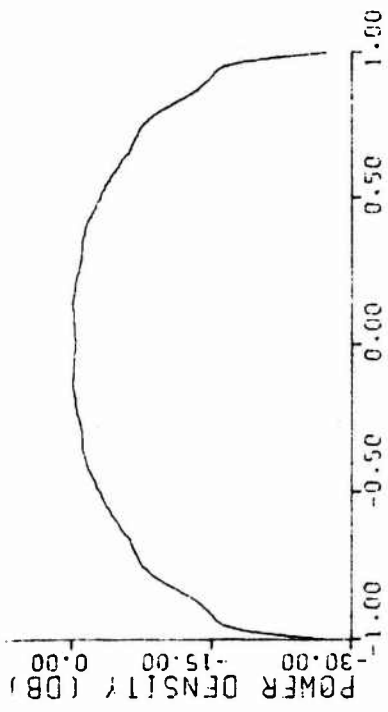


Figure 4-5. Measured far-field pattern of the antenna shown in Figure 4-4.



FIRST SIDELOBE - -24.01 DB
 GAIN FACTOR - 0.7272
 BEAMWIDTH - 70.99 DEGREES

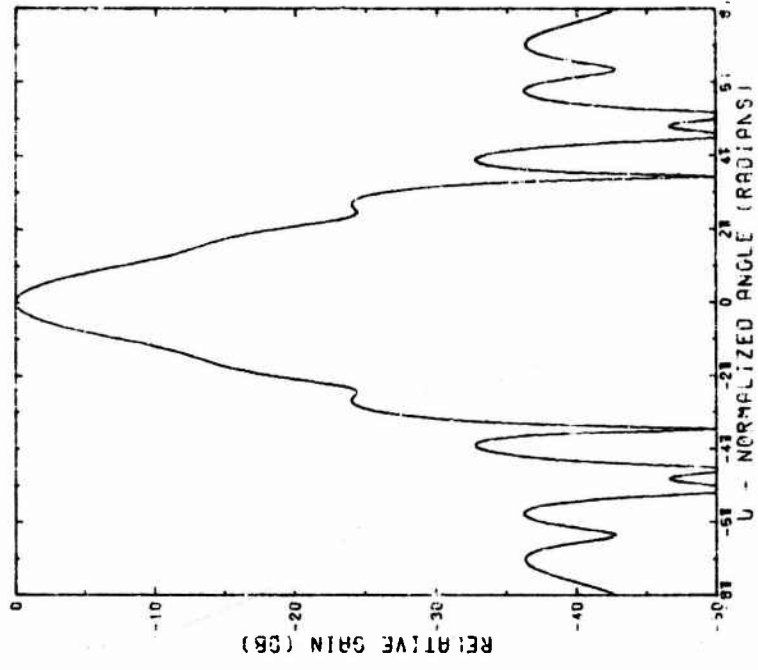


Figure 4-6. Measured aperture distribution and computed far-field pattern of the test horn.

FIRST SIDELOBE : 3.52 DB
 CPIN FACTOR : 0.7984
 BEAMWIDTH : 67.10 DEGREES

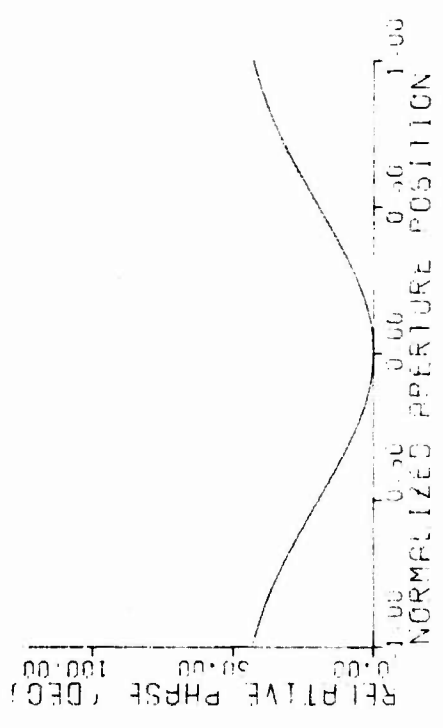
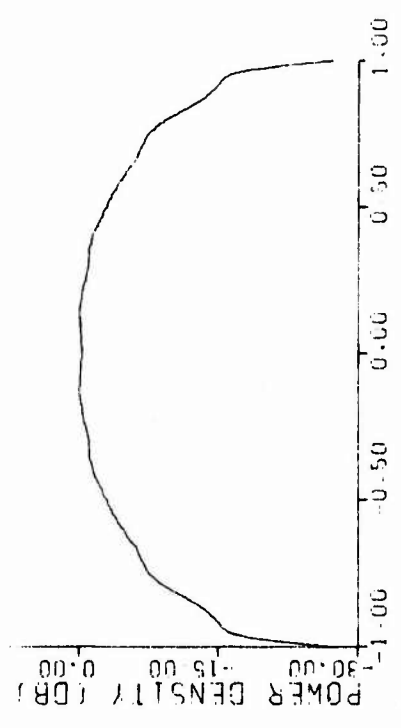
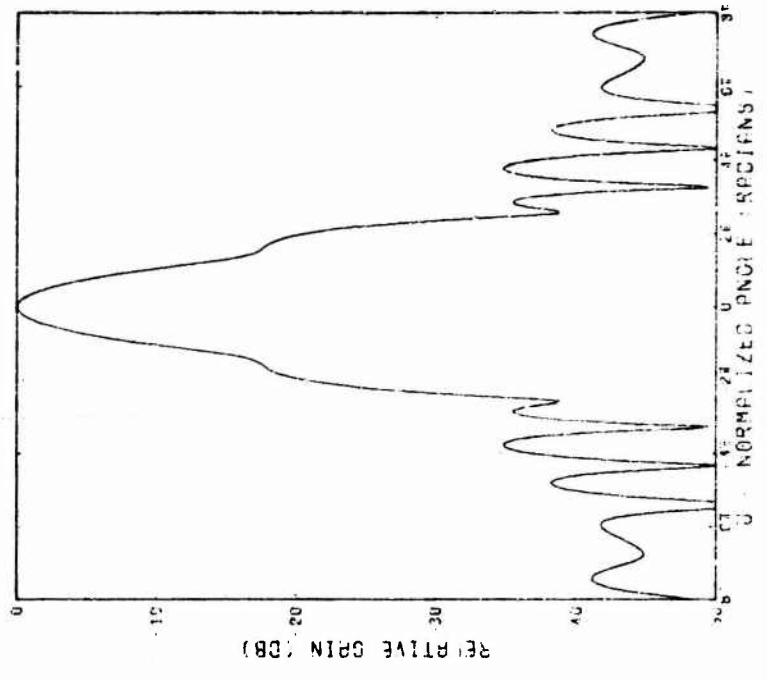


Figure 4-7. Test horn aperture distribution with a Gaussian phase distribution, and computed far-field pattern.

TABLE 4-1

PERFORMANCE COMPARISON OF TEST HORN AND
TEST HORN WITH LENS AT SEVERAL FREQUENCIES

Phase Distribution	Frequency (MHz)	First Sidelobe Level (dB)	Maximum Sidelobe Level (dB)	Gain Factor	3-dB Beamwidth (degrees)	10-dB Beamwidth (degrees)
Measured, no lens	9375	-24	-24	0.73	71.0 λ/a	135 λ/a
Desired (Gaussian)	9375	-35	-35	0.80	67.1 λ/a	120 λ/a
Measured, with lens	9375	-28	-23	0.72	69.0 λ/a	135 λ/a
Measured, with lens	9385	-42	-35	0.69	74.2 λ/a	145 λ/a
Measured, with lens	9405	-37	-33	0.71	76.4 λ/a	135 λ/a

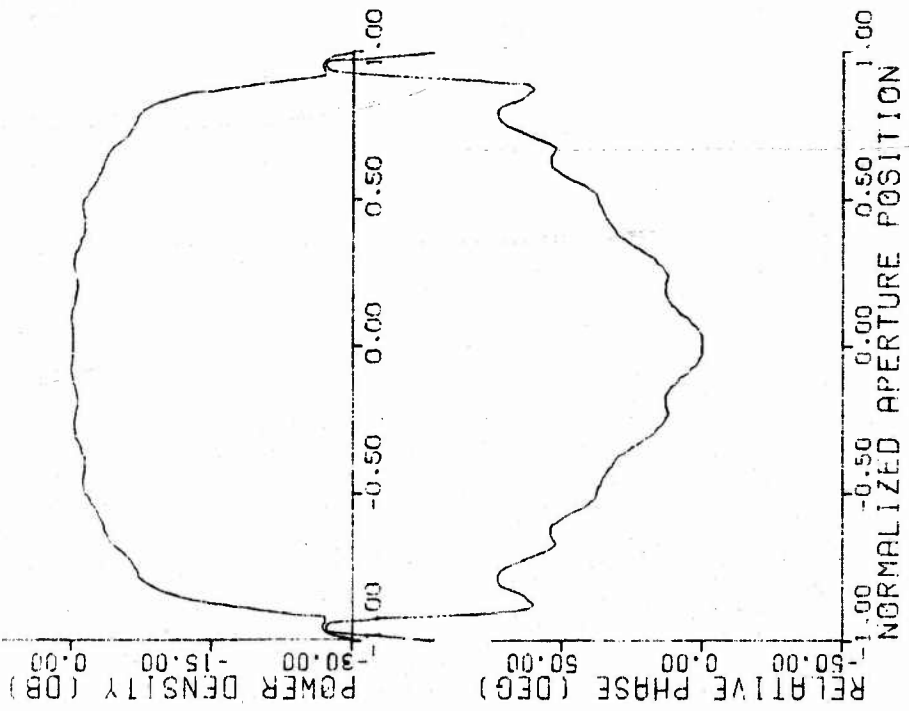
a. Near-Field Measurements

Figure 4-8 shows the measured phase and amplitude distribution and computed far-field pattern of the lens at 9375 MHz. The phase distribution is similar to the distribution without the lens, and only a small improvement in the computed pattern is achieved. However, the lens was frequency sensitive, and better results were achieved at frequencies between 9385 and 9405 MHz. At these frequencies the measured phase distribution approaches the desired shape, although the amplitude distribution is also modified by the lens. Figures 4-9 and 4-10 show the measured phase and amplitude distributions and computed far-field patterns for frequencies of 9385 and 9405 MHz, respectively. The results of the experiments with the test horn are summarized in Table 4-1.

The improvement in sidelobe level is greater than 10 dB at 9385 and 9405 MHz with the lens, although the gain factor is slightly lower than for the antenna without the lens. This is a significant improvement in performance, especially when compared to the theoretical performance achievable with amplitude tapering alone. For example, at 9405 MHz, the gain factor (0.71), first sidelobe level (-37 dB), and maximum sidelobe level (-33 dB) for the test horn with lens compare favorably with the theoretical gain factor (0.67) and sidelobe level (-32 dB) of an antenna with a cosine-squared amplitude taper. Similarly, the normalized 3-dB ($76.4 \lambda/a$) and 10-dB ($135 \lambda/a$) beamwidths of the test horn with lens are narrower than the corresponding 3-dB ($83.2 \lambda/a$) and 10-dB ($165 \lambda/a$) beamwidths for the cosine-squared taper.

b. Far-Field Measurements

The far-field patterns, both with and without the lens, were measured at several frequencies. Figures 4-11 through 4-14 show the measured patterns at



FIRST SIDELobe - -27.75 DB
 GAIN FACTOR - 0.7199
 BEAMWIDTH - 69.02 DEGREES

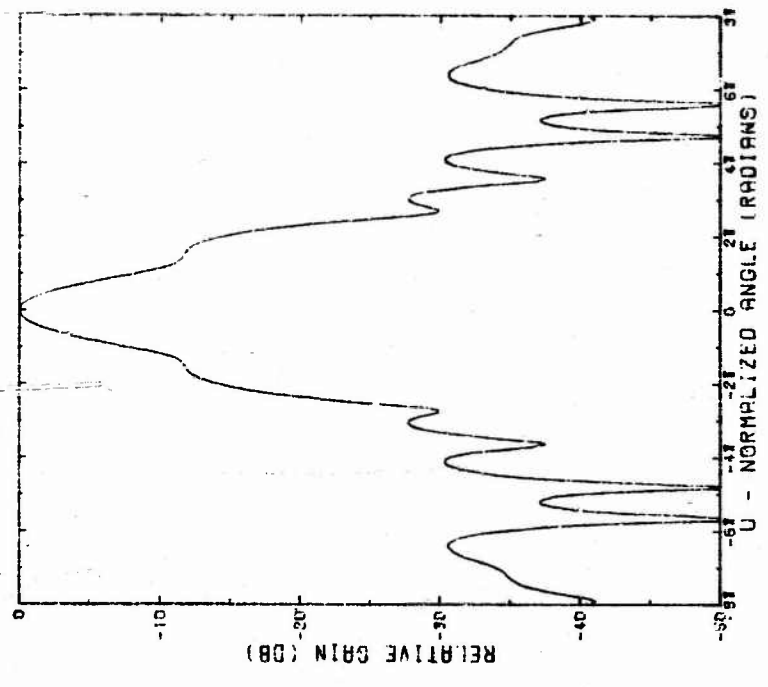


Figure 4-8. Measured aperture distribution and computed far-field pattern of the test horn with lens at 9375 MHz.

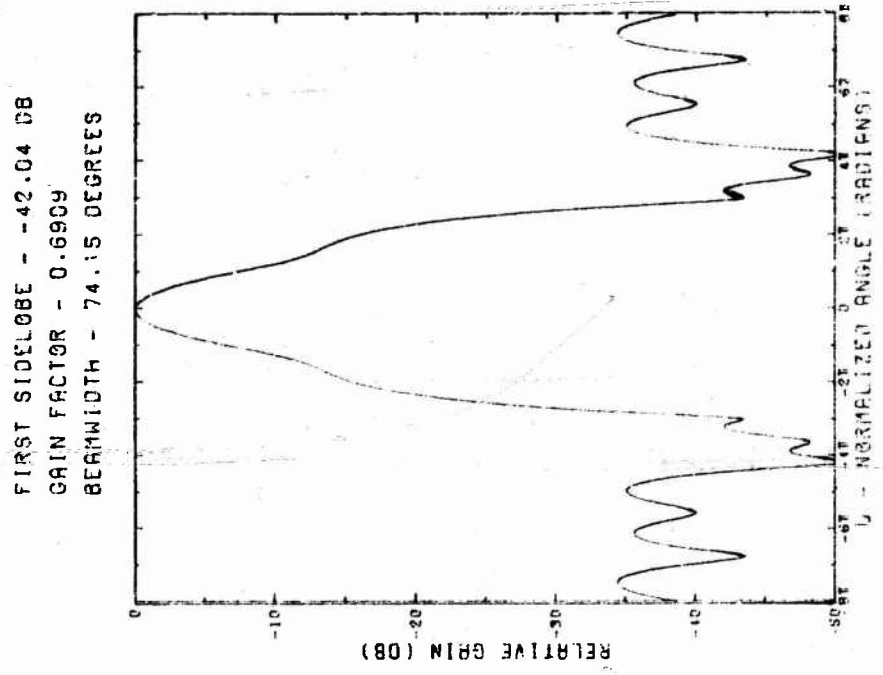
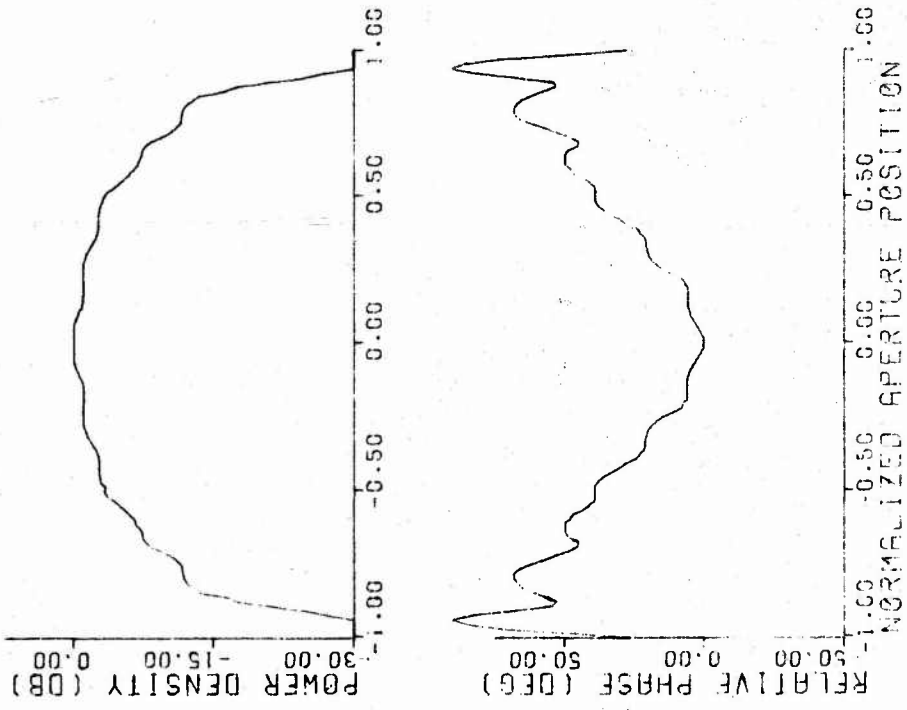
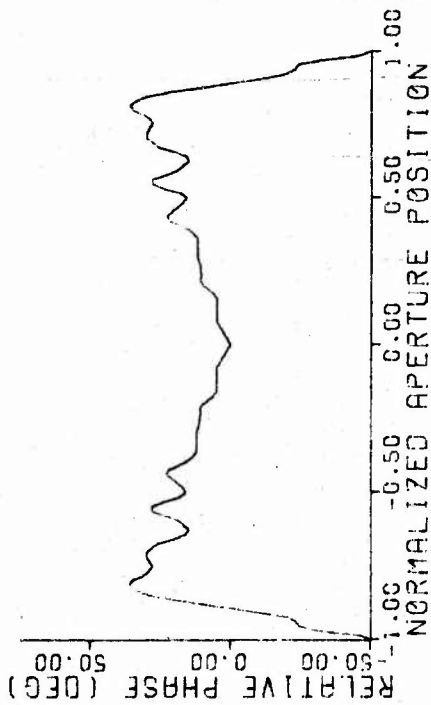
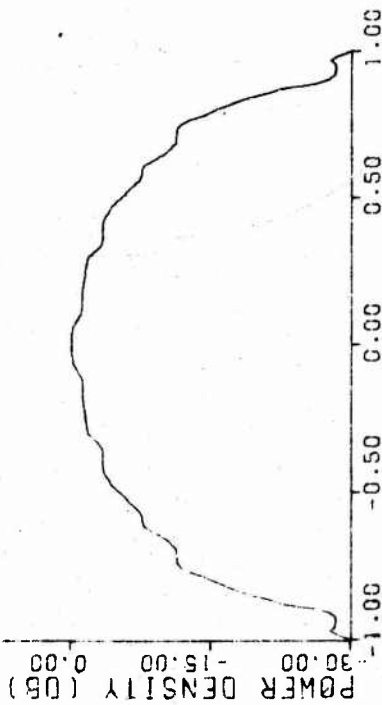


Figure 4-9. Measured aperture distribution and computed far-field pattern of the test horn with lens at 9385 MHz.



FIRST SIDELobe - -36.62 DB
 GAIN FACTOR - 0.7131
 BEAMWIDTH - 76.30 DEGREES

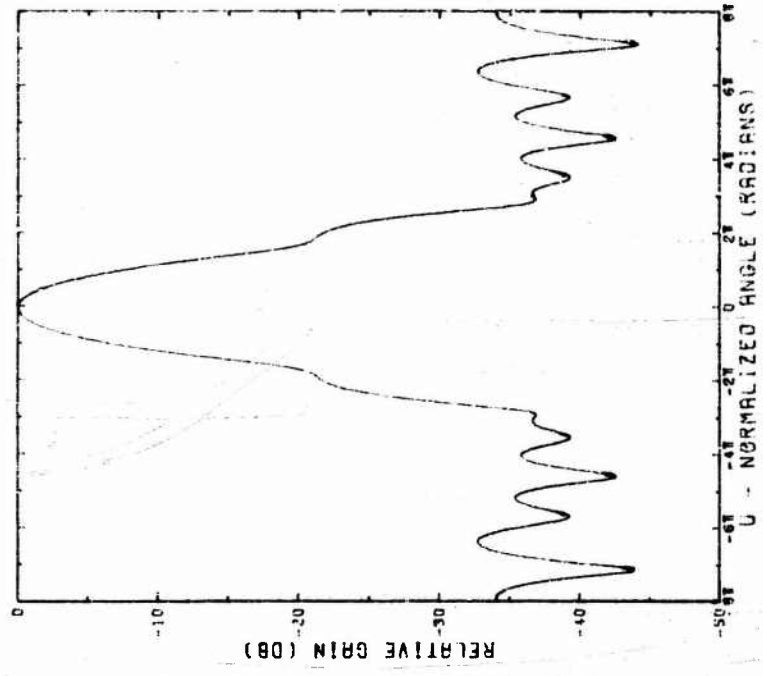


Figure 4-10. Measured aperture distribution and computed far-field pattern of the test horn with lens at 9405 MHz.

9385 and 9405 MHz of the test horn with lens, and without lens, respectively.

The patterns with the lens are essentially the same as the patterns without the lens down to a level of -10 dB; below this level, the beamwidth with the lens in place is slightly larger. The reduction in sidelobe level is clearly shown, although the noise level on the antenna range made it difficult to determine the exact sidelobe level with the lens installed. However, the improvement in sidelobe level at both frequencies was at least 6 dB. If only the close-in sidelobes are considered, the improvement is even larger, which is consistent with the predicted far-field patterns discussed in the previous subsection.

Although it was not possible to achieve the optimum theoretical improvement in both sidelobe level and gain factor with the dielectric lens, we do believe that the usefulness of phase tapering techniques has been demonstrated. It would be more practical to design an antenna with a Gaussian phase taper, thereby avoiding the problems associated with the design of a practical dielectric lens.

3. STANDARD GAIN HORN

A brief investigation of the feasibility of using a Gaussian phase taper to improve the sidelobe level and gain factor of an X-band standard gain horn revealed that a theoretical improvement of 4 dB in sidelobe level was possible, with a 10 percent higher gain factor. However, because of the mismatch problems encountered with the dielectric lens for the square horn, no attempt was made to confirm the theoretical results. The measured aperture distributions and computed far-field patterns for the standard gain horn with the measured phase distribution, and with a Gaussian phase distribution are

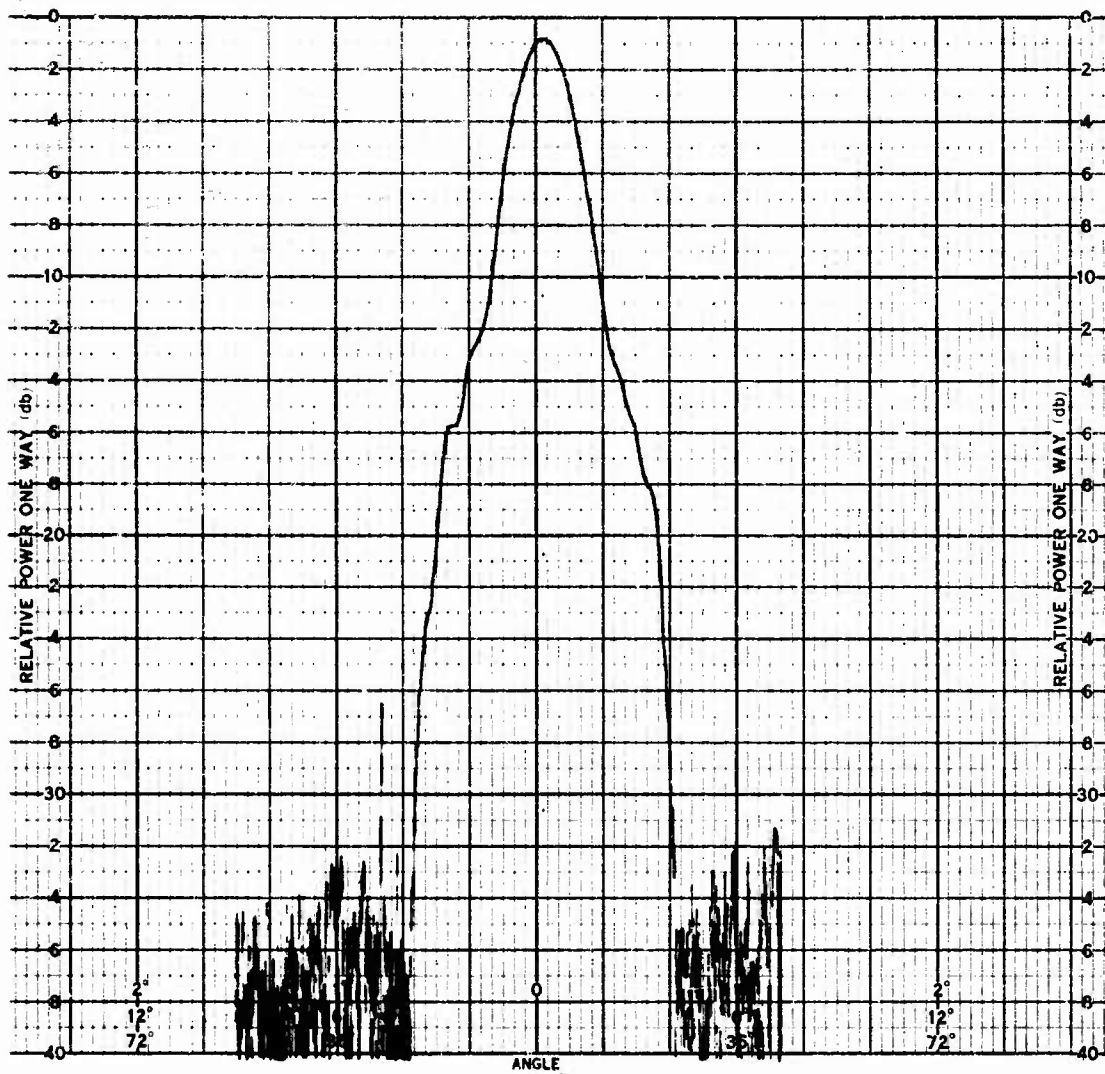


Figure 4-11. Measured far-field pattern of the test horn with lens at 9385 MHz.

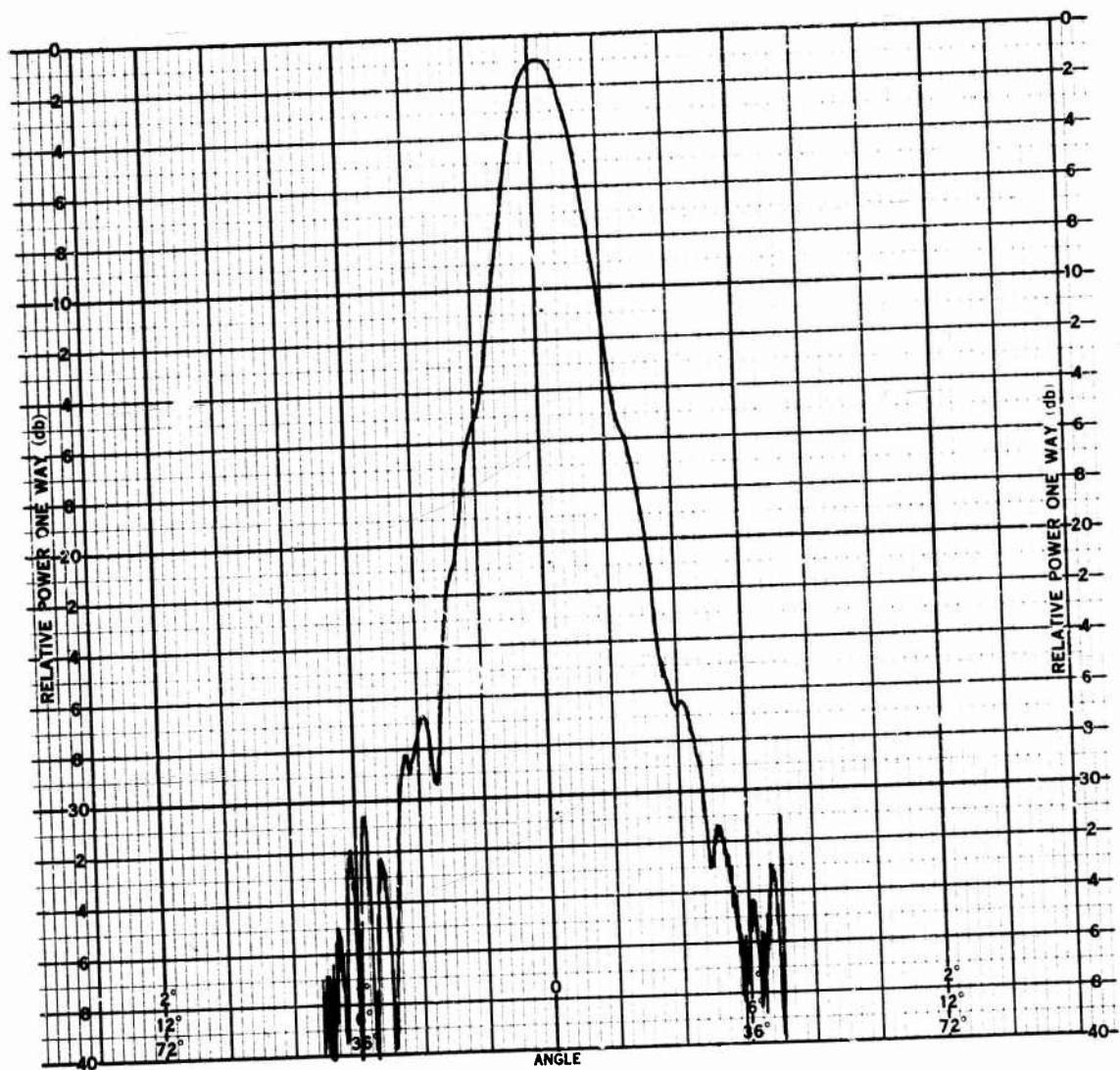


Figure 4-12. Measured far-field pattern of the test horn at 9385 MHz.

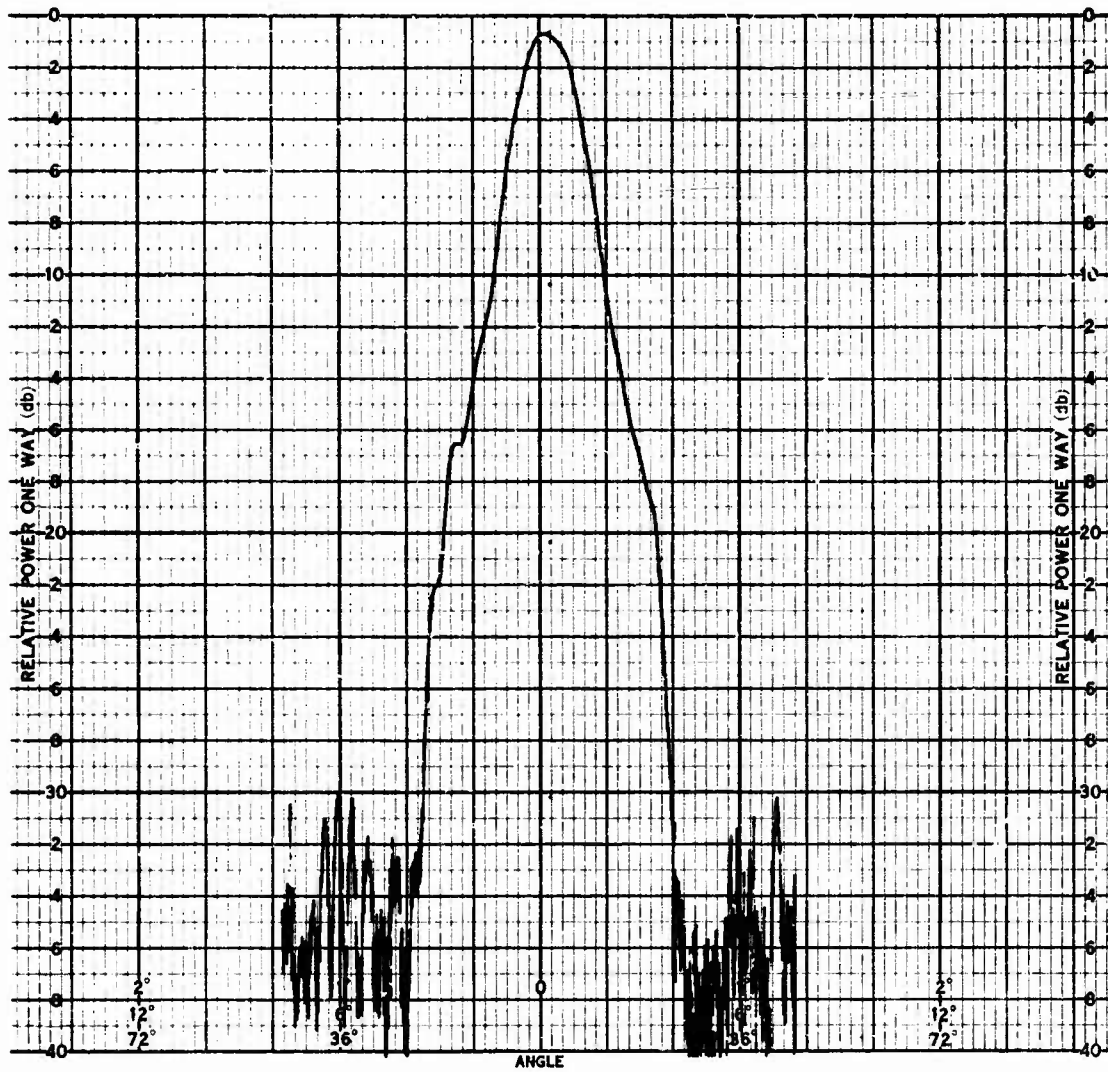


Figure 4-13. Measured far-field pattern of the test horn with lens at 9405 MHz.

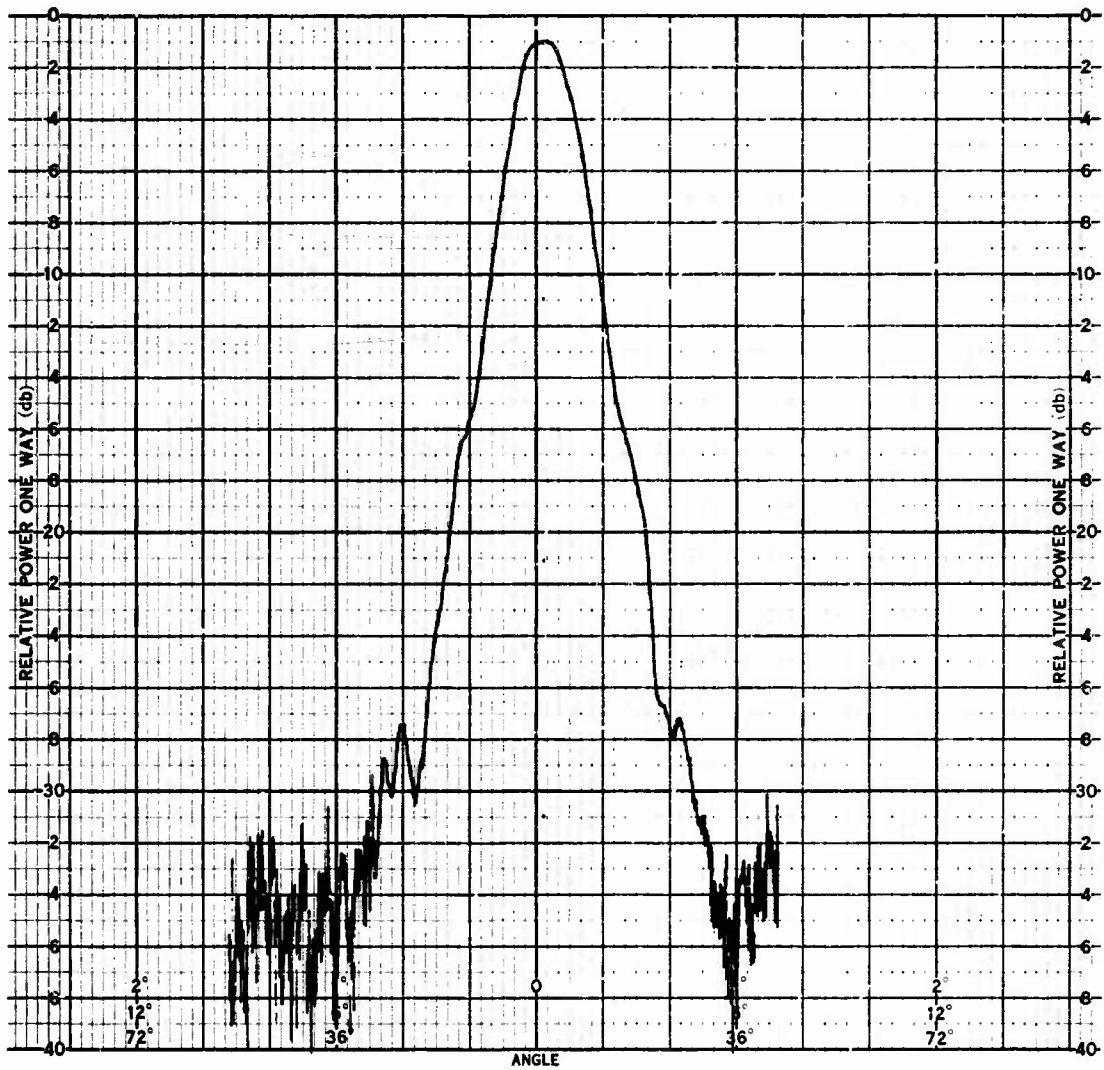


Figure 4-14. Measured far-field pattern of the test horn at 9405 MHz.

shown in Figures 4-15 and 4-16, respectively. The results are summarized in Table 4-2.

TABLE 4-2
THEORETICAL PERFORMANCE OF STANDARD GAIN HORN WITH
QUADRATIC AND GAUSSIAN PHASE DISTRIBUTIONS

Phase Distribution	First Sidelobe Level (dB)	Gain Factor	3-dB Beamwidth (degrees)
Measured	-30	0.66	74.3 λ/a
Gaussian	-34	0.73	69.1 λ/a

4. LINE SOURCE

Shaping the aperture phase distribution with a dielectric lens is a difficult task, as discussed in the previous sections of this report. For this reason, an existing line source antenna with eleven elements was chosen for study. This antenna is an X-band linear array of monopoles spaced at three-eighths of a wavelength. The amplitude distribution was generated by placing probes across the front of a sectoral horn which were connected to the array with small semi-rigid coaxial cables. Figure 4-17 shows the measured aperture distribution and computed far-field pattern of this antenna with an essentially constant phase distribution. Figure 4-18 shows the computed far-field pattern for this antenna with a theoretical Gaussian phase distribution. A reduction in side-lobe level of 4 dB should be possible by modifying the phase distribution alone. However, it was not possible to modify the phase distribution without also modifying the amplitude distribution, as shown in Figure 4-19. There is a significant dip in the amplitude distribution at the point where the change in phase begins. This was observed in every case examined, with the depth of the distortion in the amplitude pattern a linear function of the change in phase,

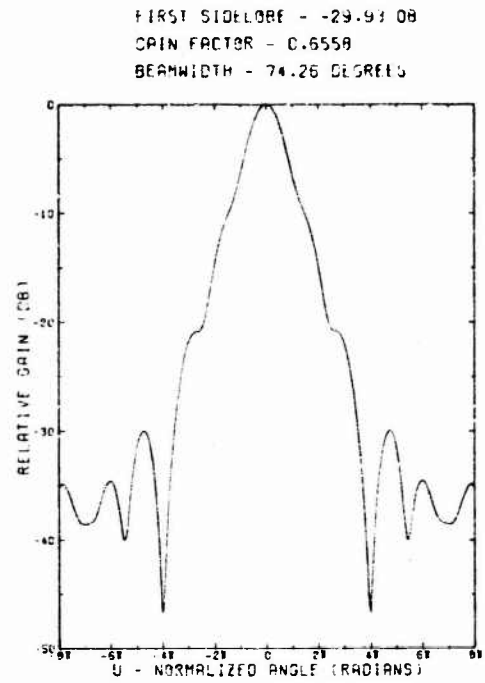
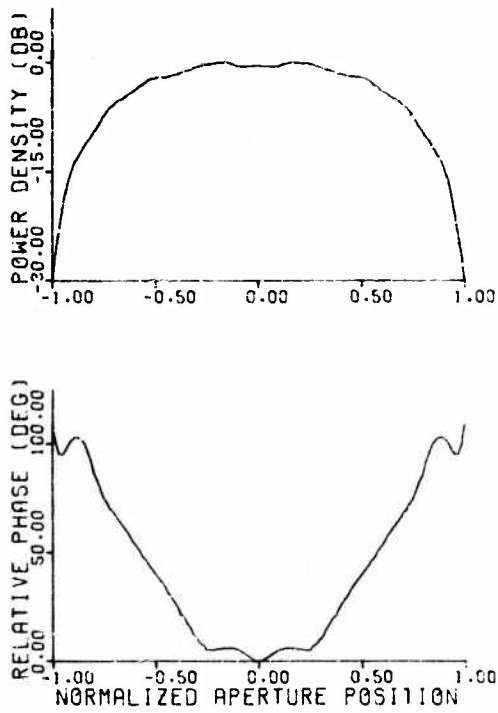


Figure 4-15. Measured aperture distribution and computed far-field pattern of the X-band standard gain horn.

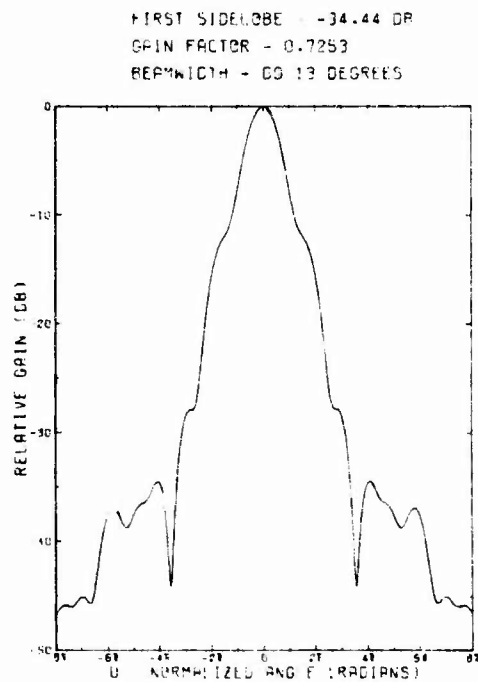
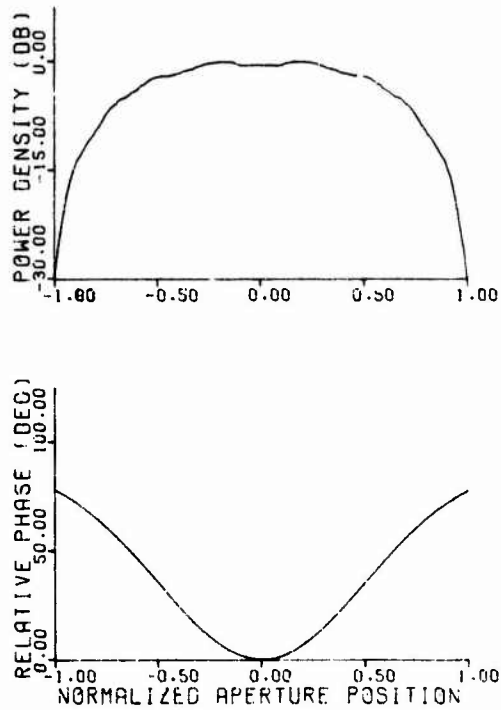


Figure 4-16. Standard gain horn aperture distribution with a Gaussian phase distribution, and computed far-field pattern.

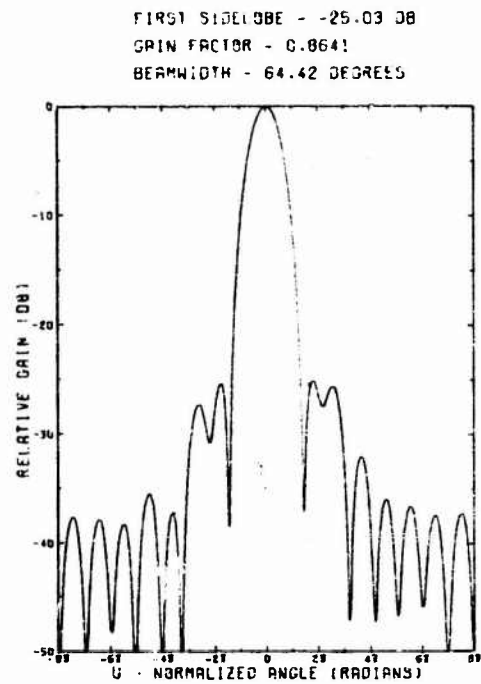
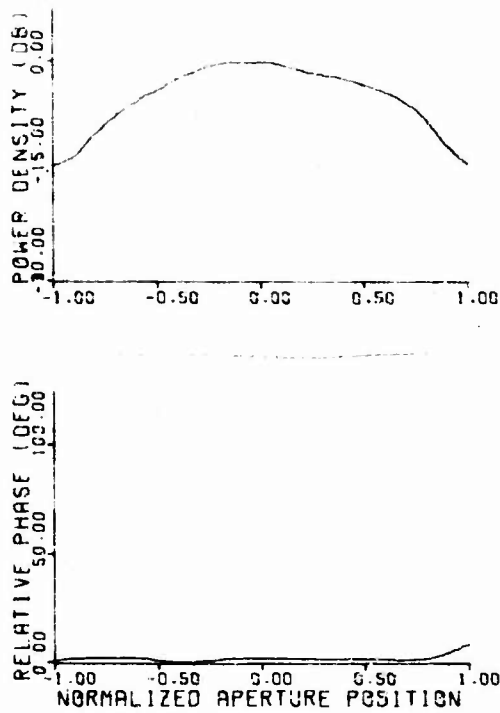


Figure 4-17. Measured aperture distribution and computed far-field antenna pattern of the line source antenna.

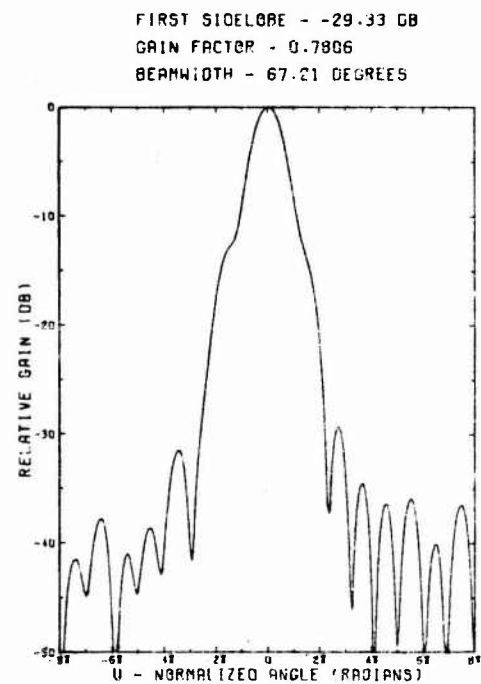
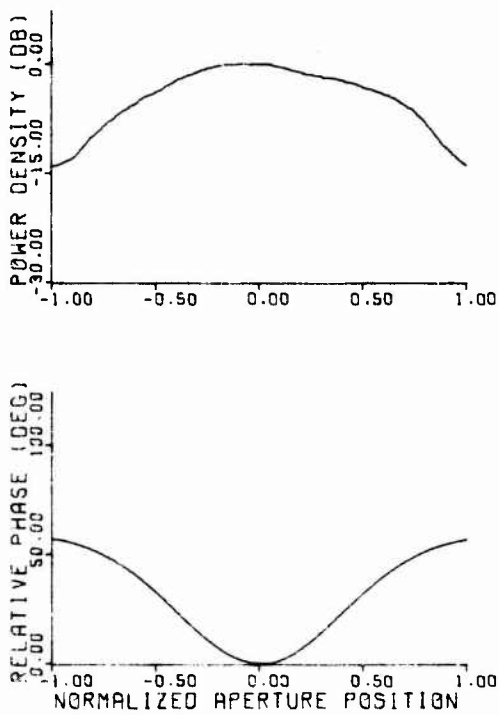
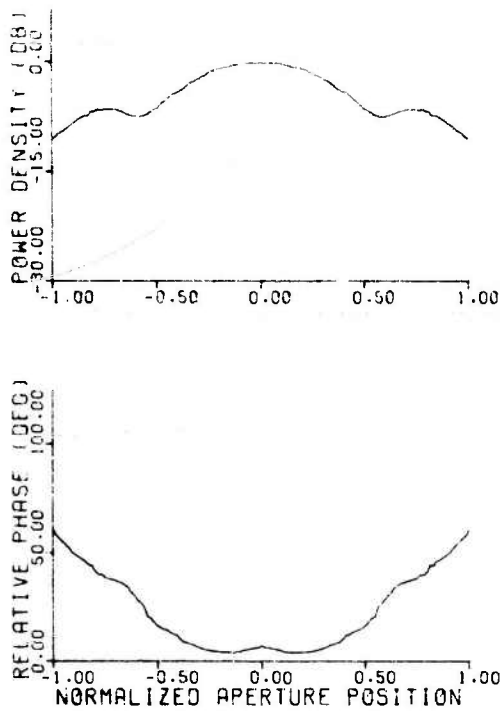


Figure 4-18. Line source aperture distribution with a Gaussian phase distribution and computed far-field pattern.

i.e., the more rapid the change in phase, the deeper the dip in amplitude (Figure 4-20). This appears to be a classic case of mutual coupling in a linear array.

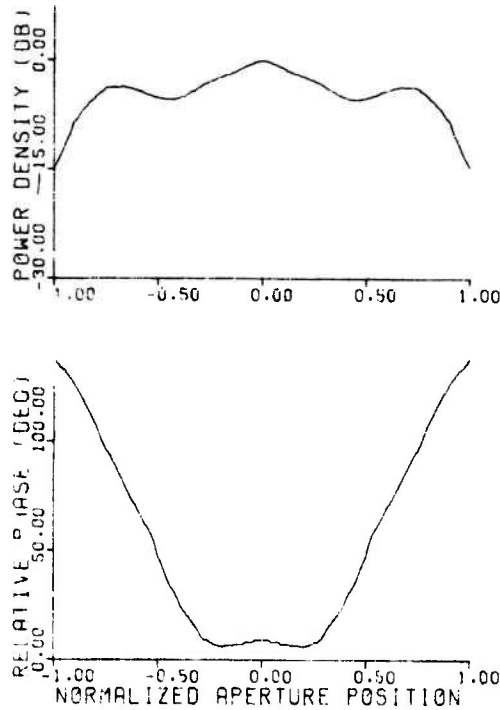
Unfortunately, independent control of both amplitude and phase was not available in the experimental setup, as phase control was obtained by changing the length of the cables feeding the array. No provision was made for changing the amplitude distribution. However, in a phased array with fully independent control of phase and amplitude, it should be possible to achieve the theoretical reduction in sidelobe level.

One useful result of the line source experiments is the demonstrated potential of the X-Y-Z probe and positioner for the analysis of mutual coupling in phased arrays. The rapid evaluation of changes in design and the detection of bad elements in the array are some of the possible applications of this system.



FIRST SIDELOBE - -17.97 DB
 GAIN FACTOR - 0.8163
 BEAMWIDTH - 62.55 DEGREES

Figure 4-19. Measured line source distribution and computed far-field pattern, showing the effect of mutual coupling on the aperture distribution.



FIRST SIDELOBE - -13.78 DB
 GAIN FACTOR - 0.5345
 BEAMWIDTH - 76.43 DEGREES

Figure 4-20. Measured line source distribution and computed far-field pattern, showing the effect of an abrupt change in the phase distribution.

SECTION V

DESIGN INFORMATION

The antenna designer will make the final decision to include phase tapering in his design procedure, or to use conventional amplitude tapering alone. The information in this section is presented as a guide for the designer who must make this choice.

A series of computed patterns which were chosen as representative of the best gain factor and beamwidth performance possible at specific sidelobe levels using a combination of modified Taylor amplitude and Gaussian phase tapering will be given in Part 1. These can be used directly to compare the performance of existing antennas (with constant or quadratic phase variations, for example) to that possible using a combination of phase and amplitude tapering that is close to the optimum.

Part 2 consists of a series of computer plots of gain factor and sidelobe level versus amplitude taper for many different Gaussian phase tapers. These can be used to determine the degree of improvement possible using phase tapering, and whether the improvement is worth the additional expense involved in shaping the phase distribution.

1. OPTIMUM PHASE AND AMPLITUDE TAPERS

The series of curves shown in Figures 5-1 through 5-8 can be used to determine the optimum modified Taylor amplitude and Gaussian phase distributions to achieve sidelobe levels from -15 to -50 dB. For sidelobe levels of -15 and -20 dB, amplitude tapering alone is superior to a combination of amplitude and phase tapering. However, for levels lower than -20 dB, phase tapering improves performance. A description of the modified Taylor amplitude and Gaussian

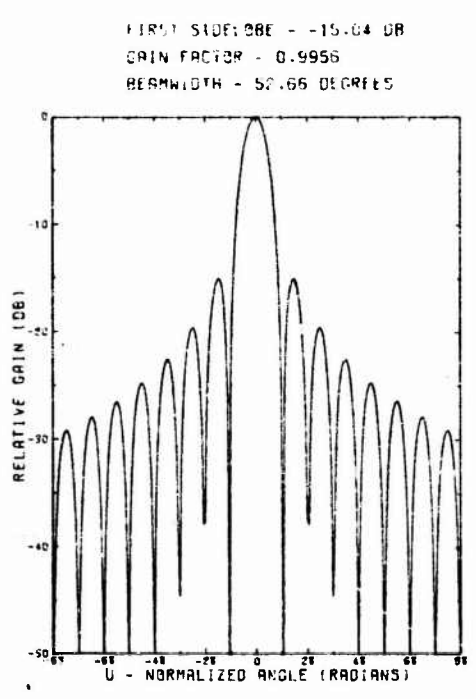
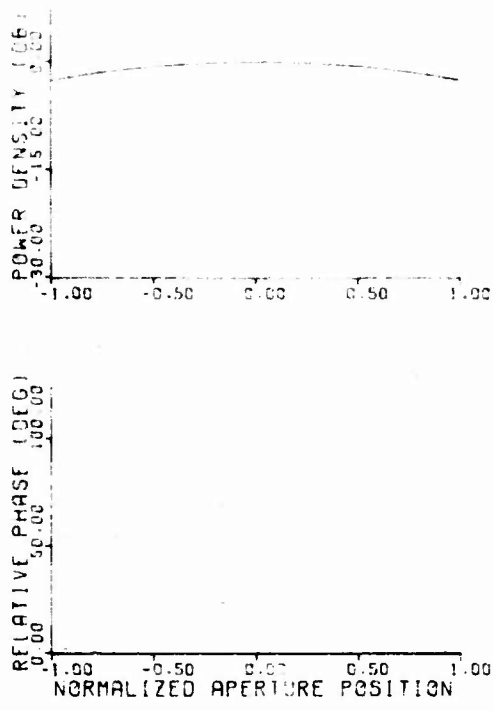


Figure 5-1. Optimized modified Taylor amplitude and Gaussian phase aperture distribution for a sidelobe level of -15 dB.

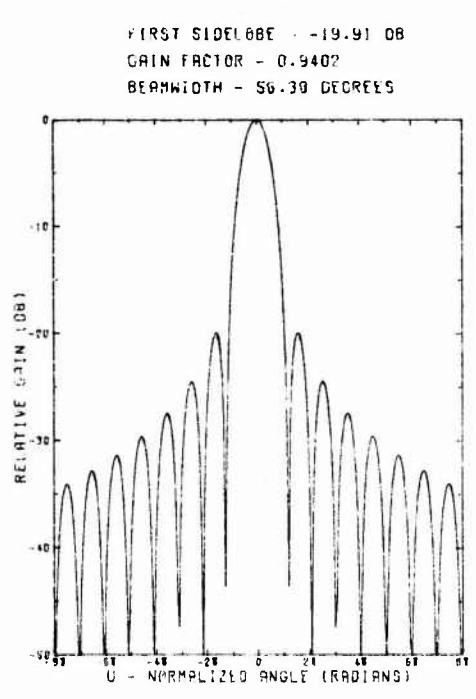
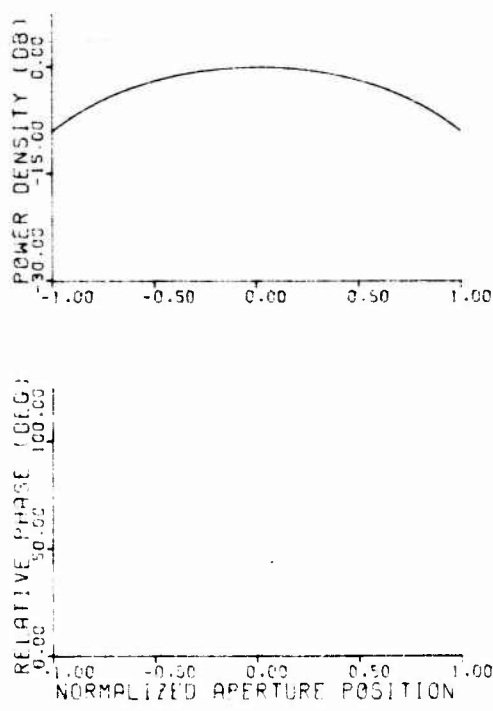


Figure 5-2. Optimized modified Taylor amplitude and Gaussian phase aperture distribution for a sidelobe level of -20 dB.

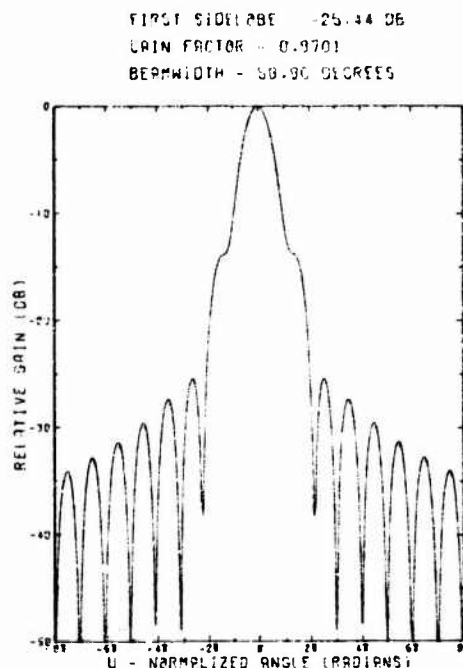
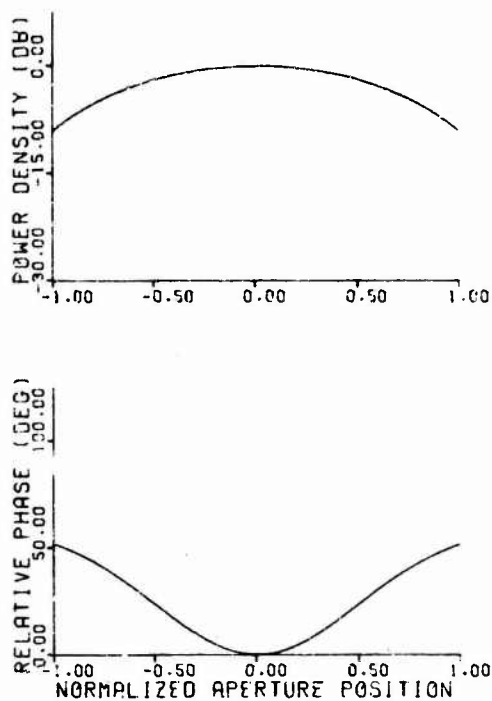


Figure 5-3. Optimized modified Taylor amplitude and Gaussian phase aperture distribution for a sidelobe level of -25 dB.

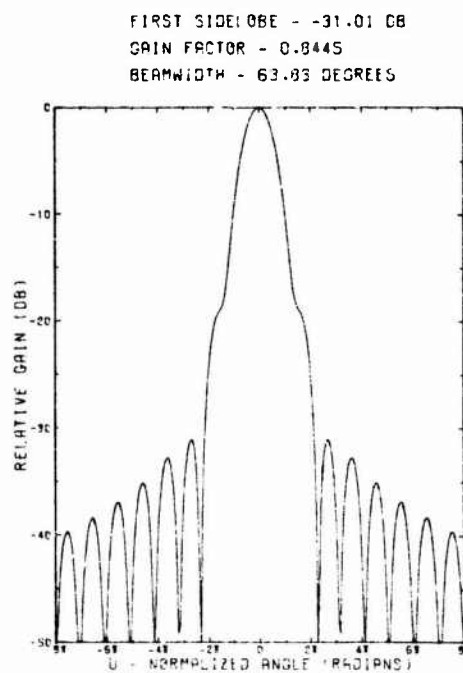
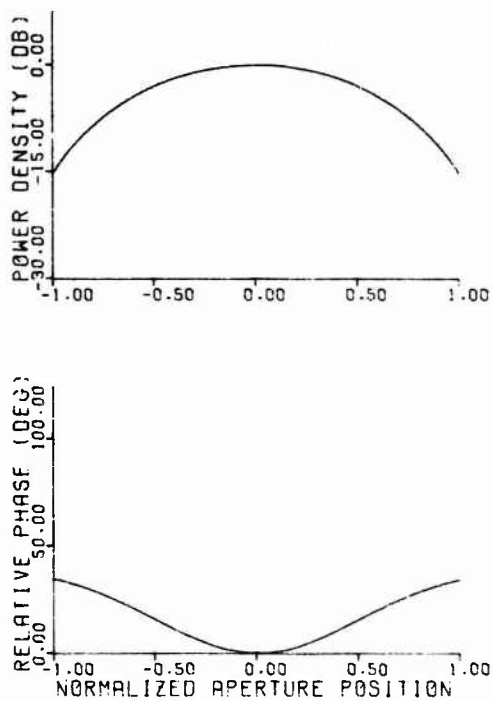


Figure 5-4. Optimized modified Taylor amplitude and Gaussian phase aperture distribution for a sidelobe level of -30 dB.

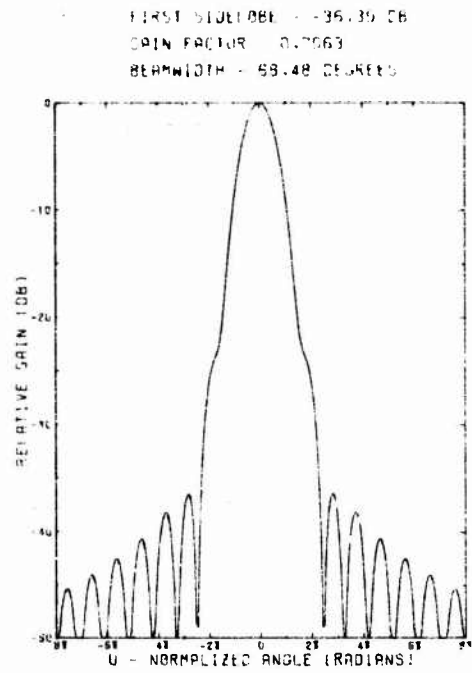
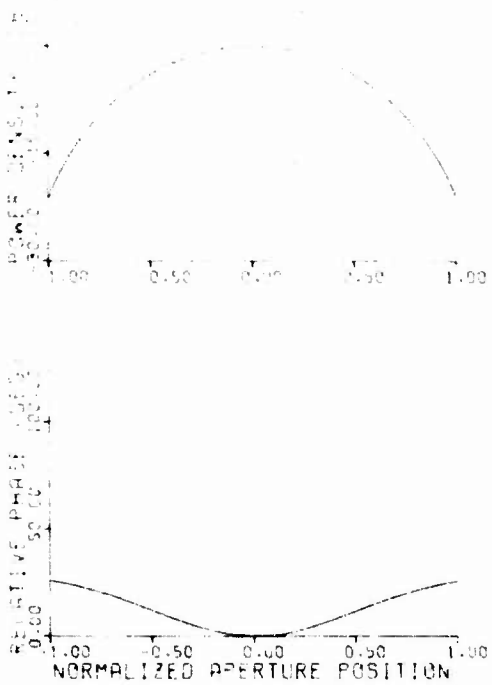


Figure 5-5. Optimized modified Taylor amplitude and Gaussian phase aperture distribution for a sidelobe level of -35 dB.

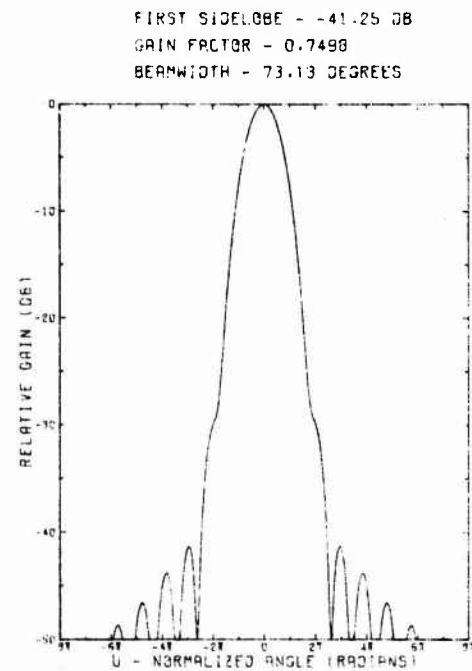
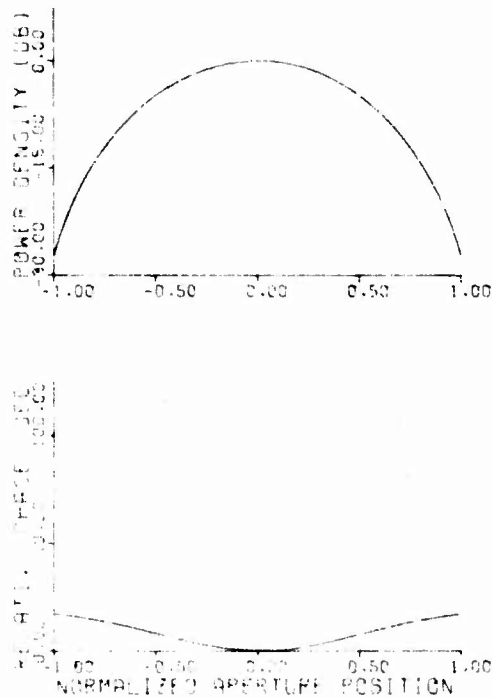
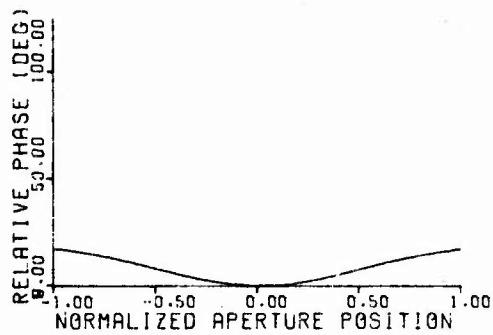
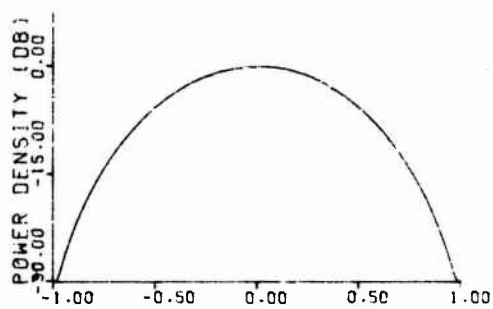


Figure 5-6. Optimized modified Taylor amplitude and Gaussian phase aperture distribution for a sidelobe level of -40 dB.



FIRST SIDELobe - 45.95 DB
 GAIN FACTOR - 0.7092
 BEAMWIDTH - 77.22 DEGREES

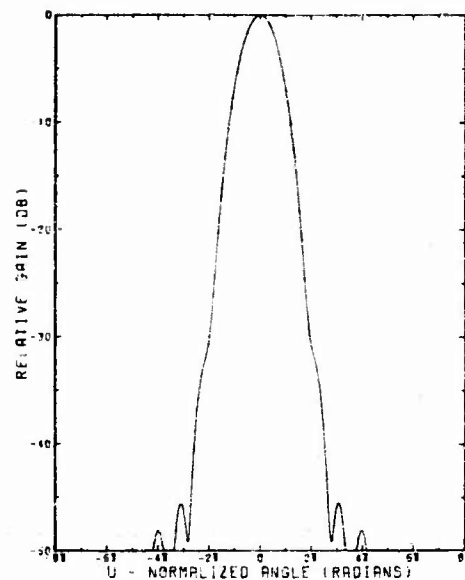
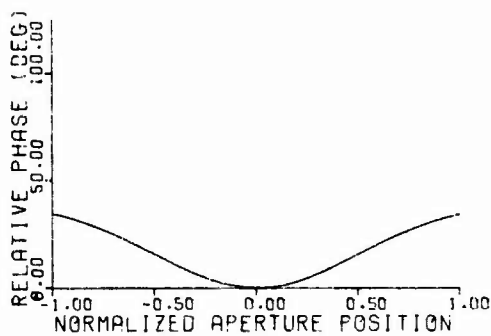
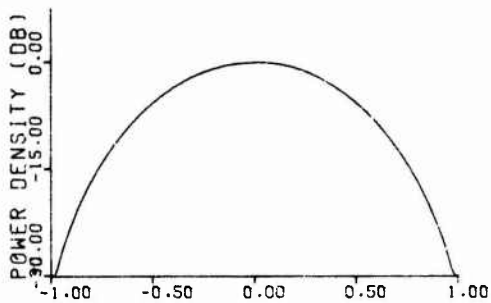


Figure 5-7. Optimized modified Taylor amplitude and Gaussian phase aperture distribution for a sidelobe level of -45 dB.



FIRST SIDELobe - -49.15 DB
 GAIN FACTOR - 0.6959
 BEAMWIDTH - 77.94 DEGREES

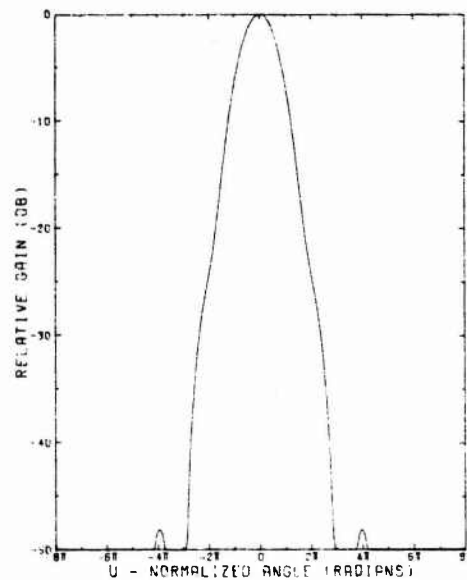


Figure 5-8. Optimized modified Taylor amplitude and Gaussian phase aperture distribution for a sidelobe level of -50 dB.

phase distributions was given in Section III. Table 5-1 summarizes the data shown on the figures and lists the equations used to generate the aperture distributions.

2. GAIN FACTOR CURVES

Figures 5-9 through 5-18 show the gain factor and sidelobe level as functions of amplitude taper (modified Taylor) and maximum phase variation. In Figure 5-9, the phase is a constant; in Figures 5-10 through 5-18, the phase distribution is Gaussian, with a standard deviation of 0.5 and end point (A in Table 5-1) between 20 and 100 degrees. The constant phase curve is repeated on each plot for comparison.

An interesting feature of these curves is the existence of a break point for each phase taper. For example, in Figure 5-10, using a twenty-degree Gaussian phase taper actually increases the sidelobe level for amplitude tapers less than approximately 17 dB. However, phase tapering improves the sidelobe level for larger tapers. As the end point phase is increased (Figures 5-11 through 5-18), the break point occurs at smaller amplitude tapers, although the gain factor also decreases. The break point coincides with the merging of the first sidelobes with the main beam. In most cases, the minimum phase taper that results in the merging of the first sidelobe will provide the best gain factor; a larger phase taper will result in a lower gain factor.

Figure 5-19 shows an example of the use of these curves. At a sidelobe level of -35 dB, the gain factor with phase tapering is higher than the gain factor using no phase variation. However, at a sidelobe level of -20 dB, the gain factor is higher when the phase is held constant.

TABLE 5-1

OPTIMIZED MODIFIED TAYLOR AMPLITUDE AND
GAUSSIAN PHASE DISTRIBUTIONS

First Sidelobe Level (dB)	Amplitude Distribution $I_0(B\sqrt{1-x^2})$ (B)	Phase Distribution $A(1 - e^{-2x^2})$ (A)	Gain Factor	3-dB Beamwidth (λ/a degrees)
15	1.12	0	.996	52.7
20	2.3	0	.940	58.4
25	2.3	60	.870	58.9
31	3.2	40	.845	63.8
36	4.0	30	.796	68.5
41	4.8	20	.750	73.1
46	5.5	20	.709	77.2
48	5.5	40	.697	77.9

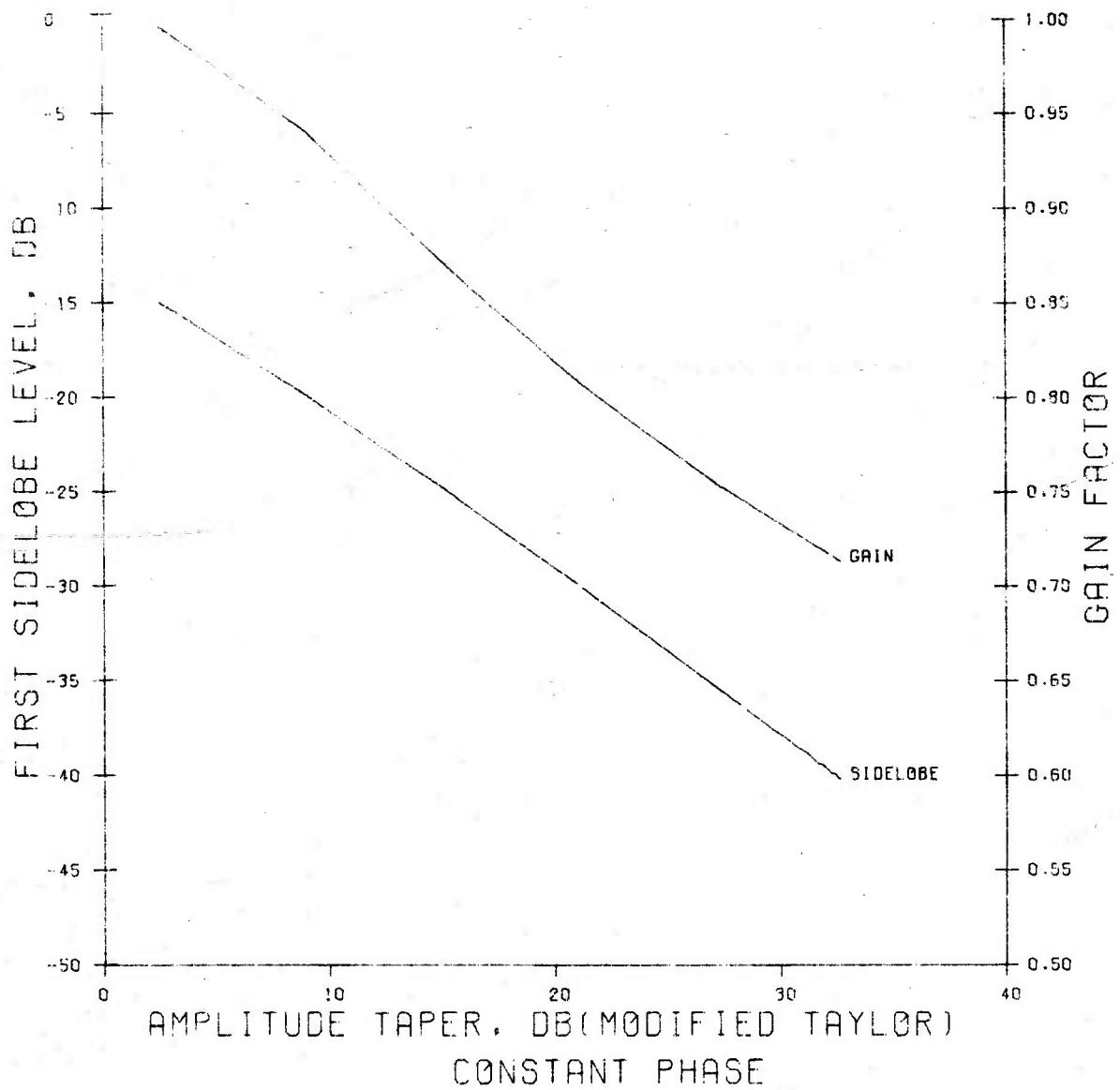


Figure 5-9. Gain Factor and sidelobe level as a function of amplitude taper, with no phase variation.

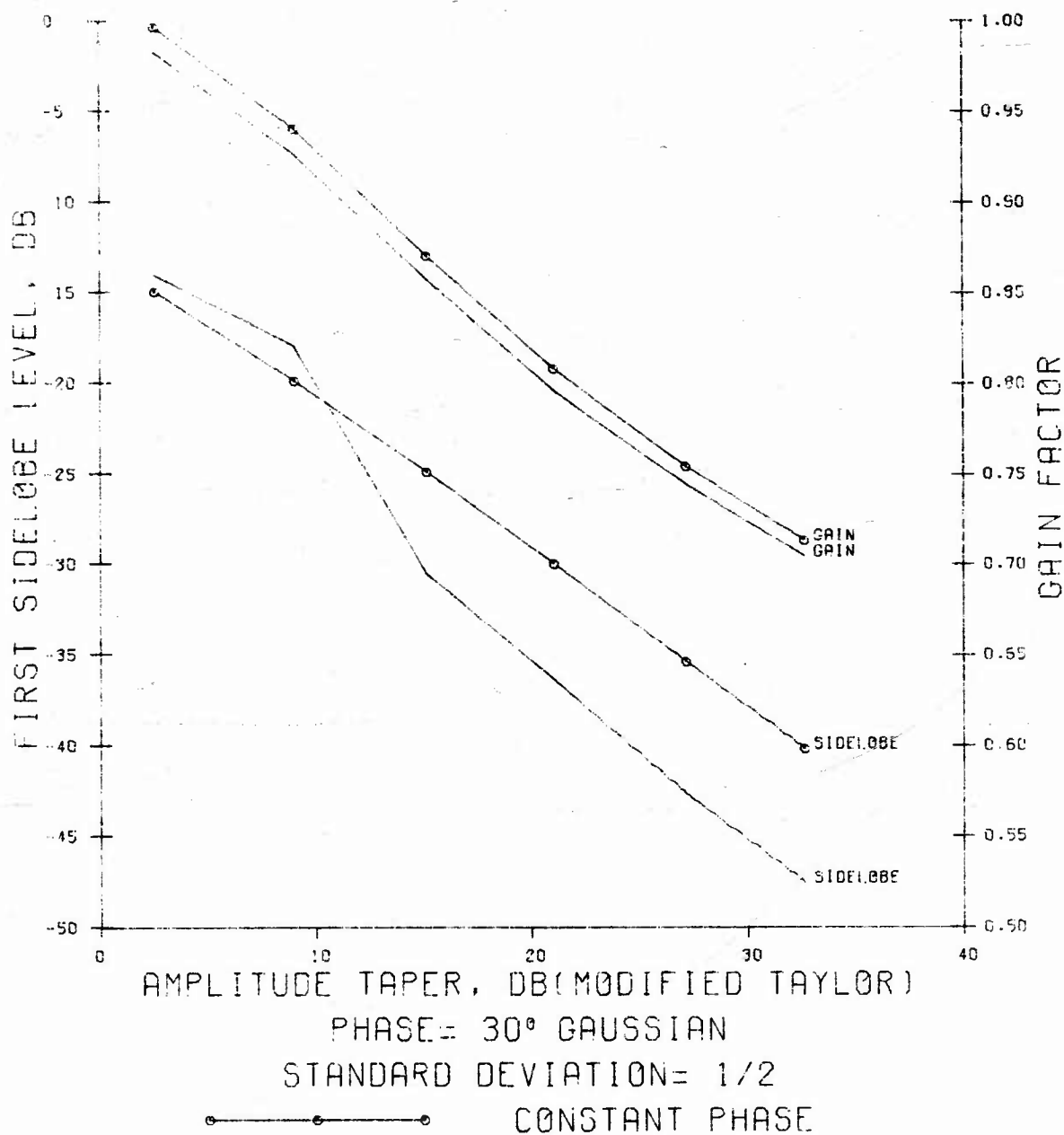


Figure 5-11. Gain Factor and sidelobe level as a function of amplitude taper, with a maximum phase variation of thirty degrees.

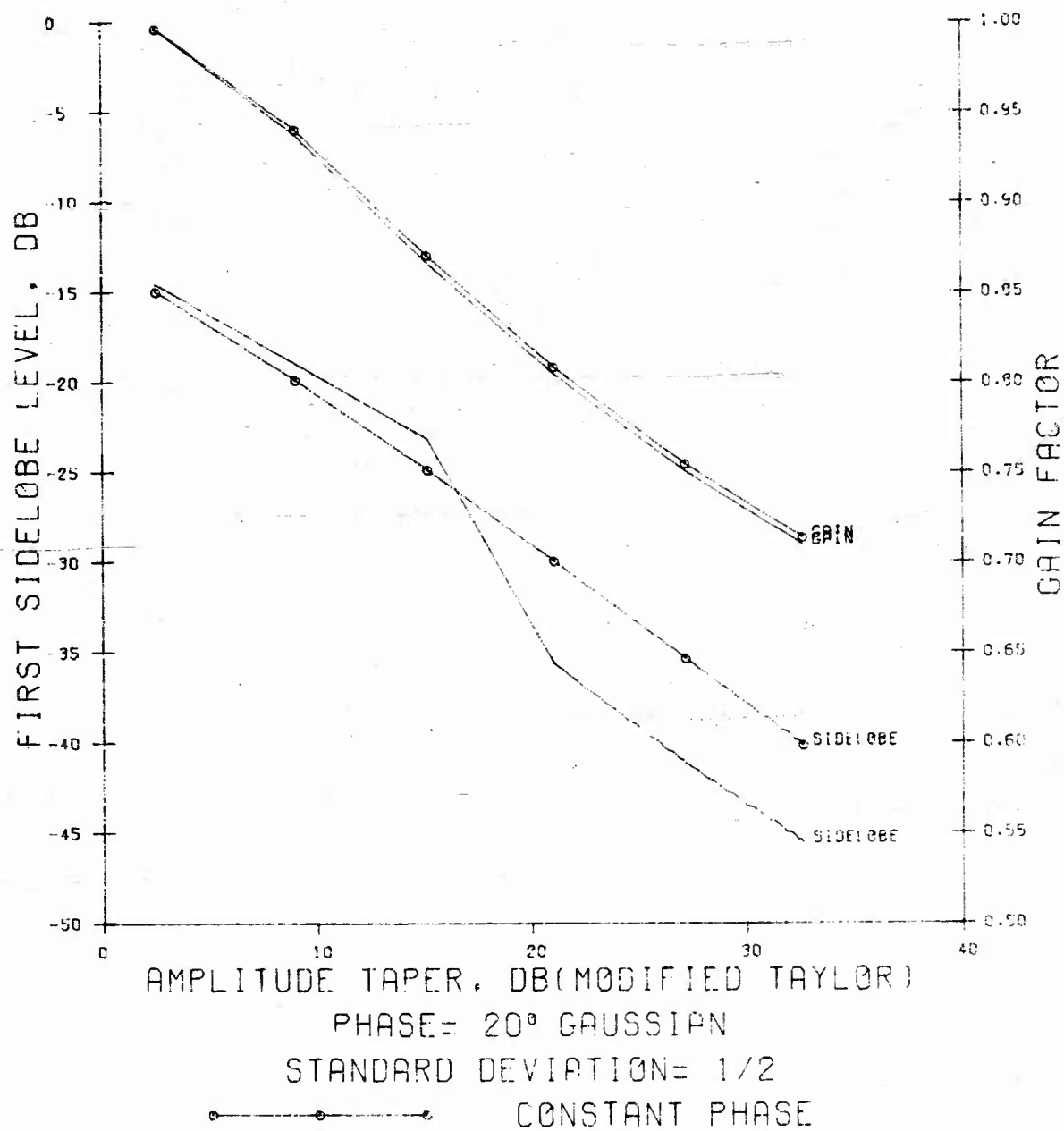


Figure 5-10. Gain Factor and sidelobe level as a function of amplitude taper, with a maximum phase variation of twenty degrees.

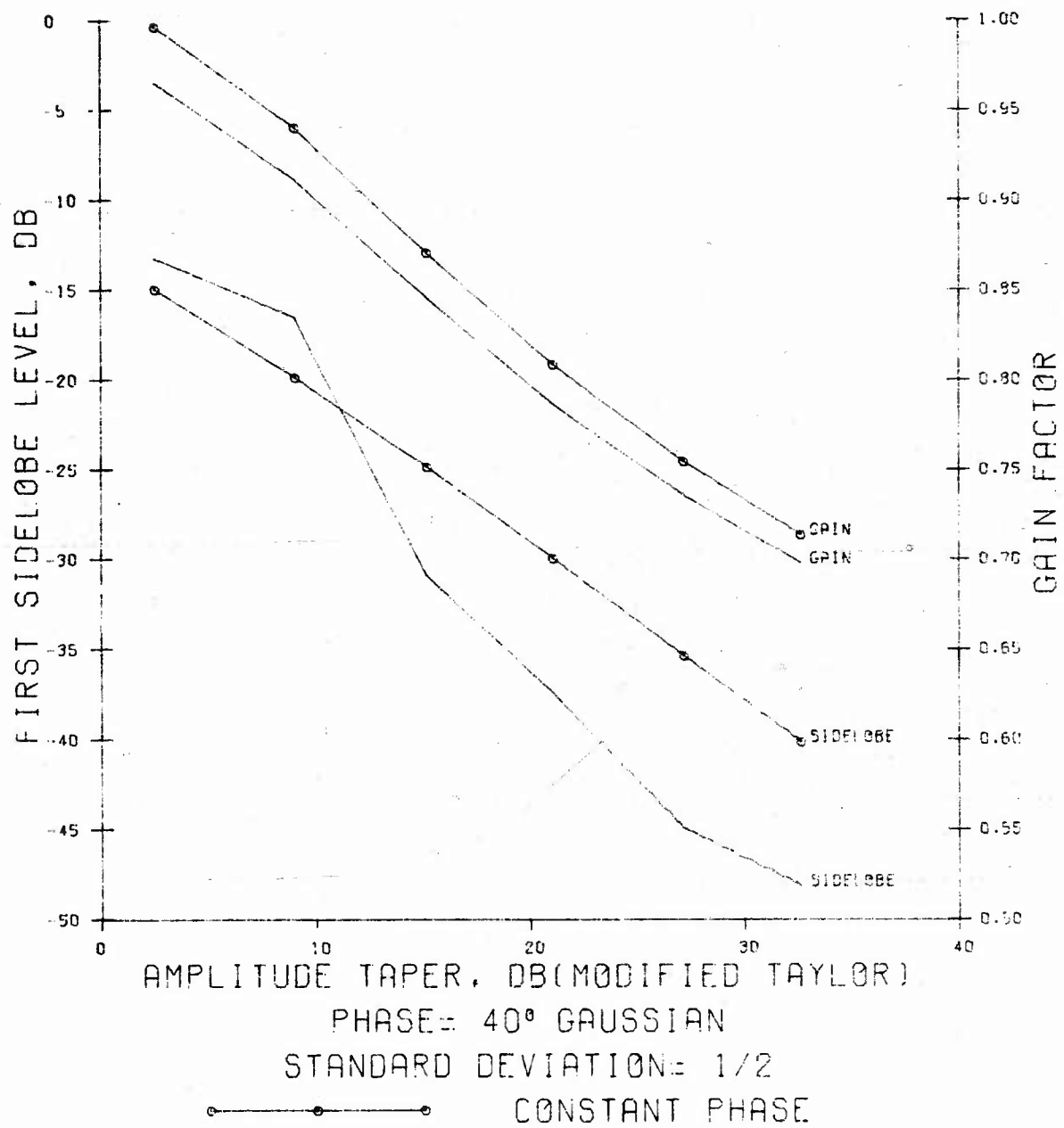


Figure 5-12. Gain Factor and sidelobe level as a function of amplitude taper, with a maximum phase variation of forty degrees.

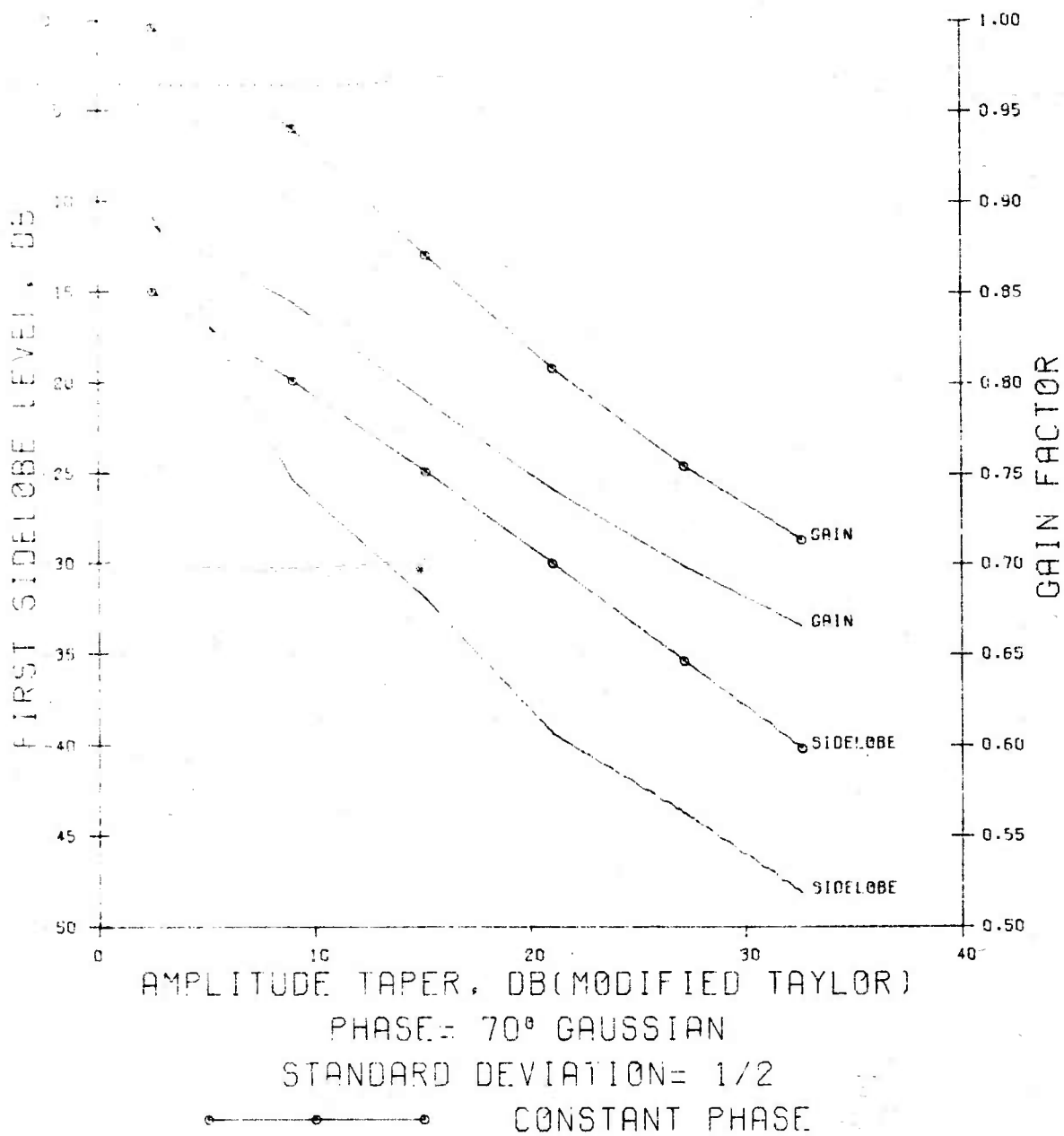


Figure 5-15. Gain Factor and sidelobe level as a function of amplitude taper, with a maximum phase variation of seventy degrees.

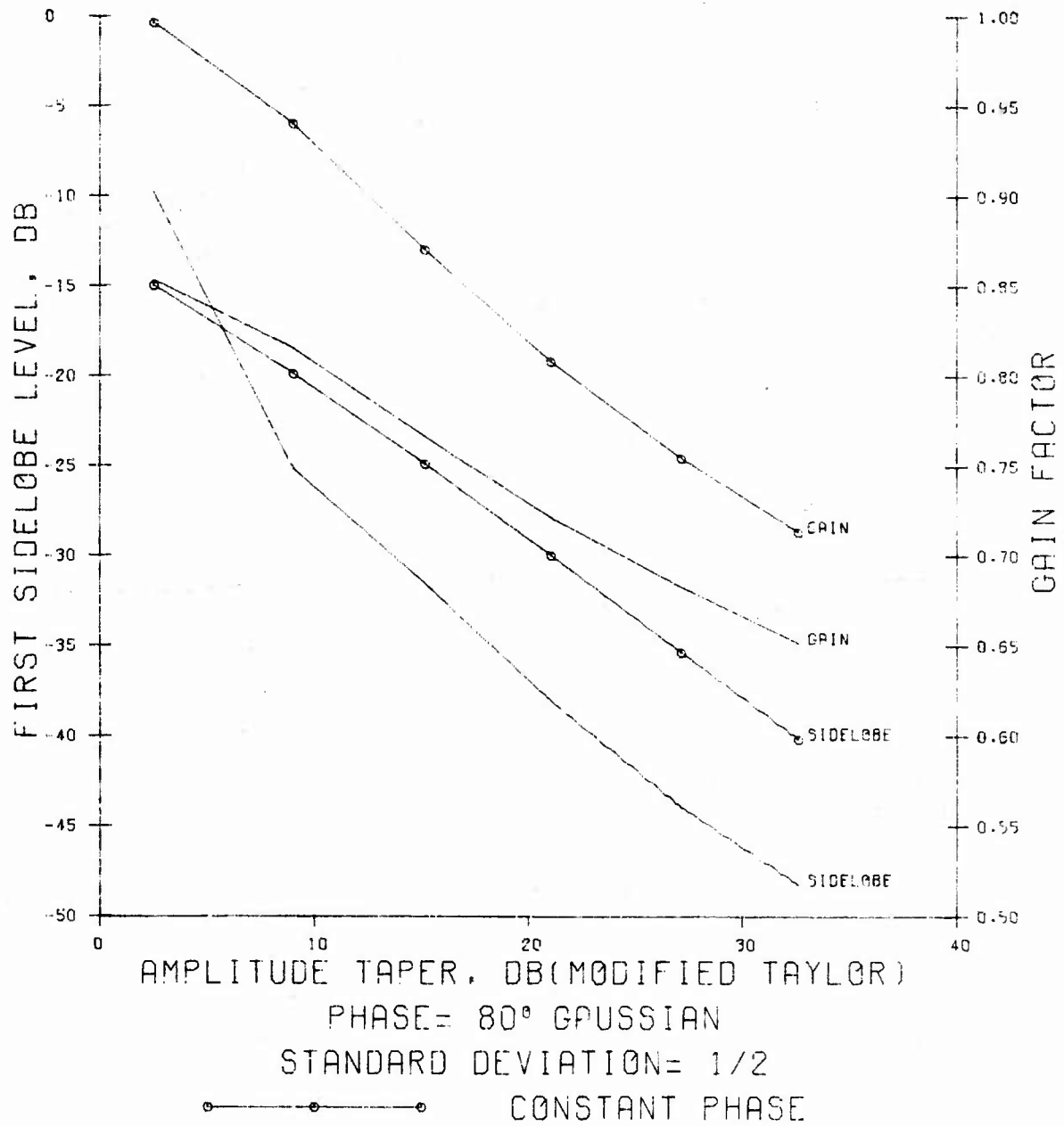


Figure 5-16. Gain Factor and sidelobe level as a function of amplitude taper, with a maximum phase variation of eighty degrees.

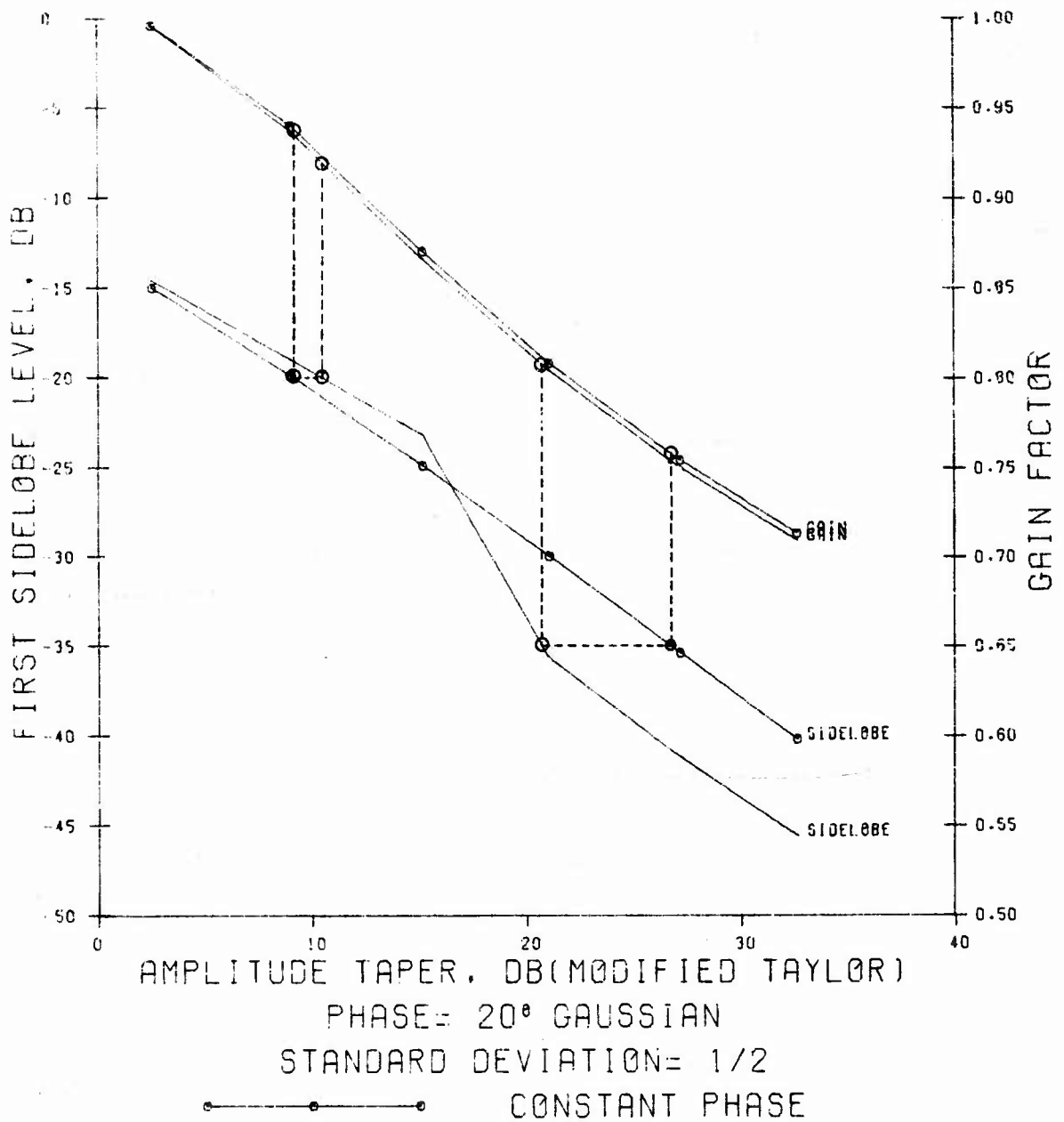


Figure 5-19. Use of the design curves to determine if phase tapering will result in a higher gain factor at sidelobe levels of -20 dB and -35 dB.

SECTION VI

CONCLUSIONS AND RECOMMENDATIONS

The theoretical analysis of the shaping of aperture distributions has demonstrated that higher gain and narrower beamwidth are possible at many sidelobe levels when conventional amplitude tapering is replaced by combined phase and amplitude tapering. The potential improvement can be easily determined by referring to the design information included in this report. It was empirically determined that a Gaussian phase taper produced the best combination of sidelobe level, gain factor, and beamwidth for a large variety of amplitude tapers.

Experiments with a horn antenna confirmed the theoretical results; a significant improvement in sidelobe level was achieved by shaping the horn phase distribution with a dielectric lens. Measurements on a standard gain horn and a line source array demonstrated that similar results should be possible with these antennas.

Recommendations for further work are 1) to determine the optimum phase distribution, and 2) to analyze a practical antenna system, such as a monopulse tracking radar antenna, to determine the improvement in total system performance possible through combined phase and amplitude tapering of the aperture distribution.

We are convinced that combined phase and amplitude tapering is an important new technique which may result in a significant improvement in the sidelobe performance of practical antennas.

APPENDIX

1. INTRODUCTION

A Scientific-Atlanta X-Y-Z near-field probe and positioner has been installed in a specially constructed laboratory in the Electronics Research building at Georgia Tech. The positioner (shown in Figures 4-1 and 4-2) enables the aperture distribution of a transmitting antenna to be measured with a receiving probe that is capable of being positioned anywhere on an 8 foot by 8 foot X-Y plane, located parallel to the plane of the aperture. Displacement of the plane in the Z direction can be varied over a 3 foot range. Such an aperture distribution may be used as input data to existing computer programs for predicting far-field patterns of antennas.

The positioner can be reset to any point in its three-dimensional coordinate system with an accuracy of $\pm .025$ inches. Because of this accuracy, it is possible to closely duplicate a particular test situation. Thus, accurate far-field patterns for a variety of antenna types can be determined from experimental measurements without the use of an outdoor antenna test range.¹⁷ The indoor measuring system makes possible the permanent installation of equipment which could not be left outdoors.

In addition to its use in determining far-field radiation patterns, the X-Y-Z positioner can be used in the evaluation of compact ranges, in aperture blockage investigations, in tuning phased arrays, and in microwave holography.

2. INSTALLATION

During the construction of the laboratory room in which the positioner is located, no special provisions were made to reduce reflections. However,

microwave absorbing material was mounted on the entire front area of the positioner frame. Also, a movable wall, approximately 16 feet by 12 feet, was constructed from wood and covered with absorbing material. This wall is positioned to intercept the main beam of the antenna being tested. Figure 4-2 shows the wall located a few feet behind the positioner to provide a background with a low reflection level. During operation, absorbing material is placed at any location on the floor that could be a possible source of reflection.

3. MEASUREMENTS AND ALIGNMENT

Relative phase and amplitude measurements were made to ensure that all the cables and rotary joints were operating properly. With a constant voltage input to the probe, the positioner was moved in the X-Y plane while the phase and amplitude of the system were recorded. Over the 8 foot by 8 foot plane, the measured phase was constant to within $\pm 5^\circ$ and the amplitude to within ± 4 dB. In another checkout test, a precision phase shifter was inserted in the system between a phase-locked transmitting source and an antenna. The phase shifter was rotated in 5° steps up to 180° and tracking in the phase-amplitude receiver was observed. Tracking was excellent and the relative phase measured with the receiver agreed to within $\pm 0.4^\circ$ (measurement accuracy) of the phase shifter setting.

After the initial system checkout tests were completed, the positioner was mechanically aligned. With the use of a clinometer, alignment was accomplished by the adjustment of the eight screw-type jacks located under the positioner. During the leveling procedure, the lower horizontal bar was found to have a slight bow near the center. Alignment in the X-Y plane was done using a jig transit which could be focused at close distances. Figure A1 is a three-dimensional

error map showing deviation in probe position from a true X-Y plane. Readings were taken every five inches along the X-axis and every five inches along the Y-axis.

This error map describes the mechanical error present at the time of measurement, but could be significantly reduced if necessary. Deviation over the X-Y plane varied from $-.040$ to $+.005$ inch, referenced to the four corners of the plane. This corresponds to a relative error of $.0225$ inch (referenced to the middle of the error plane), or a phase error of approximately 5° at X-band. In practice, a test antenna may not radiate over the entire 8 foot by 8 foot area; whether or not the inherent phase error is significant depends on the electrical size of the antenna being measured. Looking at the error map, the area with the least error is near the center of the plane. Measurements on the horn and line source antennas described in Section IV were taken in this area where the relative phase error was extremely small.

The positioner was tested using standard gain and hog horn X-band antennas. Far-field predictions were made from the measured aperture distributions and in both cases, the results obtained were consistent with far-field measurements taken previously.

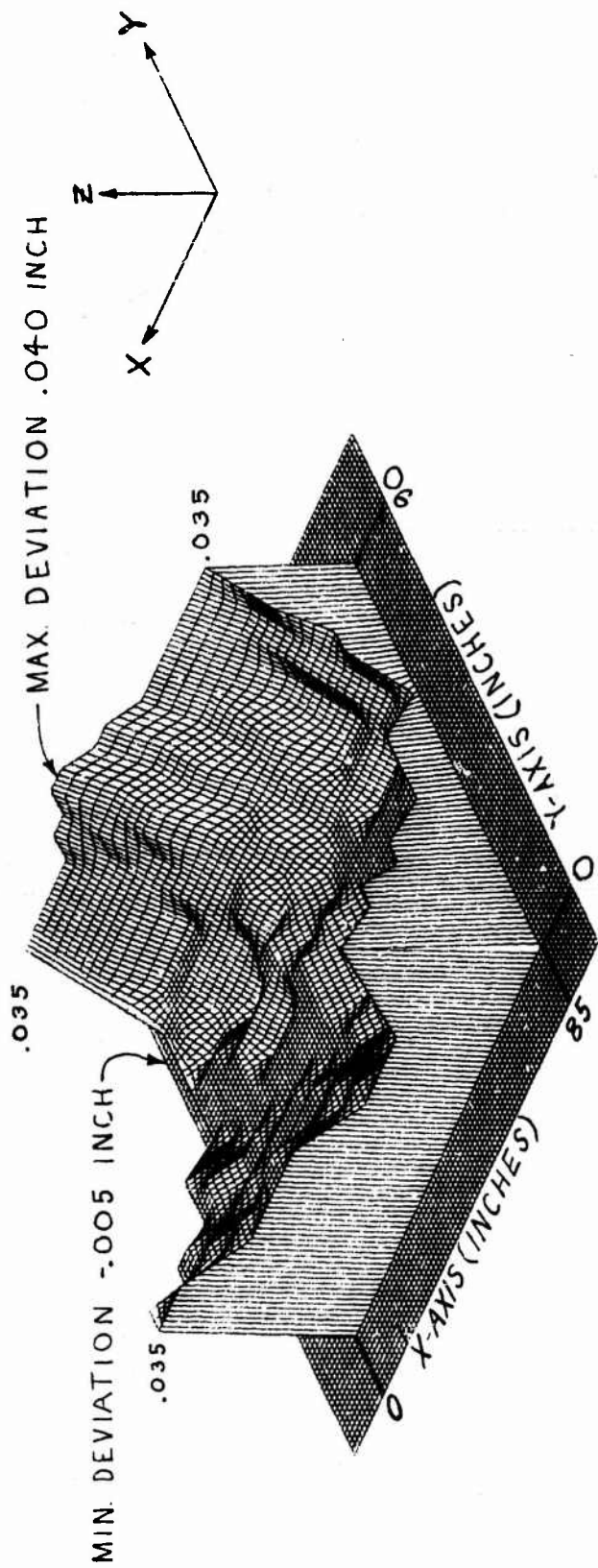


Figure A1. Three-dimensional error map of deviation in probe position from a true X-Y plane.

REFERENCES

1. Taylor, T. T., "Design of Line Source Antennas for Narrow Beamwidth and Low Side Lobes," IRE Transactions on Antennas and Propagation, Vol. AP-3(1), pp. 16-28, January 1955.
2. Dolph, C. L., "A Current Distribution for Broadside Arrays Which Optimizes the Relationship Between Beamwidth and Side-lobe Level," Proc. IRE, Vol. 34, pp. 335-348, June 1946.
3. Ecker, H. A., "Study of Directivity Optimization for Linear Antennas," 2142-1, Technical Report AFAL-TR-66-38, 28 February 1966.
4. Woodward, P. M., "A Method of Calculating the Field Over a Plane Aperture Required to Produce a Given Polar Diagram," J.IEEE (London), pt. III A, Vol. 93, pp. 1554-1558, 1947.
5. Goodman, R. M., Jr., Johnson, R. C., Ecker, H. A., Rivers, W. K., Jr., "A Folded Geodesic Luneberg Lens Antenna," Abstract, Engineering Experiment Station, Georgia Institute of Technology.
6. Johnson, R. C., "The Geodesic Luneberg Lens," Microwave Journal, Vol. 5, No. 8, August 1962, pp. 76-85.
7. Johnson, R. C., "Radiation Patterns From a Geodesic Luneberg Lens," Microwave Journal, Vol. VI, July 1963, pp. 68-70.
8. Jasik, H., "Antenna Engineering Handbook," McGraw-Hill Book Company, Inc., New York, 1961, pp. 2-31, 2-33.
9. Silver, S., "Microwave Antenna Theory and Design," MIT Rad. Lab. Ser., McGraw-Hill Book Company, Inc., New York, 1949, Vol. 12, Section 6.7.
10. Silver, Ibid, Section 6.6.
11. Silver, Ibid, Section 6.4.
12. Skolnik, M. I., "Introduction to Radar Systems, McGraw-Hill Book Company, Inc., New York, 1962, Section 7.8.
13. Taylor, T. T., "One Parameter Family of Line Sources Producing Modified $\sin \pi u / \pi a$ Patterns, Hughes Aircraft Company Technical Memorandum 324, Contract AF 19(604)-262-F-14, September 4, 1953.
14. Sandrin, W. A., and Glatt, C. R., "Computer Aided Design of Optimal Linear Phased Arrays," Microwave Journal, Vol. 13, No. 9, September 1970, pp. 57-61.

15. Silver, op. cit., Section 6.
16. Kinsey, R. R., "Line Source Aperture Monopulse Excitations," General Electric Company, Heavy Military Electronics Department, Project No. 8683, Final Report, Contract AF 19(628)-5905. April 1968.
17. Joy, E. B., "Spatial Sampling and Filtering in Near-Field Measurements," Doctoral Dissertation, Georgia Institute of Technology, 1970.